LA-UR-19-31408
Approved for public release; distribution is unlimited.

Title: STRENGTHENING TECHNICAL SAFEGUARDS OF FRESH FUEL THROUGH INTERNATIONAL COOPERATION

Author(s): Favalli, Andrea
Broughton, David Paul
Croft, S.
Grund, M.S.
McElroy, R. D.
Renha, G

Intended for: Report

Issued: 2021-02-11 (rev.1)

STRENGTHENING TECHNICAL SAFEGUARDS OF FRESH FUEL THROUGH INTERNATIONAL COOPERATION

PROJECT REPORT ON ACTION SHEET 26

Between

The United States Department of Energy (DOE) And

The National Nuclear Energy Commission of Brazil (CNEN)

For

Fuel Bundle Measurements

A.Favalli[1], D.P.Broughton[1], S.Croft[2], M.S.Grund[3], R.D. McElroy[2], G.Renha[3]

[1]Los Alamos National Laboratory, Los Alamos, USA
[2]Oak Ridge National Laboratory, Oak Ridge, TN, USA
[3]The National Nuclear Energy Commission of Brazil (CNEN), Rio de Janeiro, Brazil

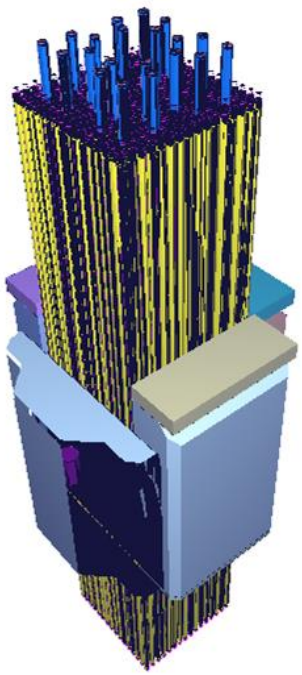

Executive Summary

Over time, nuclear fuel designs have shifted towards having higher initial enrichments and a greater number of burnable poison rods. This enables increased burnup for commercial reasons. These changes have made safeguards measurements of the ^{235}U content in modern fresh fuel more challenging. This is addressed here through a re-evaluation of the UNCL (Uranium Neutron Collar – Light Water Reactor Fuel) poison rod correction factor. Coefficients of the poison rod correction factor were updated by simulating response of Angra II PWR fuel with a wide range of both burnable poison rods and Gd_2O_3 content per rod. Benchmark comparisons are made to experiments performed at Resende (Brazil) and CNEN/LASAL in Brazil. By updating these coefficients, while maintaining the same mathematical form to allow INCC to be used without software modification, it was possible to reduce error in experimental ^{235}U linear density assay by an order of magnitude.

This work was conducted under the framework of a collaboration between the U.S. Department of Energy (DOE) and the National Nuclear Energy Commission of Brazil (CNEN). The collaboration leveraged facilities and expertise to: (1) design and construct a short mock-up of a modern fresh fuel assembly, as a reference assembly for training and R&D, (2) model the fuel bundle as built, and in a number of different configurations to predict the UNCL detector response in MCNP, (3) verify outcomes of simulated response against tested performance of correction factors generated using simulated cases on commercial fuel assemblies. Follow-up experimental studies using the short fuel mock-up with Burnable Poison (BP) rods may be used to further build upon the simulation studies conducted here.

Under AS-26, the UNCL LANL-2 was shipped from LASAL to the Brazilian Fuel Fabrication Plant and it was calibrated. Following the calibration, fuel assemblies with and without Gd were measured in order to evaluate the UNCL performance. A technical report on how to perform measurements with collar was written by CNEN with DOE staff. The fabrication of a reference short mock-up assembly was completed in November 2017 in Brazil. The name of this assembly is Elemento Combustivel Curto (EC Curto) and is based on 16×16 PWR Angra II design. This assembly, constructed in Resende, at Nuclear Industries of Brazil (INB), is supported by detailed destructive assay measurements of the nuclear material and by detailed engineering drawings.

On Wednesday March 21 2018 at approximately 3:14 pm Brazil local time the team completed the *historic first ever non-destructive assay* measurement of the new reference short fuel assembly. Then, comparative measurements were made at INB between production assemblies and the certified reference short fuel bundle. The short bundle, as well as the UNCL and Am-Li neutron source was moved in 2018 to CNEN in Rio de Janeiro, where a laboratory was set. It is being used for training and will be used for substitution and other research studies.

The MCNP model of EC Curto used in simulations to evaluate sensitivities and to extend the calibration, was based upon the detailed engineering drawings and destructive assay

measurements of the nuclear material used for the construction, ensuring that it very precisely represents the geometry and material within the nuclear fuel. This enabled high fidelity absolute MCNP simulations which predicted the Doubles rates within 1.3% of the experimental value for the reference short fuel mock-up. Further simulations corresponding to Angra II fuel used in reactors that follows the same basic design, but use a longer active length, were similarly found to be in accord with measurements. Absolute simulated Doubles were within 1.2% for two commercial fuel assemblies containing BP rods.

The remainder of this report is arranged as follows. *Part I* consists of a simulated sensitivity study used to estimate overall Doubles uncertainty for both simulations and experimental measurements of the short fuel assembly by varying factors such as the lateral fuel position, polyethylene density and AmLi spectrum. From this it was estimated that the respective simulation and experimental Doubles uncertainty for the short mock-up assembly are in the range of 1.91% and 1.39% (includes 0.76% statistical uncertainty). *Part II* of this report focuses on re-evaluating the poison rod correction factor using 40 simulated cases with assemblies having 4, 8, 12, 16, 20, 24 poison rods, each with Gd_2O_3 wt% ranging from 2% 11%. The numerical values for the coefficients from the original poison rod correction factor based on Menlove's pioneering work and implemented in the INCC code were optimized for these simulated cases and then applied to verification measurements of five different commercial Angra II fuel assemblies, each with 12 poison rods. For these experimental validation cases, the relative error in the ^{235}U linear density was reduced from >10% to <4% by adopting self-consistent cross calibration parameters and changing from the original to updated burnable poison rod correction coefficients. These results provide a pathway for how to improve current safeguards of fresh fuel of modern designs, since, by updating coefficients of the existing poison rod correction factor equation, it is possible to significantly improve verification measurements of modern light water fuels. Part III of the report is dedicated to reporting of the results, simulations and experiments, and of the method developed, as part of the AS, by the team to study the emergent neutron spectra from the AmLi sources used in the collar. The developed method used an Active Well Coincidence Counter, which is a typical safeguards counter, and a set of two sources in moderating material, to identify features of the AmLi neutron energy spectrum. *Part IV* of the report discusses the gamma related activities performed at the CNEN/LASAL laboratory in Rio de Janeiro where standards of enriched uranium were available, as well as $LaBr_3$ scintillation detectors. The data shows the robustness of the pair of $LaBr_3$—gamma detector based systems analyzed using the NaIGEM code.

In addition the project succeeded *to transfer needed software* to CNEN: Peak Easy for gamma spectra analysis (from Los Alamos National Laboratory by following the export control requirement) and NaIGEM (from IAEA, A.Berlizov). Both of these codes were used in the joint AS activities.

To summarize several of the main findings of this work:

- **EC Curto (short mock up) was constructed as a unique high fidelity reference nuclear fuel assembly (one of only 4 in the world for safeguards/nonproliferation)**

  - Excellent provenance and documentation (technical drawings, destructive assay of the pellet materials, details on the construction process in the INB fuel factory)
  - Demonstrated to be a good surrogate for full length fuel assemblies
  - Useful for experimental research, calibration, and training

- **Validation demonstrated simulation-experimental consistency**
  - ~1%, within estimated uncertainty budget

- **Overall simulation uncertainty low enough (~2%) to justify updating the k_3 parameter used in the INCC algorithm to reduce the >10% assay error with commonly used *k* correction factors**

- **The poison rod correction in thermal mode has been updated for modern PWR fuel**
  - Optimized coefficients improves verification assay by order of magnitude (~10x)
  - These coefficients are directly usable by IAEA without modification to analysis code (INCC)

For completeness, here is the list of the neutron tasks as in the AS-26, and their mapping in the present report.

- CNEN is to provide Los Alamos National Laboratory (LANL) and Oak Ridge National Laboratory (ORNL) detailed engineering drawings and DA data for the short mock-up fuel bundle.

  Final technical design of the short mock up fuel assembly were provided for construction of models (they are not included here as they contain proprietary information). Reference CNEN, Technical Note NT-COSAP/LS-001/15. 29/09/2015, and Standard Pellets for the In-the Field DA Calibration (COMPUCEA). 2013-03-15 reported the isotopic analysis by DA of the fuel (see Part I of the present report).

- LANL and ORNL are to develop a detailed MCNP model of the short mock-up fuel bundle based on the data provided by CNEN.

  Part I and Part II of the report on the MCNP simulations and the full sensitivity analysis.

- LANL and ORNL sensitivity studies to AmLi spectrum are to be performed using well counter measurements. Rates and ring-ratios are to be compared to predictions as a function of moderation.

  Part I, sections 1.5-1.7 discuss the sensitivity of the results of the AmLi spectrum, while the PART III reports on the well counter measurements methods on the analysis of energy

neutron emission from AmLi sources used in the uranium collar.

- LANL, ORNL, and CNEN are to develop a neutron measurement plan for the short mock-up fuel bundle.

  The upgraded UNCL unit was moved from CNEN to INB in Resende and set up again to work during a first DOE (LANL & ORNL) and CNEN measurement campaign in August & September 2017. LANL, ORNL, and CNEN are to perform neutron measurements on the short mock-up fresh fuel bundle. These measurements allowed the team to create a joint suitable plan of measurement to be used in the measurement campaign with the short-fuel assembly.

- LANL, ORNL, and CNEN are to compare MCNP results with the neutron measurement data to calculate new correction factors and reevaluate the correction factors currently in use.

  On March 2018 the team completed the first measurement campaign with short-fuel assembly. The high fidelity modelling and benchmark of the measurement are reported in the Part I and Part II of the report, where Part II focuses on the detailed re-evaluation of the correction factors, providing a new set of correction coefficients that allow an improvement of an order of magnitude in the verification of the linear ^{235}U mass in modern fresh fuel assembly.

- LANL, ORNL, and CNEN are to draft a report with specific recommendations to improve current safeguards measures on fresh fuel with modern designs.

  The present report reports on the neutron activities and including an updated recommendation for the correction factors to be used in the verification of modern reactor fresh fuel assembly with Gd poison rods to control reactivity. The new coefficients were also tested with new measurements of Angra Fuel by CNEN on February 2019.

The joint project also had gamma related activities. Here is the list of the gamma measurements related tasks as in the AS-26, and their mapping in the present report.

- LANL, ORNL, and CNEN are to develop a list of their respective gamma measurement systems and analysis software (including version numbers) for evaluation.

  The gamma measurement systems and analysis in LASAL are the following: Detectors NaI 2"×2", NaI 2"×0.5", NaI 3"×3" (well), $LaBr_3$ 1.5"×1.5", HPGe GL 0213R (30 L cryostat), HPGe GL 0515R (bigmac cryostat); MCA GBS 166, Canberra DSA1000,

Inspector 2000, Acquisition Softwares- Gamma acq and analysis v. 3.1, WinSpec v. 2.04.0000, WinU235 v. 2.00.0005, WinUF6 v. 1.00.0014; Analysis software MGAU v. 4.0 and NaIGEM 1.52a. The NaIGEM 1.52a were updated to 2.1.4, under this AS making LASAL able to analyse $LaBr_3$ spectra.

- LANL, ORNL, and CNEN are to develop a detailed benchmarking and uncertainties evaluation of spectrum analysis code (for LRGS spectroscopy), based on measurements available from CNEN.

  A plan of measurements to compare 2 systems was established. LASAL has SRM 969 Standards (Uranium Enrichment standards from NBL): 031; 071; 194; 295 and 446 and a set of Steel attenuators: 0, 4, 8, 12 and 16 mm.

- CNEN, LANL, and ORNL are to jointly evaluate the NaI(Tl) well-geometry detector available at CNEN as an alternative to the current counting geometry. This includes source type and placement, data acquisition parameters, spectrum quality control tests, analysis methods, speed and accuracy.

  A description including recommendations from DOE team are enclosed to this report.

- CNEN, LANL, and ORNL are to study potential source of bias and evaluate uncertainties in spectrum analysis codes (such as MGAU and FRAM) commonly used in nuclear safeguards practice in the analysis of High Resolution Gamma Spectroscopy (HRGS)

  Analysis of the data in particular, using the NaIGEM code transferred to CNEN, is reported in Part IV of the report.

Contents

Appendices

Introduction

The application of international safeguards to commercial nuclear power prompts the need to assay fresh nuclear fuel assemblies against the manufacturer declaration. Active UNCL (Uranium Neutron Collar – Light Water Reactor Fuel) measurements have been developed to assay the linear density of fissile mass in fuel assemblies for prevention of nuclear material diversion. The demonstration and implementation of the UNCL approach has been the subject of a collaboration between the US and Brazil starting in the early 1980s. Calibration of such instruments by direct measurement is difficult because there are few facilities with traceable assemblies that can be reconfigured and because the dynamic range and number of configurations of interest is so broad. Consequently, the current analytical response models are founded on quite a narrow exploration of the overall parameter space of interest. Modern low enriched fuel has both higher enrichment and higher burnable poison content than was available for calibration and so there is interest in extending the calibration to ensure the quality of verification measurements. In Part II of the current report the Monte Carlo simulation approach to this problem is used to quantify Doubles variations resulting from changes in the number and Gd contents of Burnable Poison (BP) rods. Simulation of these scenarios is faster, cheaper and allows exploration of a wider parameter space than is feasible experimentally, but poses a different set of challenges. For instance, although high fidelity neutron transport models are absolute, in practice their accuracy is insufficient for safeguards purposes. This is due to limitations in basic nuclear data and imperfect knowledge of the materials and geometry of the instrument and AmLi neutron source. Some of these limitations are explored in Part I of this report to understand reasonable expectation for simulation-experimental consistency. Therefore, it is necessary to use simulations to make only relative adjustments to benchmark data.

In the framework of a collaboration project between the Department of Energy (DOE) and the National Nuclear Energy Commission of Brazil (CNEN), a research activity is ongoing to develop a reconfigurable reference short fresh fuel assembly of modern design for calibration and research, to also model the fuel bundle, and predict the UNCL detector response. The reference fuel assembly constructed as part of this project at Nuclear Industries of Brazil (INB) has excellent provenance and documentation as engineering drawings used during manufacturing were made available for reference when constructing MCNP models. Fuel characterization included destructive analysis by LASAL (Rio de Janeiro, Brazil) of the uranium concentration and uranium isotopic concentrations by the IAEA NML (Seibersdorf, Austria). The assembly will be readily available at CNEN for training, pin substitution, and other research studies including the exploration of the influence of varying burnable poison pin number, position and concentration.

This current work benefits from a collaboration over decades, between instrument developers, regional inspectorate, and fuel fabricators. It rests on team work between a multi-discipline group of technical experts. By leveraging facilities and talent in this way a robust technical solution has been achieved, one that uses international resources effectively and leads to strong stakeholder involvement. The concept and approach will also benefit the larger safeguards community. This report focuses on (Part I) a Monte Carlo sensitivity study varying parameters

expected to make the greatest contributions to Doubles uncertainty both experimentally and in simulation space, and (Part II) simulation of 40 cases varying the Gd content (number of BP rods and Gd_2O_3 wt%) in fuel assemblies of constant ^{235}U linear density to re-evaluate coefficients of k_3, the BP rod correction factor used in INCC by safeguards inspectorate. Expected outcomes are quantification of simulation sensitivity to parameters that are known to have variation, as well as an updated set of coefficients that may be implemented in existing versions of INCC to improve verification measurements for assemblies containing BP rods.

Fabrication of Short Fuel Assembly

To effectively use the UNCL for training and calibration, a physical library of fuel pins and fuel assembly jigs must be available. To the best of our knowledge, there are only three other locations worldwide that have had fuel pin libraries (LANL at Los Alamos, EC-JRC, IAEA HQ in Vienna). Under AS 26, the fabrication of a reference short mock-up assembly was completed in November 2017 by INB. The name is Elemento Combustivel Curto (EC Curto) and is based on 16×16 PWR Angra II design. A batch of 3.2% enriched uranium dioxide pellets, which were analyzed by destructive assay techniques, was used in making the rods of the short assembly, and all the technical drawings of the construction were made available to the CNEN/DOE collaboration. This care and detail was necessary to ensure that short mock up fuel assembly has the excellent pedigree and traceability needed to be designated a reference calibration assembly.

On Wednesday March 21 2018 at approximately 3:14 pm local time the team completed the *historic first ever non-destructive assay* measurement of the new reference short fuel assembly. The technical team is shown in Fig. 1 during the deployment of CNEN's UNCL to acquire passive and active coincidence count data on the short fuel bundle at the INB Resende Nuclear Fuel Fabrication Plant.

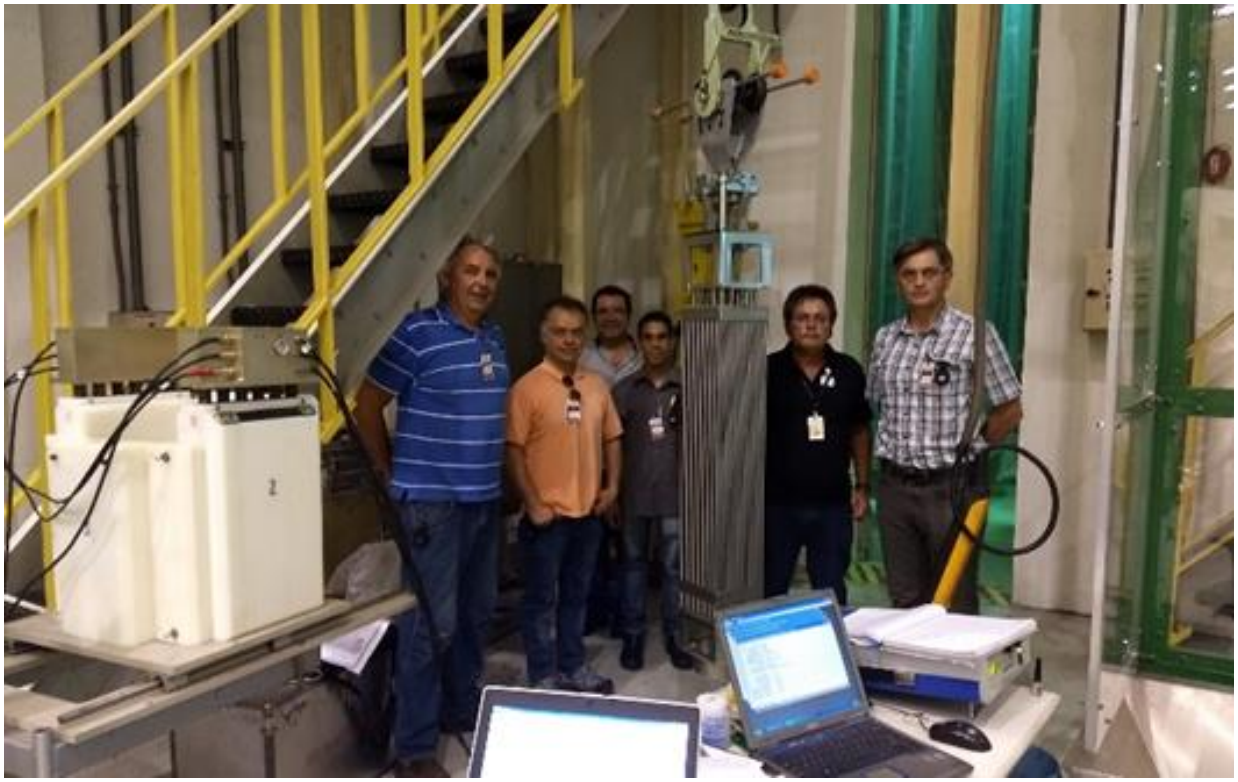

Figure 1. CNEN, DOE and INB staff beside the new reference short fuel bundle – March 2018. The collar is on the left and the JSR-12 on the right.

Part I – Monte Carlo Sensitivity Analysis

1.1 Background and Model Validation

To demonstrate that the MCNP model realistically corresponds to the PWR fuel used in the Brazilian Angra II and III reactors it was validated by comparing simulation and experimental results for three specific fuel assemblies. This included two measurements of full length fuel assemblies with poison rods (A1 and A2) and the shorter reference fuel assembly named Elemento Combustivel Curto (EC Curto) described in Tables 1 and 2. The density values reported in Table 2 are based on the reported fuel length, radius and mass assuming that gaps between pellets and chamfering are negligible. The high fuel densities in the UO_2 at the ends of the fuel rods may be due to actual BP rods differing slightly in length from the schematics provided (INB fabricates fuel rods and imports BP rods). Since the A1 and A2 fuel assembly measurements were taken in the middle region of the fuel the simulations omit the end regions that do not contain Gd_2O_3. These measurements of full length fuel assemblies are simulated using the considerably shorter 80.3 cm active length corresponding to the active length of EC Curto to demonstrate that for active simulations and measurements the short fuel assembly can be interchanged with full length fuel assemblies. This is done to demonstrate practical equivalence in support of future work involving experimental measurement of a variety of BP rod configurations using the short fuel assembly. The UNCL in this work is the original UNCL type I detector which was brought to Brazil by Dr. Howard Menlove in the 1980's early on in the evaluation of the neutron collar. A visual of the geometry simulated in all cases is shown in Fig. 1, based INB (Everaldo 2017). The specific UNCL detector used both experimentally and in modelling corresponds to the type 1 neutron collar as described by Menlove et al. (1985), which consists of 18 ^{3}He tubes, each 1 inch (2.54 cm) in diameter with an active length of 33 cm. Each of the 3 polyethylene segments (with 6 ^{3}He tubes) has its own pre-amplifier and the output signal is a summation of the signals, which is connected to a shift register to record the total Singles and Doubles rates. A MCNP model of the type I UNCL was used for the simulations (private communication from Anthony Belian).

Fuel type	**PWR**
Reactor design	Angra type II and III reactors
Pin array	16×16
Commercial assembly active length	390 cm (Gd_2O_3 in poison rods are only in central 330 cm for type-A fuel)
Short laboratory assembly ('EC Curto') active length	80.3 cm (Gd_2O_3 in poison rods extends full length)
Rods / guide tubes per assembly	236 / 20
Clad outer diameter / thickness	1.075 cm / 0.065 cm
Clad material / density	Zircaloy-4 / 6.55 g/cm^3
Fuel pellet diameter	0.911 cm
Pitch	1.43 cm

Table 1. Simulated fuel assembly parameters (fuel parameters as reported in da Silva et al. 2011)

Assembly name	Pin type (region)	^{235}U enrichment [wt%]	$\frac{m(Gd_2O_3)}{m(Gd_2O_3)+m(UO_2)}$ [wt%]	Density [g/cm^3]
EC Curto	Fuel	3.1995%	-	10.270
A1	BP (Middle)	4.2307%	2.0119%	9.936
	Fuel	4.2470%	-	10.260
A2	BP (Middle)	2.9203%	6.9430%	9.804
	Fuel	4.2540%	-	10.172

Table 2. Fuel parameters of experimentally measured fuel

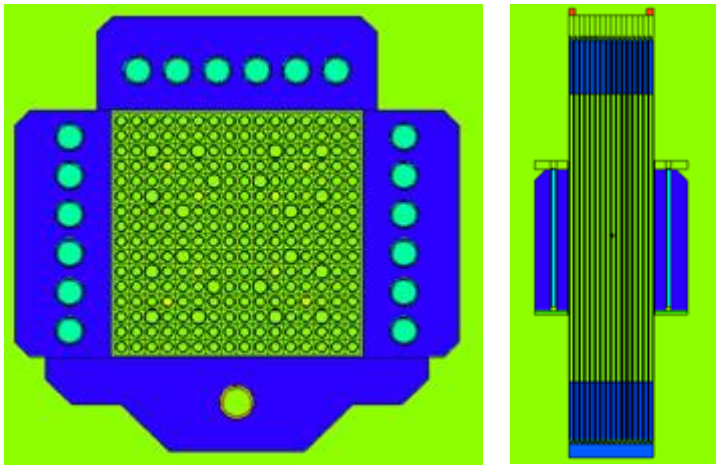

Figure 1. Cross sectional images of MCNP geometry showing **(a)** horizontal and **(b)** vertical cross sections at center of fuel assembly

When simulating fuel at a given enrichment, E_i, the declared fuel density of the as built EC Curto was scaled using

$$\rho_{E_i} = (10.270\ g/cm^3) * \left(\frac{(M_{UO_2})_i}{(M_{UO_2})_{3.1995\%}}\right)$$

Where $(M_{UO_2})_i$ refers to the UO_2 molar mass at a given enrichment, i. The reference theoretical relation for determining UO_2-Gd_2O_3 density as a function of Gd_2O_3 wt% (as defined in the header of Table 2) is defined by Bairiot et al. (1995) as

$$\rho_{UO_2-Gd_2O_3} = 10.962\ g/cm^3 - 0.0348 * (Gd_2O_3\ wt\%)$$

The density of 10.962 g/cm^3 should correspond to the density of fuel with a Gd_2O_3 wt% of zero, however since the density of the fuel being simulated here has a density lower than this a scaling factor was added to adjust the equation. The idea being that the relative change in density as Gd_2O_3 content increases should not vary, but since it appears that the overall density of the fuel of interest here differs from that of the reference equation a scaling factor should allow the determination of density as a function of Gd_2O_3 wt% for the fuel of interest. This scaling factor

was determined by minimizing the sum of squares between the estimated and declared UO_2-Gd_2O_3 densities for assemblies A1 and A2. With the scaling coefficient of 0.9128 the resulting equation used in this work to determine poison rod density is

$$\rho_{UO_2-Gd_2O_3} = 0.9128 * [10.962\ g/cm^3 - 0.0348 * (Gd_2O_3\ wt\%)]$$

which suggests the Gd rods used here have greater porosity than those included in the optimization of standard equation of Bairiot et al. (1995) as the optimized scaling factor is less than the typical scaling factor of 0.95 used to convert from theoretical density to effective density (effective density is reduced due to gaps between pellets).

Simulations were conducted using MCNP 6.2 (Werner et al. 2017), using the ENDF/B-VII.0 (i.e. XXXXX.70c) cross section library (Chadwick et al. 2006), using available room temperature thermal scattering S(α,β) tables. Specifically, the S(α,β) tables used are the ENDF70SAB based on ENDF/B-VII.0 poly.10t, fe56.12t, al27.12t, and the combination of u/o2.10t and o2/u.10t for UO_2 (Trellue and Little 2008).

The Singles, Doubles and Triples count rates were tallied using analog capture with F8 shift register tallies with a predelay of 4.5 μs and coincidence gate width of 64 μs (only Doubles are reported herein). Additionally, the 1-D Rossi-alpha distribution (RAD) was constructed using a series of 40 F8 tallies where the predelay was increased 5 μs increments with a constant gate width of 5 μs. Simulations were run on a Windows cluster using between 10^8 to 10^9 source neutrons (most commonly 5×10^8) to achieve reasonable statistical precision within approximately 10 minutes. Relative error values were all <1% for Doubles in all cases.

Simulation results corresponding to the fuel assemblies described in Table 2 are presented in Table 3, where the simulated AmLi spectra corresponds to the experimentally evaluated spectra from Obninsk Laboratory, Russia (Rinard and Menlove 1998; Rinard 2001; Croft et al. 2011). As the simulated Doubles for these three different fuel assemblies are consistent within overall uncertainty of the measured rates, discussed later in Table 12, the MCNP model is considered to have high predictive capability despite the simulation corresponding to an active length of 80.3 cm instead of the full length of 330 cm for A1 and A2. The effect of simulated fuel length on measurement results is quantified later in this report. The ability to approximate a full length fuel assembly with one that has a much shorter active length is important as the short fuel assemblies are much more convenient for handling during calibration and characterization measurements in laboratories. The apparent bias low for simulation results in Table 3 may result from a number of parameters that include room return, anisotropic neutron emissions from AmLi, position of fuel, and other factors investigated in Part 2 of this report.

Assembly name	Simulated net active Doubles	Measured net active Doubles	Relative difference	σ_{exp} from measurement

	$\pm \sigma_{MC}$ [s^{-1}]	$\pm \sigma_{exp}$ [s^{-1}]		
EC Curto	161.2 ± 1.5	163.3 ± 1.2	-1.32%	1.8σ
A1	158.8 ± 1.4	160.8 ± 1.2	-1.22%	1.7σ
A2	153.2 ± 1.1	154.5 ± 1.2	-0.88%	1.1σ

Table 3. Comparison of simulated to measured rates in thermal mode (no Cd) with FA centered within UNCL (Source strengths used in simulations were 39706.52 neutrons per second for EC Curto, measured Mar 2018, and 39738.37 neutrons per second for A1 and A2, both measured Aug 2017. See section 1.10 for details on source strength calculation. σ_{MC} refers to Monte Carlo statistical uncertainty and σ_{exp} to experimental statistical uncertainty)

Although current verification measurements use net active Doubles rates, the comparison of other simulated and experimental responses such as the passive response and timing characteristics of coincidence events can increase confidence in simulations. Ideally experimental and simulated Rossi-alpha distributions (RADs) would be compared directly, however as they are not currently available the effective detector die-away time is evaluated. The simulated die-away time from a pure ^{252}Cf source of 0.1 cm radius is compared to the reference value. The RAD was simulated using a series of 40 gates, each 5 μs in width with an initial 4.5 μs pre-delay after the initial neutron capture event, or "trigger" as shown in Fig. 2.

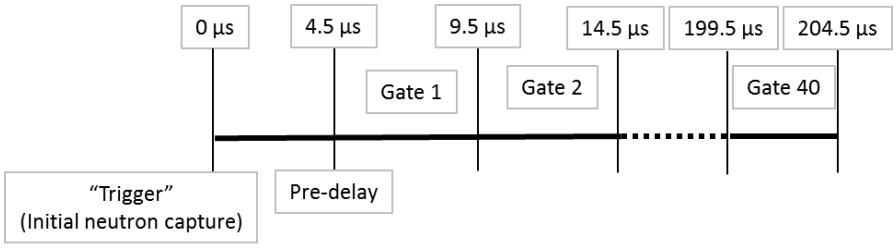

Figure 2. Illustration of sequential gates used to tally RAD in MCNP

The die-away time of the system was determined by fitting the exponential over the range 4.5 μs to 99.5 μs as shown in Fig. 3. (a). This range was used because as Fig. 3. (b) shows that the fit becomes distorted in the early region when the full RAD is analyzed by a single curve. Using the fit in Fig. 3 (a) the die-away, τ, is 54.1 μs based on the relation,

$$D(t) = D_0 \cdot e^{-\frac{t}{\tau}}$$

which corresponds to an optimal gate width of 64.9 μs based on $g_{opt} \approx 1.2 \cdot \tau$ for Accidentals dominated coincidence counting. As experimental list mode measurements are not documented this would be a useful measurement to verify with the UNCL LANL-2 used in Brazil. Such a measurement would require use of a list mode device such as the Advanced List Mode Module (ALMM) and would be most beneficial for research purposes if the signals were individually output from each tube or detectors within each of the 3 HDPE segments of the UNCL, however overall die-away can be measured in list mode without any hardware changes.

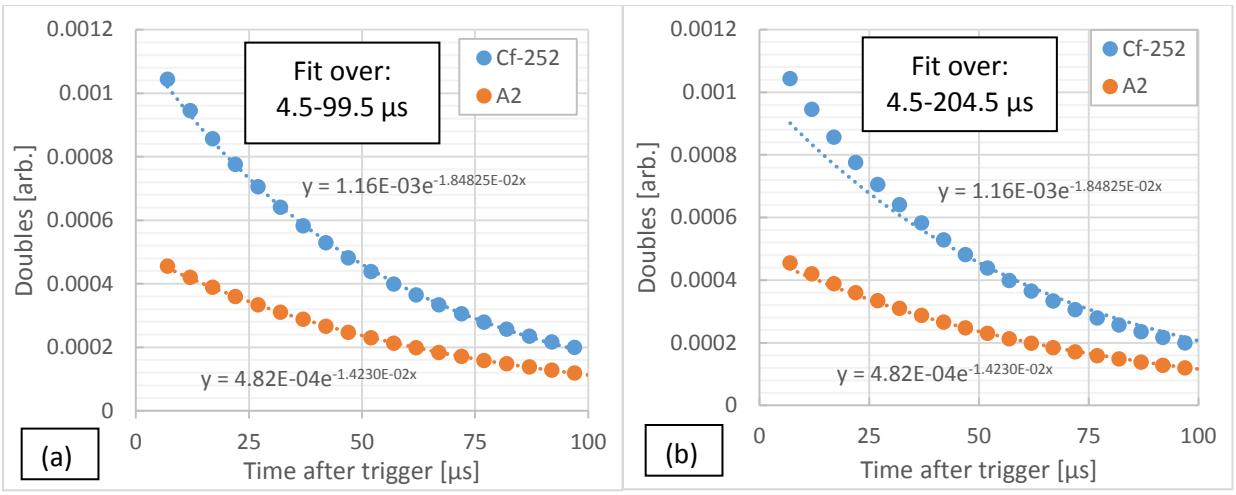

Figure 3. Simulated RAD for spherical ^{252}Cf source, with r = 0.1 cm, at center of UNCL (without fuel), and for the A2 fuel assembly **(a)** fit over: 4.5-99.5 µs, and **(b)** fit over: 4.5-204.5 µs

In August 2017 the die-away of A2 was measured with LANL-2 using 32 µs and 64 µs gates. The die-away was found to be 59.1 ± 9.1 µs (1σ), corresponding to an ideal gate width of 70.9 ± 10.9 µs (1σ). The equivalent simulated two-gate analysis for A2 yields die-away and ideal gate widths of 66.0 ± 1.3 µs and 79.2 ± 1.5 µs, respectively (simulation uncertainty estimates are only Monte Carlo uncertainties). Equivalent die-away and ideal gate widths of 67.2 µs and 80.7 µs, respectively, were also determined by fitting the die-away curve for A2 in Fig. 3 over the range 4.5 µs-99.5 µs. The RAD-based die-away has some sensitivity to the specific range over which the curve is fit and shows almost exact agreement with the two gate method by fitting over the 4.5 µs-44.5 µs time range where the die-away is 66.2 µs. This illustrates the consistency of the two methods, demonstrating that longer experimental measurements with 32 µs and 64 µs gate widths could be used to more precisely determine the ideal gate and die-away time.

While the die-away times for A2 from simulations are within experimental uncertainty they are greater than the experimental results by nearly 1σ greater, suggesting that higher precision experimental results may change the conclusion. In either case 64 µs may be slightly smaller than the ideal gate, which appears to be at least 70 µs. The conventional approach of determining the ideal gate width from ^{252}Cf might be improved through the use of a fuel assembly measurement as the goal is to minimize Doubles uncertainty when measuring fuel assemblies. To do this a reference assembly would need to be defined and applied to all cases, but in any case it is likely to be more representative of fuel assemblies in general than the use of ^{252}Cf.

The overall consistency between experiments and simulations suggests that the MCNP model is an accurate representation of modern PWR fuel used for Angra II in Brazil and can reasonably be used for extrapolating to hypothetical enrichments and BP configurations that extend beyond those currently in commercial use. The small negative bias when comparing simulations to experiment appears relatively consistent across different types of fuel assemblies, suggesting general trends in simulations should not be affected. By simulating an extensive range of cases it may be possible to improve coefficients for the existing correction factors used to determine ^{235}U

linear density in fuel assemblies containing BP rods. Prior to the optimization study a sensitivity analysis is conducted to evaluate effects of varying simulation parameters within the known uncertainty. By understanding the limits of simulations and measurements the expectations for both simulation-to-experimental and experimental-to-reference calibration agreement can better be defined.

1.2 Sensitivity of collar measurements to fuel length

The experimental EC Curto fuel assembly (Favalli et al. 2018) and corresponding simulation analysis presented here rely on the assumption that the short fuel assembly is a good approximation of a full length fuel assembly. The set of simulation results presented here used fuel assemblies of varying lengths to determine the infinite fuel length, which is used here in reference to the distance from the detector at which there is a negligible contribution to the UNCL count rates. The length of fuel assayed during a given collar measurements is also useful in practice to optimize measurements aimed at scanning the entire length of the fuel.

The set of simulations for fuel of varying lengths ranges from the length of the UNCL detector (43 cm) up to 100 cm above and below the UNCL (243 cm total) at increments shown in Fig. 4. Results of these simulations are given in Fig. 5 as a ratio to the simulation result for the short fuel assembly which has an active length of 80.3 cm, corresponding to fuel length of +20 cm in the notation where fuel length is measured based on the length of fuel above and below the collar.

The active signal is much more localized than the passive signal since the fissions induced by the AmLi source are concentrated in fuel within the collar. Coupled with the strong spatial dependence of Doubles efficiency this results in 90% of the active Doubles being detected from the 43 cm of fuel contained within the length of the UNCL. The 10 cm of fuel above and below the UNCL accounts for most of the remaining signal, contributing ~9% of the overall Doubles, which equates to ~99% of the signal being from 63 cm of fuel. This analysis supports the claim from the original report of Menlove et al. (1985) that

> "This active length of the fuel assembly must extend at least 15cm beyond the bottom of top of the collar to avoid reduction in the measured response because of end losses from neutron leakage".

Therefore the 80.3 cm active length of EC Curto satisfies the infinite active length as it produces a Doubles rate that is just 0.2% less than the longest simulated length of 243 cm. There would be a negligible further increases from the additional 87 cm for real fuel of 330 cm in length.

As the passive source is distributed, source strength corresponds directly to fuel length. This results in the passive signal not reaching a plateau as soon or as flat as the active signal. The position of the collar on the fuel assembly is likely to have a slight effect for passive measurements of ^{238}U linear density using the Doubles. While the use of a single passive measurement to determine net active Doubles when scanning a fuel assembly could introduce bias, it is likely a minor effect as the passive Doubles measurement generally accounts for <10%

of the active Doubles signal, meaning that a 5% error in the passive rate affects the net Doubles by <0.5%.

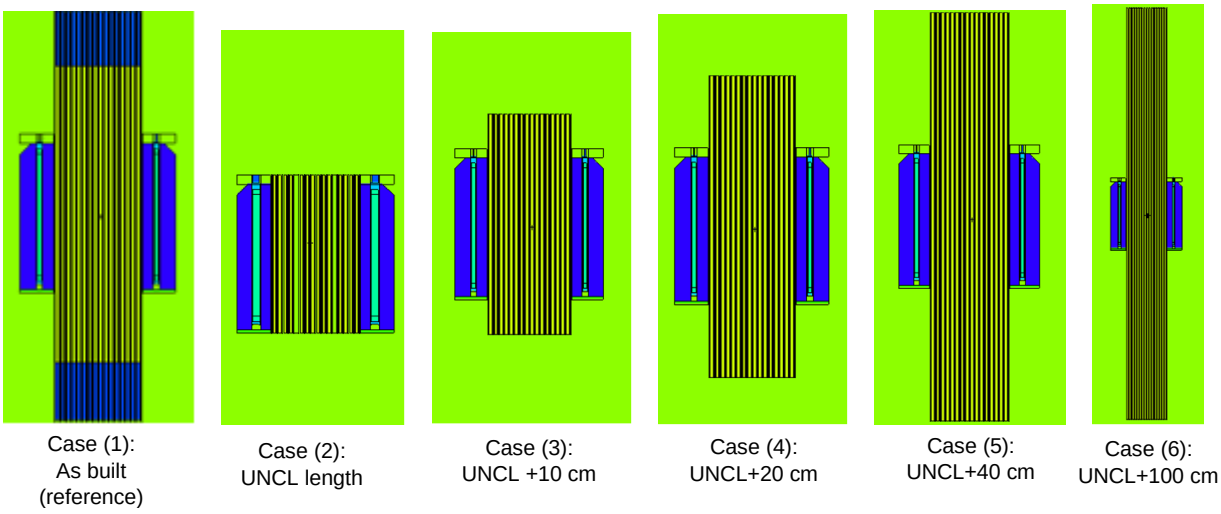

Figure 4. Illustration of the five fuel length variations simulated

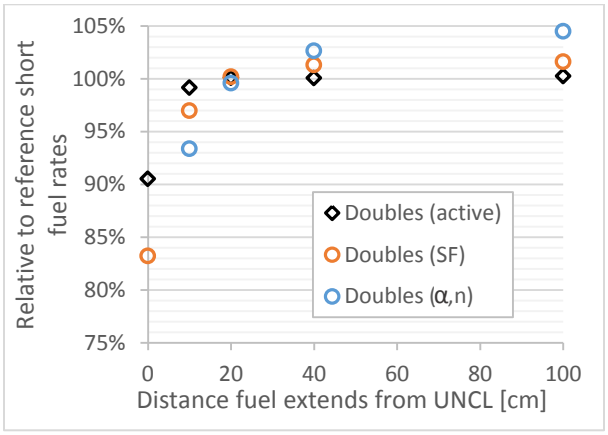

Figure 5. Active AmLi and passive SF and (α,n) Doubles count rates for varying fuel lengths relative to reference short fuel simulation (case (1) in Fig. 4) for fuel enriched 3.1995 wt% ^{235}U

Overall this suggests that the short fuel assembly is a reasonable surrogate for the purpose of active measurements of full length fuel assembly as the net active Doubles rate is not affected by the slight underestimation of the passive Doubles. For studies directly using passive count rates a scaling factor might be required to make rates comparable to a full length fuel assembly. If desired, this should be determined with the full length assembly hanging from a crane slightly above the floor and the collar near the bottom of the assembly as this is the standard measurement position.

1.3 Assembly position within the collar

The UNCL was designed to be slightly larger than the fuel assemblies being measured to avoid the need to physically touch the operator's fresh fuel. This gap contributes to experimental and simulation uncertainty as it is difficult to visually center the fuel assembly within the detector. As an alternative to improve reproducibility some opt to position the collar so that the front (AmLi side) of the collar is just touching the fuel, which reduces the uncertainty to variations left or right for a given set of measurements. Though there is just slightly more than 0.25 cm on each side of a 16×16 Angra fuel assembly when centered it is useful to quantify how much small variations in position can contribute to the systematic uncertainties.

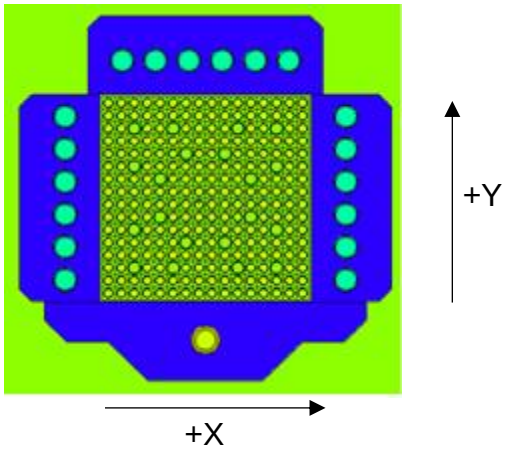

Figure 6. Illustration of the fuel assembly centered within the UNCL with axial labels corresponding to Table 4

The results in Table 4 correspond to simulations with a number of 0.25 cm translations corresponding to the directionality shown in Fig. 6. The variability in the Doubles is just 0.50%, indicating that there is relatively little sensitivity to fuel assembly position. The active Doubles signal results from induced fissions which are increased slightly when the assembly is either shifted closer to the AmLi source or off to one side, respectively corresponding to increased interrogation and detection efficiencies. These results are amenable to direct comparison with experimental measurements in the future.

Assembly position (x,y) translation	Singles [cps]	Doubles [s^{-1}]
Centered (0, 0)	2229.76	160.79
Close to source (0, -0.25 cm)	2217.65	161.53
Far from source (0, +0.25 cm)	2232.15	160.72
Left (-0.25 cm, 0)	2224.46	161.19
Left back (-0.25 cm, +0.25 cm)	2231.76	160.90
Left front (-0.25 cm, -0.25 cm)	2217.26	161.38

Table 4. Comparison of count rates when fuel assembly (3.1995 wt% ^{235}U) position is shifted

1.4 Sensitivity of active measurements to polyethylene density

It is well known that the density of high density polyethylene (HDPE) can vary considerably, with one of the wider ranges referred to being 0.912 to 0.962 g/cm^3 (Awaschalom and Sanna 1985). As conventionally it has been found to vary to a lesser extent around 0.95 g/cm^3, simulation results are reported in Table 5 and Fig. 7 over the density range of 0.94-0.96 g/cm^3. As the Doubles rate increases proportional to the density this suggests that higher density HDPE moderation the AmLi neutrons to a greater extent to increase the induced fission rate. The rate of change in the Doubles relative to 0.95 g/cm^3 appears to have an approximately linear trend, which follows from the variation shown in Fig. 7. Variations in the exact polyethylene thickness and diameter of the holes for the ^{3}He detectors within fabrication tolerance are additional factors affecting moderation that have not been considered here. Experimentally the detector response normalization factor, k_2 (Menlove et al. 1990), is intended to account for these slight fabrication differences between detectors built using the same design.

Active AmLi(α,n)	HDPE ρ 0.94 g/cm^3	HDPE ρ 0.945 g/cm^3	HDPE ρ 0.955 g/cm^3	HDPE ρ 0.96 g/cm^3	Variation between max/min
ΔDoubles*	-1.35%	-0.63%	0.76%	1.29%	2.64%

Table 5. Percent differences relative to 0.95 g/cm^3 for simulated count rates using various polyethylene densities ranging 0.94-0.96 g/cm^3 for short fuel simulation with fuel enriched 3.1995 wt% ^{235}U

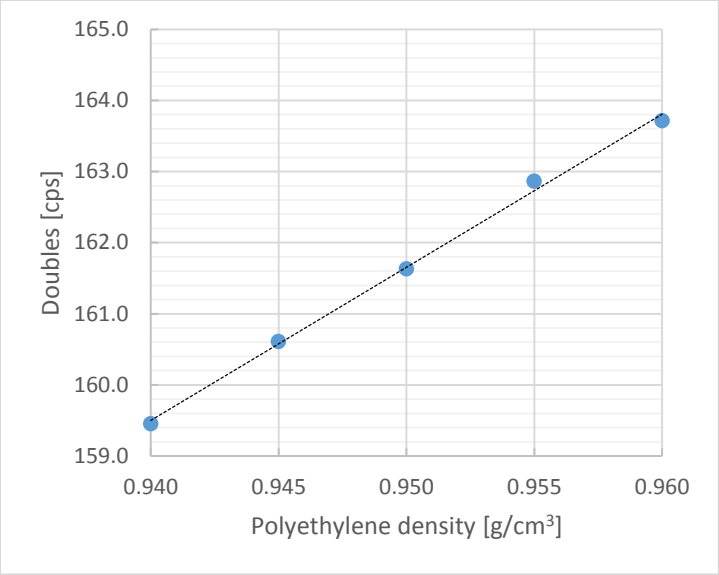

Figure 7. Simulated active Doubles rate as a function of polyethylene density (linear line of best fit added to guide the eye)

1.5 Sensitivity of passive simulation results to (α,n) spectra

The sensitivity of both active and passive response variations resulting from the choice of simulated (α,n) neutron energy spectra is of interest. For passive measurements the (α,n) source is mainly driven by the 4.76 MeV ^{234}U alpha decay particles interacting with ^{17}O (exothermic) or ^{18}O (0.847 MeV threshold), however lesser alpha emitting U isotopes have a minor effect as for example in 3.2% enriched fuel the mean alpha energy is 4.72 MeV. As a general approximation the neutron spectra is determined here by averaging the intensity weighted spectra measured from 4.5 MeV and 5 MeV alpha particles impinging on UO_2 targets from Jacobs and Liskien (1983). The averaged (4.5 MeV and 5 MeV) spectra is also show extrapolated to 0 from 0.3 MeV as there are larger uncertainties at low energies resulting from effects including low intensity, uncertainty in detector efficiency, and thermal neutron room return. The extrapolated spectra used the intensity weighted spectra measured from 4.5 MeV and 5.0 MeV alpha particles impinging on UO_2 targets and then extrapolated to 0 from 0.25 MeV while maintaining a constant cumulative probability of 1 to maintain normalization consistent with all spectra in Fig. 8. Each of the four spectra used for the UO_2 (α,n) distributions are shown in Fig. 8, with the corresponding mean neutron energies listed in Table 6. There is a relatively small difference between the 4.5 MeV and 5 MeV distributions, however if the true spectrum best approximated by the average and extrapolated to 0 than other spectra are too soft.

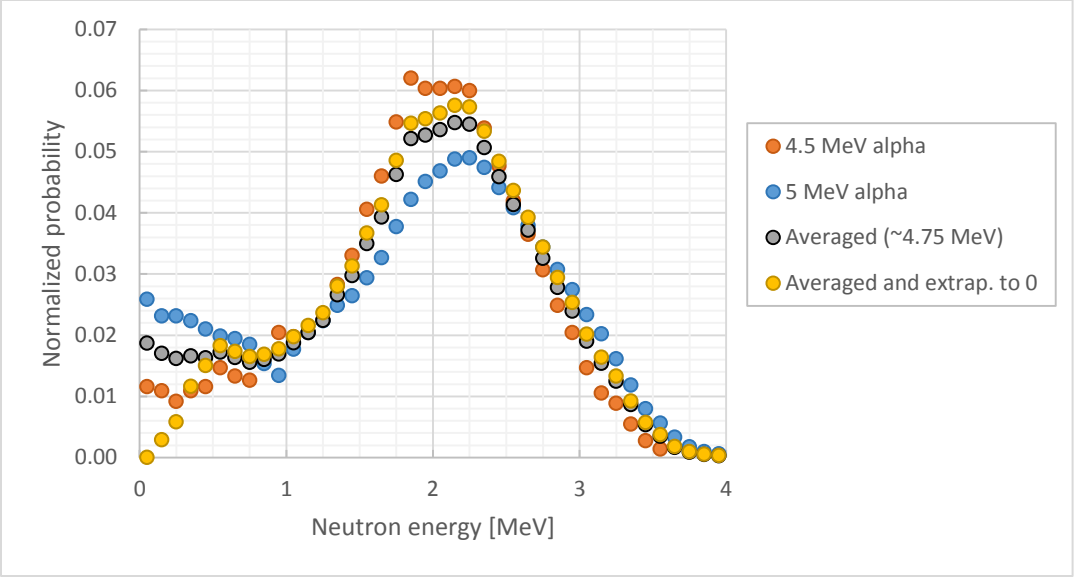

Figure 8. Various neutron energy distributions for UO_2 (α,n) based on Jacobs and Liskien (1983) (each spectra normalized to 1 and reported in MCNP usable format in Appendix A)

Alpha particle energy	Mean neutron energy [MeV]
5 MeV	1.86
4.5 MeV	1.89
Average (5 and 4.5 MeV)	1.88
Averaged and extrapolated to 0	1.97

Table 6. Mean neutron energies corresponding to the distributions in Fig. 8

Simulated count rates for the short fuel assembly (EC Curto) using each of the spectra are summarized in Table 7. Variations are compared both between the 4.5 MeV and 5 MeV alpha spectra and from all four simulated options because extrapolating to 0 makes a significant difference and may not be an appropriate modification (it is included in the study as indication of potential systematic uncertainty).

Passive (α,n) source	**4.5 MeV**	**5 MeV**	**Average**	**Average & extrapolated to 0**	Difference between 4.5 MeV/5 MeV	Difference between max/min
Doubles [s^{-1}]	0.287	0.289	0.287	0.284	0.60%	1.59%

Table 7. Percent difference values for simulated Doubles rate using various UO_2 (α,n) spectra for simulations of short fuel assembly (EC Curto) with fuel enriched 3.1995 wt% ^{235}U

1.6 Active simulation variations resulting from choice of AmLi spectra

Traditionally all active collar measurements conducted by the IAEA have used AmLi sources to interrogate ^{235}U in the fuel. It has been established that variations in source fabrication and contamination affect the microstructure of source materials, altering the emergent spectra slightly

between different AmLi sources. Unfortunately, it is difficult to determine the expected spectra for a given source as most AmLi sources in use have outlived documentation and knowledge of specific fabrication details (matrix materials, chemical compositions, etc.). Factors that alter the neutron spectra are inclusion of either O or OH as part of Li compounds, variations in bulk density, and variations in particle size due to the ball mill used, which is also a point during production where contamination such as Be is introduced if a given mill is used for fabrication of multiple types of sources. If Be or O are present within the AmLi source (α,n) reactions occur producing neutrons with notably higher energies. The variations in material density and particle size affect spectra and neutron yield as they define the energy loss and probability of an alpha particle reaching a target Li, O or Be atom.

Instrument response was simulated for a set of 19 AmLi spectra generated from semi-empirical and theoretical calculations and direct experimental measurements. These simulated spectra simulated were corrected back to the initial AmLi spectra by Weinmann-Smith (2017), with the exception of the Obninsk (emergent) spectra (Rinard and Menlove 1998; Rinard 2011; Croft et al. 2011) and those semi-empirical and theoretical spectra reported as initial spectra. The correction of Weinmann-Smith (2017) from emergent to initial spectra was conducted as an iterative process where the initial spectra is perturbed and simulated within the reported (or approximated) source encapsulation until the neutron spectrum emergent from the surface of the source was consistent with the experimentally measured spectra. The complete set of simulated spectra are reported both as the initial launch and emergent spectra where appropriate in Appendix B.

The response variations are summarized in Fig. 9, where Doubles and Singles are reported normalized per source neutron. Overall the Doubles standard deviation of 0.76% is small relative to the 12% standard deviation in the mean energy reported in Table 8. The Doubles response varies up to 3% depending on what spectra is used, which is large compared to the ~1% experimental uncertainties in Table 3. This suggests that scaling the simulated active Doubles conducted using the Obninsk emergent spectra throughout all other sections of this work up by ~1% to better agree with experimental results could be appropriate, however no scaling was applied in this report. Finally, by comparing the initial and emergent Obninsk spectrum (Rinard and Menlove 1998; Rinard 2001; Croft et al. 2011) the correction for perturbations from the source encapsulation appear to have minor effects on detector response.

The bounding results in Fig. 9 for the Doubles correspond to the SGTS1 and SGTS2 spectra (Beddingfield 2016). These spectra were respectively based on benchmark measurements of Singles and Doubles for Monsanto and Gammatron sources. The measurements were conducted in both the UNCL and AWCC, then simulated energy responses were used to create least squares optimized spectral fits. These results support the conclusions of Weinmann-Smith et al. (2017) where it is suggested that source-specific neutron spectra may be useful.

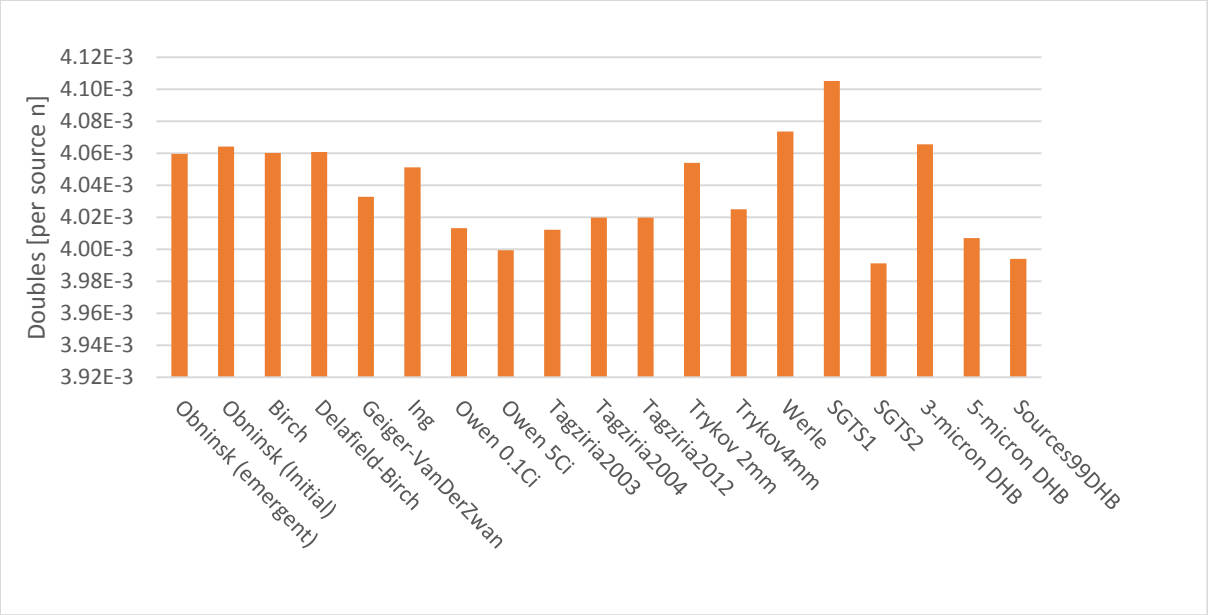

Figure 9. Active Doubles per source neutron for various measured and computed (α,n) spectra with EC Curto (all measured emergent spectra were corrected by RWS back to the initial spectra using MCNP)

Doubles are related to fission neutron production and are directly proportional to the net multiplication, defined here as the average number of neutrons produced per initial AmLi source neutron. This results in similar trends for the Doubles and net multiplication in Figs. 9 and 10, and the Doubles plotted as a function of net multiplication in Fig. 11 illustrating the correlation directly.

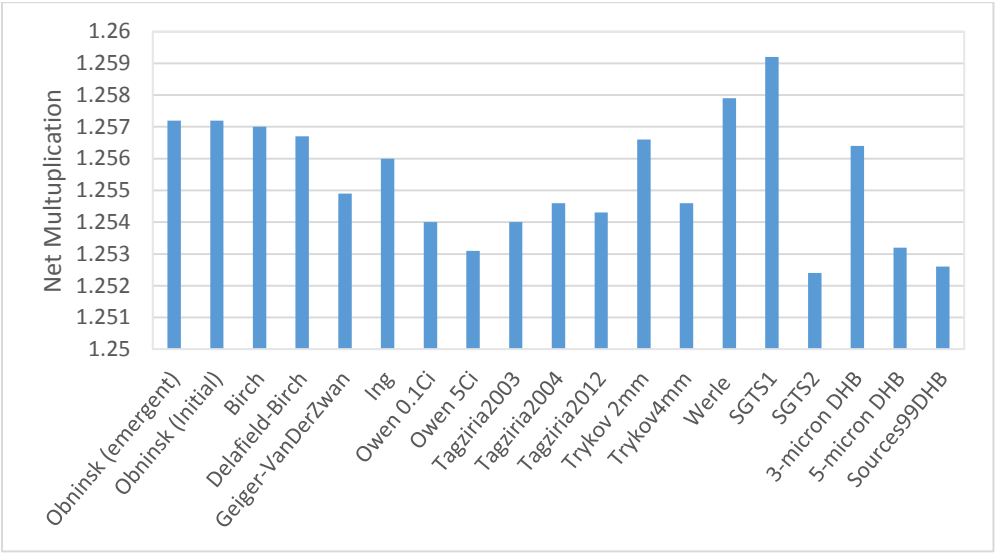

Figure 10. Net multiplication for each of the AmLi spectra simulated with EC Curto (note variation appears large due to suppressed origin and narrow net multiplication range)

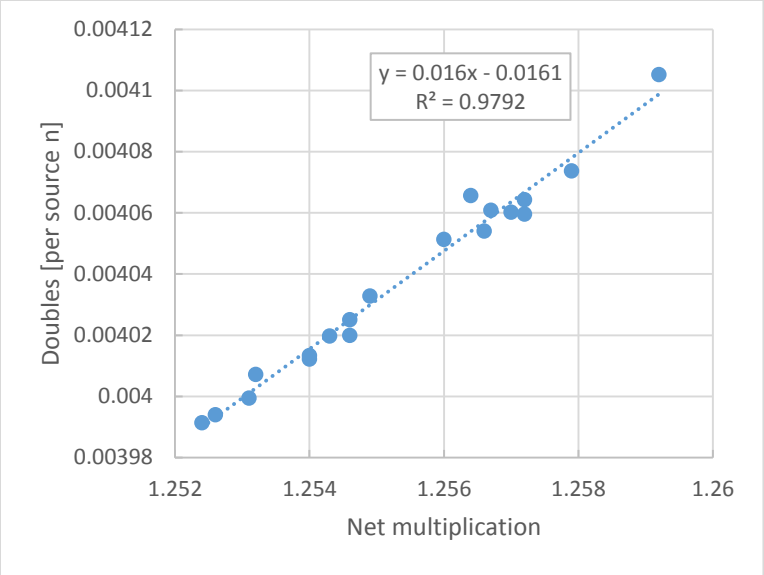

Figure 11. Doubles as a function of net multiplication for simulations with EC Curto

AmLi spectra	Mean energy [MeV]	Net Mult	Doubles [normalized]
Obninsk (emergent) (Rinard and Menlove 1998; Rinard 2011; Croft et al. 2011)	0.492	1.257	1.006
Obninsk (initial) (Rinard and Menlove 1998; Rinard 2011; Croft et al. 2011)	0.495	1.257	1.007
Birch (Birch et al. 1984)	0.447	1.257	1.006
Delafield-Birch (Delafield and Birch 1989)	0.474	1.257	1.006
Geiger-VanDerZwan (Geiger and van der Zwan 1971)	0.537	1.255	0.999
Ing (Ing et al. 1981)	0.488	1.256	1.003
Owen 0.1Ci (Owen et al. 1982)	0.547	1.254	0.994
Owen 5Ci (Owen et al. 1982)	0.577	1.253	0.991
Tagziria2003 (Tagziria et al. 2003)	0.481	1.254	0.994
Tagziria2004 (Tagziria et al. 2004)	0.556	1.255	0.996
Tagziria2012 (Tagziria and Looman 2012)	0.558	1.254	0.996
Trykov 2mm (Trykov et al. 1997)	0.467	1.257	1.004
Trykov4mm (Trykov et al. 1997)	0.533	1.255	0.997
Werle (Werle 1970)	0.435	1.258	1.009
SGTS1 (Beddingfield 2016)*	0.455	1.259	1.017
SGTS2 (Beddingfield 2016)*	0.605	1.252	0.989
3-micron DHB (Beddingfield 2016)*	0.549	1.256	1.007
5-micron DHB (Beddingfield 2016)*	0.695	1.253	0.993
Sources99DHB (Beddingfield 2002)*	0.584	1.253	0.989
Standard deviation	**12.0%**	**0.151%**	**0.759%**

Table 8. Summary of AmLi spectra response characteristics using the UNCL where normalized Doubles have been divided by the mean Doubles rate including all 19 spectra (*Information on privately communicated Beddingfield spectra included in Appendix B)

Following from the minor variations in the induced fissions the die-away characteristics also appear nearly unaffected by the different energy distributions in Fig. 12 (a). The slight differences are made more apparent in Fig. 12 (b) where the relative percent difference between the best fit line generated from all 19 die-away data sets and each given data set is shown, however even in this case the differences are generally small between the spectra. The mean die-away fits over the 4.5 to 44.5 μs range of the RAD are 66.01 μs ± 0.5% (where 66.01 μs is both the average of all die-away times and the die-away time obtained when RAD of all simulated spectra are fit together, and ±1σ is the relative standard deviation assuming each simulated die-away is an equally valid estimate), with fits over the full 4.5 to 204.5 μs range showing greater consistent at 73.76 μs ± 0.1%, albeit the fits over the full range are likely less accurate.

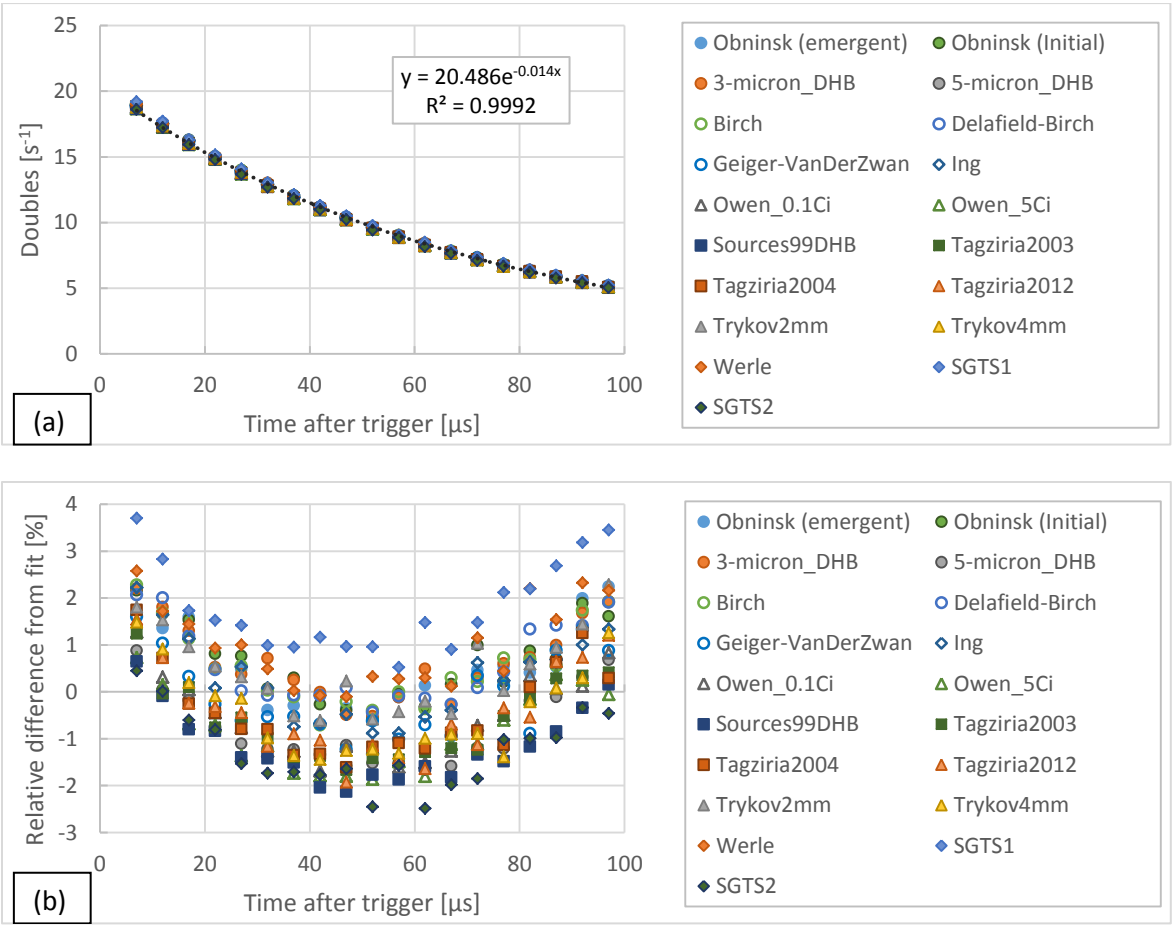

Figure 12. (a) RAD shown for each of the simulated AmLi source spectra simulated in the UNCL with a 3.1995% enriched fuel assembly (best fit line corresponds to all simulated spectra together), and **(b)** relative difference between each individual spectra and the best fit line corresponding to data from all 19 simulated spectra

1.7 Sensitivity to AmLi Source Contamination

Previous studies on the characterization of AmLi sources (Ravazzani et al. 2001; Weinmann-Smith et al. 2017) have noted contributions from Be and O (α,n) reactions and estimated relative

contributions. The Li matrix composition is generally not well known, but based on the measured AmLi spectra and potentially matrixes consisting of LiH, Li_2O or LiOH and the potential for Am to be present as AmO_2 there is a reasonable probability that O(α,n) reactions will be present in a given AmLi source (Croft et al. 2011). The relative contribution of O(α,n) reactions was estimated to range 6.7% to 8.1% over a large sample set of 17 AmLi including: Gammatron-C (3), Gammatron-N (8); and Monsanto Research Corporation (6). As it was noted that the relative lithium and oxygen contributions may be incorrect, the O(α,n) fractional yield is considered here to potentially range 4% to 9% of the total neutron emission.

The study of Ravazzani et al. (2001) is a more precise contamination measurement as the Be was quantified directly using the 4438 keV Be gamma emission shown in Fig. 13 along with the several other Am based (α,n) sources with the characteristic gamma emissions labelled (note many of these emissions are affected by Doppler broadening). It should also be noted that gamma measurements of Weinmann-Smith et al. (2017) did not find Be, demonstrating that this may be source specific, as opposed to manufacturer specific, as it could be dependent on glovebox contamination present during AmLi preparation. Ravazzani et al. (2001) measured a different set of 17 AmLi sources, with the relative Be(α,n) contributions reported to range 0.3% to 3% of the neutron emission rates for the 4 sources where Be emission fraction was reported. The factor of 10 variation in this limited sample size shows that there is a wide range in possible contamination. It is assumed, but not explicated stated, that Be concentrations were below the limit of detectability for the remaining 11 AmLi sources as it was reported that gamma measurements were conducted for 15 of the 17 sources. A gamma spectroscopy measurement was made in Aug. 2019 using 1 ½ x 1 ½ $LaBr_3$ detector to determine whether the AmLi source used in Brazil, MRC-118, has significant Be contamination (this has yet to be analyzed).

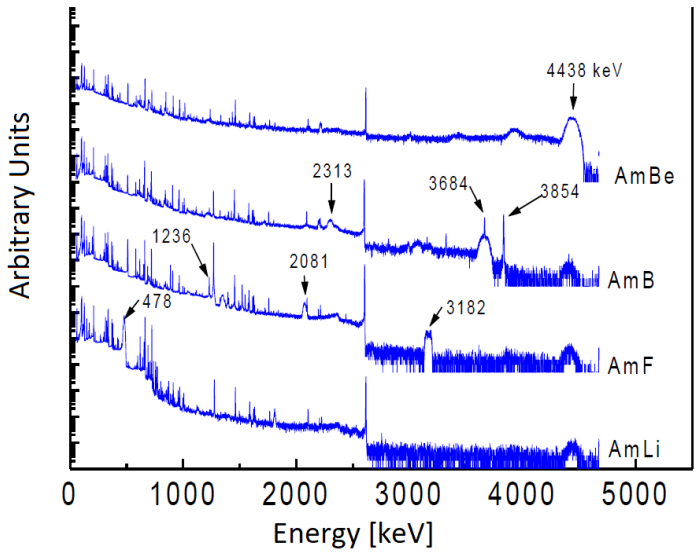

Figure 13. Comparison of typical gamma spectra, taken with a coaxial detector, for a ^{241}AmBe(α,n), ^{241}AmB(α,n), ^{241}AmF(α,n), and ^{241}AmLi(α,n) neutron source (from Ravazzani et al. 2001)

When considering the effects of various relative contributions of the Li, O and Be (α,n) reactions the difference in the neutron energy distributions need to be considered. The distinct AmLi, AmO and AmBe spectra are shown in Fig. 14 together to illustrate the difference. Although actual AmLi(O) or AmLi(Be) spectra are not simply equivalent to the summation of individual AmLi and AmO or AmBe spectra due to alpha slowing down effects in the matrix, the summation approach is used here as an illustrative approximation of the effects on spectral shape. The experimental AmLi spectra of Tagziria and Looman (2012) is used in this sub-section as it is an example of a clean AmLi spectra that does not contain neutrons from O or Be as it has a maximum neutron energy of approximately 1.5 MeV, corresponding to approximately half of the maximum energy of the broad AmO peak. The AmBe spectra is most unique as it peaks at 3.75 MeV and extends up to 12 MeV, with the much higher neutron energies likely to result in a reduced number of ^{235}U induced fissions, an increased number of ^{238}U fast fissions and a reduction in the total neutrons detected.

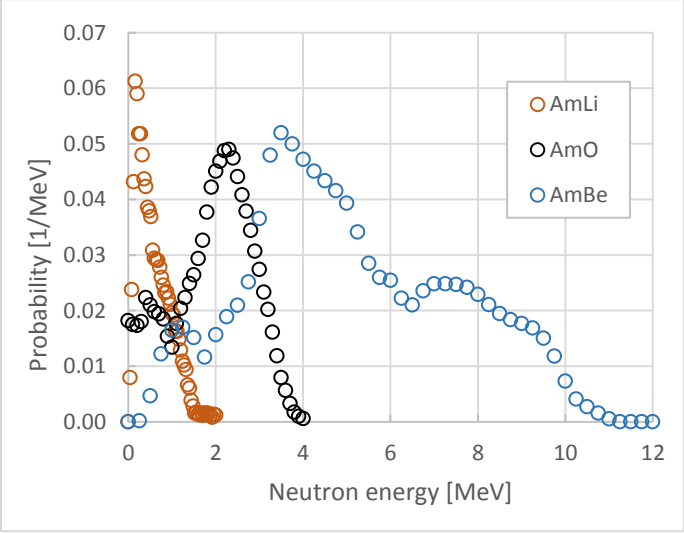

Figure 14. Neutron spectra resulting from (α,n) reactions in AmBe (SOURCES 4A (Madland et al. 1999)), AmLi (Tagziria and Looman 2012), AmO (averaged 5 MeV and 5.5 MeV alpha particles impinging on O from Jacobs and Liskien 1983) (note each spectra is normalized to 1, but with different number of energy bins: AmBe (48), AmLi (50), AmO (48))

The effect of Be contamination on detector efficiency is reviewed precisely with the following formalism. Let S_{Li} and S_{Be} be the neutron emission rates inside the AmLi source material. Ignoring multiplication and other factors to first order we can express the dead time and background corrected net Singles counting rate as follows

$$T = \varepsilon_{Li} \cdot S_{Li} + \varepsilon_{Be} \cdot S_{Be} = \varepsilon \cdot S$$

Where ε is the average efficiency and S is the total neutron emission rate which would be determined using a detector with an energy independent efficiency. Re-arranging this overall efficiency can be determined as

$$\varepsilon = \varepsilon_{Li} \cdot \left[S_{Li}/(S_{Li} + S_{Be}) + \frac{S_{Be}/(S_{Li} + S_{Be})}{\varepsilon_{Li}/\varepsilon_{Be}} \right]$$

Ravazzani et al. (2001) report that the Gammatron produced source labelled ANHP-C282 has a fractional yield from Be of 3% (sources ANHP-N086, ANHP-N008 and ANHP-N253 respectively are reported to have fractional Be yields of 0.3%, 0.5% and 0.7%). For the JCC-12, JCC-14, and MPC-01 neutron counters used in that study the efficiency ratio $\varepsilon_{Li}/\varepsilon_{Be}$ is about 1.62. Inserting the maximum and minimum Be relative yield values we find

$$\varepsilon \approx \varepsilon_{Li} \cdot \left[0.97 + \frac{0.03}{1.62} \right] = \varepsilon_{Li} \cdot [0.989]$$

$$\varepsilon \approx \varepsilon_{Li} \cdot \left[0.997 + \frac{0.003}{1.62} \right] = \varepsilon_{Li} \cdot [0.995]$$

Given an approximate ε_{Li} of 5.75% from simulation of the Tagziria and Looman (2012) AmLi spectra, the presence of 3% and 0.3% Be fractional yields respectively reduce the overall efficiency to 5.69% and 5.72%. Considering other analysis here showing that trends differ significantly between the Singles and Doubles the effects of this on the coincidence count rate is considered here.

The three neutron spectra corresponding to Li, O and Be (α,n) neutrons were simulated independently for the reference EC Curto assembly and two experimental BP rod cases (A1 and A2). These simulations include two approximations: (1) while the source spectra were altered to reflect the O(α,n) and AmBe neutron energies, in these cases the material which they were emitted from was still AmLi, which does not include the ^{9}Be(n,2n) reaction contribution; and (2) independent AmLi, O(α,n) and AmBe are used as approximations that are not precisely equivalent to the spectra seen when O and Be are within an AmLi source.

These simulated rates are compared against the measured results in Table 9 to illustrate the potential extreme variations. The highest Doubles rates are seen using the AmLi source, which follows expectations as neutrons from the softer distribution are readily thermalized to induce fissions in ^{235}U, while the harder O(α,n) and especially AmBe spectra are less likely to induce fission. Overall, the simulated count rate variations are relatively small for the EC Curto assembly containing only fuel, where the maximum variation is 1.1%. For the assemblies containing poison rods the variation is more than twice as much at 3.0%. Resulting effects on the calculated ^{235}U linear density are then shown with Table 10, where the maximum variation between simulations of EC Curto, A1 and A2 are respectively 2.24%, 6.67%, 6.85%. This demonstrates that AmLi source characterization is important if simulations are to be used in place of experimental measurements. The fact that contamination appears to have a greater effect on the fuel assemblies containing poison rods also suggests that a simple source normalization may not be sufficient to fully account for effects of the harder AmLi spectra that result from contamination. This could be demonstrated by simulating a full set of cases with multiple AmLi spectra corresponding to different types and degrees of contamination to determine what the

overall effect is and if a general correction is a feasible solution. As a harder AmLi spectrum is more likely to induce fission in ^{238}U through the fast interrogation flux the current practice of scaling by neutron emission rates alone is unlikely to fully account for resulting variations.

AmLi Source components	Doubles rate [s^{-1}] – by fuel assembly type		
	EC Curto (3.1995%)	A1	A2
Experimental measurement with MRC-118	163.3 ± 1.2	160.8 ± 1.2	154.5 ± 1.2
100% AmLi	159.31 ± 0.14	154.04 ± 0.14	151.71 ± 0.14
5% O(α,n) + 95% AmLi	158.36 ± 0.15 (4.43% from O)	153.31 ± 0.15 (4.55% from O)	150.89 ± 0.14 (4.48% from O)
9% O(α,n) + 91% AmLi	157.60 ± 0.16 (8.01% from O)	152.73 ± 0.15 (8.22% from O)	150.24 ± 0.15 (8.10% from O)
0.3% AmBe + 99.7% AmLi	159.22 ± 0.14 (0.25% from Be)	153.58 ± 0.14 (0.25% from Be)	151.26 ± 0.14 (0.25% from Be)
3% AmBe + 97% AmLi	158.44 ± 0.15 (2.47% from Be)	149.42 ± 0.14 (2.56% from Be)	147.16 ± 0.14 (2.59% from Be)

Table 9. Count rate variations resulting from source contamination using the spectra: AmBe (SOURCES 4A, Madland et al. (1999)), AmLi (Tagziria and Looman 2012), O(α,n) (approximated from average of 5 MeV and 5.5 MeV alpha particles impinging on UO_2 from Jacobs and Liskien (1983))

AmLi Source components	Calculated ^{235}U linear density [g/cm] – by fuel assembly type		
	EC Curto (3.1995%)	A1	A2
Experimental measurement with MRC-118	44.28	52.31	51.80
100% AmLi	42.02	47.39	49.65
5% O(α,n) + 95% AmLi	41.50	46.89	49.04
9% O(α,n) + 91% AmLi	41.09	46.50	48.56
0.3% AmBe + 99.7% AmLi	41.97	47.08	49.31
3% AmBe + 97% AmLi	41.54	44.33	46.36
Declared ^{235}U linear density [g/cm]	**44.52**	**58.89**	**58.03**

Table 10. Count rate variations resulting from source contamination (AmBe (SOURCES 4A, (Madland et al. 1999)), AmLi (Tagziria and Looman 2012), O(α,n) (approximated from average of 5 MeV and 5.5 MeV alpha particles impinging on UO_2 from Jacobs and Liskien 1983)

Throughout the rest of this report the default AmLi spectra used was the experimentally measured Obninsk spectra, chosen due to good consistency with experimental results in previous studies (Rinard and Menlove 1998; Rinard 2001; Croft et al. 2011). Comparing the Tagziria and Looman (2012) AmLi spectra to the Obninsk and the AmO_2 spectra in Fig. 15 makes it clear that the Obninsk contains an AmO_2 component. Other notable distinctions include the most probably AmLi energy in the Obninsk occurring at a 0.4 MeV as opposed to the lower value of 0.2 MeV from the Tagziria and Looman (2012) measurement. Due to the slight spectra difference in both the AmLi and AmO_2 portions of the Obninsk spectra from the two component spectra it is not

possible to reconstruct the spectra from its components (specifically the dip between 1.3 and 1.5 MeV in the Obninsk is not present in the other spectra). The differences may partially be due to energy loss of the alpha particles as they pass through O prior to reaching Li in the actual source affecting the resulting neutron spectra. It is also probable that different AmLi source spectra have inherent distinctions resulting from the specific particle size, molecular form, and potential contamination and packing density. The sensitivity of the unfolded spectra to the chosen a priori is also a factor that is generally difficult to evaluate in reported spectra. These appear to be in line with the conclusions drawn from the studies of Weinmann-Smith et al. (2017) and Ravazzani et al. (2001). The effort towards source specific spectra recommendations for use in simulations as presented in Weinmann-Smith et al. (2017) may be expanded to more sources as they appear to be required at minimum based on manufacturer and potentially specific to individual sources. When considering the use of a single spectra the Obninsk does appears to be a reasonable choice for Gammatron C and N-series sources, as well as the Monsanto Research Corporation (MRC) sources analyzed by Weinmann-Smith et al. (2017). This supports the decision to use the Obninsk spectra in this work as the source used by CNEN is an MRC source.

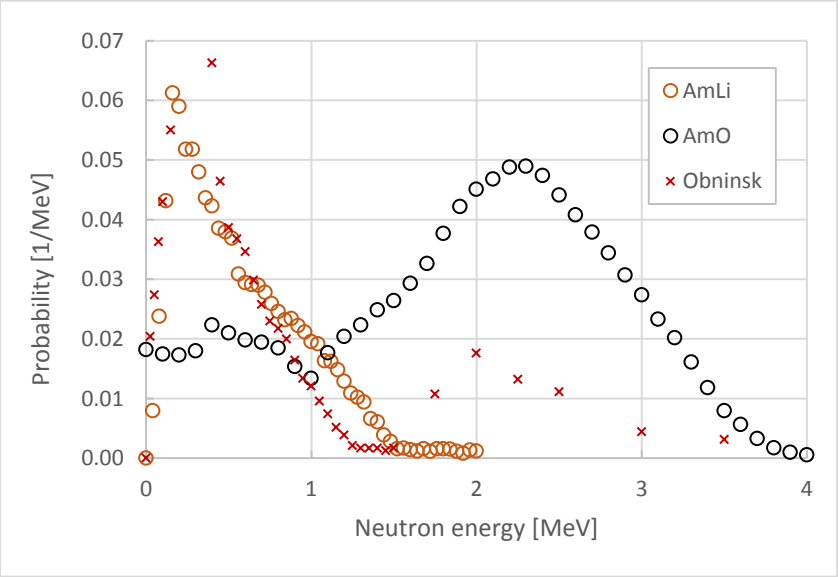

Figure 15. Neutron spectra resulting from (α,n) reactions in AmLi (Tagziria and Looman 2012), O(α,n) (approximated by averaging spectra from 5 MeV and 5.5 MeV alpha particles impinging on UO_2 from Jacobs and Liskien 1983) and the Obninsk spectrum which includes components of both Li and O (α,n) (Rinard and Menlove 1998; Rinard 2011; Croft et al. 2011)

1.8 Source position within tungsten pot

The AmLi source generally has a slightly smaller diameter than the inner diameter of the tungsten pot it is contained within. This results in there being a slight angular dependence on the emission rate dependent on the specific configuration of a given source. A set of experimental measurements were conducted using MRC-118 rotating at 45 degree increments, where 0 degrees was indicated by marking the AmLi source and detector in the direction facing away from the fuel assembly. The results are reported in Table 11 and show a 34 cps variation in the

Singles depending on the angle, while the Doubles remain at 0 within uncertainty for all angles. The fact that there is variation is not necessarily an issue as long as effort is made to maintain a consistent measurement geometry. For the results presented here the AmLi source was consistently kept in the 0° position (note that the position is relative to an arbitrary mark made on the AmLi source container). Unexpected variations in the Singles during the AmLi source normalization measurement could also be used to indicate if there has been a shift of the source material within the tungsten, which could be verified by repeating the rotation measurements. An interesting follow-up would be to repeat this experiment with EC Curto inside the collar to evaluate effects on a well characterized fuel assembly to inform potential variation in measurement uncertainty if care is not taken during verification measurements (the ideal experiment would be to repeat this exercise with a number of the AmLi sources used in UNCL measurements on the same fuel assembly).

AmLi Angle	Singles [cps]	Uncertainty [cps]*	Doubles [s^{-1}]	Uncertainty [cps]*
0°	1871.350	4.348	0.988	2.133
45°	1880.430	4.355	-1.072	2.148
90°	1890.000	4.366	-1.242	2.154
135°	1904.980	4.391	2.198	2.172
180°	1904.990	4.383	-1.762	2.164
225°	1899.250	4.376	-1.452	2.158
270°	1892.990	4.376	1.888	2.155
315°	1874.72	4.348	-0.802	2.132
360°	1872.690	4.346	-0.352	2.132

Table 11. Count rate variation due to AmLi source rotation, where angle corresponds to clockwise rotation from the arbitrary reference position facing directly away from the fuel assembly within the collar (*determined in INCC)

1.9 Effect of tungsten AmLi shield

An additional factor was considered that is not a sensitivity factor in the same sense as the others considered here. The AmLi source is placed within a tungsten shield to reduce the gamma dose during handling and measurement, however it is possible that this unnecessarily reduces the count rates during measurements. A comparison of simulations with the tungsten replaced by lead of the exact same size, but using the lower lead density of 11.34 g/cm^3 instead of 19.3 g/cm^3 for tungsten (actual AmLi tungsten shields are not constructed from elementally pure materials, but are generally alloys of some sort for machinability, so actual tungsten density may be closer to 18 g/cm^3). This change of shielding material was found to increase the Doubles rate from 161 s^{-1} to 173 s^{-1}, a change of 7.2% (note that the Doubles rates with tungsten at a density of 19.3 g/cm^3 and 18 g/cm^3 are 163.34 s^{-1} and 161.33 s^{-1}, respectively showing that a slight change in density has a negligible effect on the observed Doubles rate). This appears to be a considerable change and may warrant further assessment. There are also potential drawbacks of making this type of change as the scaling of neutron emissions relative to MRC-95 may need to be reconsidered, if the different sources have slightly different spectra that could affect the viability

of the standardized corrections currently applied. The dispersion of AmLi sources globally would also make it a challenge to change all AmLi sources using for UNCL measurements over. The practical gain in slightly reduced inspectorate measurement time from the increased Doubles rate needs to be considered along with the time and effort involved.

1.10 Overall uncertainty

The contribution of all sources of uncertainty analyzed in previous sections are considered here together to estimate the uncertainty for simulations of the short fuel assembly for comparison with measurements of full length fuel assemblies. Factors omitted from the summary of Table 12 are: (1) Be contamination as it is not known to be present within the MRC-118 source that is of primary interest here, and (2) uncertainty in the correction factor coefficients used to relate the Doubles rate to the assay ^{235}U linear density (these correction factors are discussed in Part II of this report). A gamma measurement of MRC-118 could be used to evaluate whether Be is present and the amount; such measurements are described in Ravazzani et al. (2001) using the 4438 keV (Doppler broadened) peak. As uncertainty estimates are not provided for all of the correction factor coefficients and the relative impact of a given coefficient is dependent on fuel characteristics it is difficult to accurately gauge this effect. Each uncertainty estimate from the sources evaluated in this section are now briefly summarized.

As the fuel assembly position within the collar is not precisely controlled the mean relative error in the Doubles from 0.25 cm translations in all x and y directions relative to a perfectly centered fuel assembly was taken to be 1σ [translations included: (+0.25 cm,0), (-0.25 cm,0), (0,+0.25 cm), (0,-0.25 cm), (+0.25 cm,+ 0.25 cm), (-0.25 cm,+ 0.25 cm), (+0.25 cm,- 0.25 cm), and (-0.25 cm,- 0.25 cm)].

The simulation of the active length of the fuel as 80.3 cm instead of the full length (300 cm) was approximated by the difference between the simulations using an active length of 80.3 cm and an active length of 243 cm (UNCL length +100 cm above and below). This is believed to be reasonable as often measurements of a full fuel assembly are not taken at the center of the fuel assembly, which means that the difference used here may occur it is likely conservative.

The variation in the simulated Doubles corresponding to polyethylene density ranging 0.94-0.96 g/cm^3. This was taken to be the 2σ uncertainty based on the fact that in practice the density of commercial polyethylene is relatively consistent.

The uncertainty resulting from the choice of simulated AmLi spectra was taken to be the standard deviation of the Doubles response over all of the simulated spectra. Although a better estimate of this might be obtained by investigating MRC-118 further to determine if only a smaller subset of possible spectra that best correspond to Monsanto AmLi sources were reasonable this conservative approximation considers all available possibilities.

Finally, the source of uncertainty here that is best described here as it has been directly studied is the uncertainty in the MRC-118 emission rate. The uncertainty in the neutron emission rate of MRC-118, denoted as NPS_{118}, is determined using

$$\frac{\sigma(MRC118)}{MRC118} = \sqrt{\left(\frac{\sigma\left(\frac{NPS_{118}}{NPS_{95}}\right)}{\frac{NPS_{118}}{NPS_{95}}}\right)^2 + \left(\frac{\sigma(NPS_{95})}{NPS_{95}}\right)^2}$$

where $\frac{NPS_{118}}{NPS_{95}} \pm \sigma(\frac{NPS_{118}}{NPS_{95}})$ and $NPS_{95} \pm \sigma(NPS_{95})$ respectively correspond to 1.2207 ± 0.0017 and 32737 ± 1.12%. The MRC-95 emission rate is based on a combination of JRC/NPL (S. Croft), LANL (H.O. Menlove) and NIST measurements, which respectively determined the neutron emission rate on February 14, 2014 to be 32672 ± 1%, 32802 ± 1.1%, and 32800 ± 3%, (Croft 2018).

Considering the combined sources of uncertainty the polyethylene density and AmLi neutron emission rates are the dominating factors that limit the accuracy of simulations. Of these polyethylene density is likely the most readily determined. Although it may be difficult for the current detector as disassembly is not trivial, several options are possible during the fabrication process of new detectors. Density could be evaluated via gamma transmission measurements or a combination of careful mass and either spatial measurements of water displacement. If reference detector specific values were documented simulation uncertainty would be significantly reduced.

Component	Estimated uncertainty (1σ)
Fuel assembly position	0.20%
Fuel assembly length	0.20%
Polyethylene density	1.32%
AmLi spectra	0.76%
AmLi neutron emission rate	1.13%
Overall uncertainty	1.91%

Table 12. Total uncertainty estimate for simulated net Doubles (note calculated ^{235}U linear density also includes correction factor uncertainties)

Several of these components are also applicable when considering uncertainty in experimental measurements. The fuel assembly length is again included to account for variation resulting from the collar along the length of the fuel, which is expected to show a similar degree of variation. Any variation in polyethylene density for a given detector should in principle be accounted for by the detector response correction factor, k_2.

If a given AmLi source has Be contamination it has been estimated previously to have about a 5% effect on instrument response (Ravazzani et al. 2001), which is consistent with the magnitude of variations reported here (see Table 9). This is not included in the analysis here as it appears

that generally the contamination either is or is not present based on the AmLi source in use, however when present this will create a bias greater than all estimated sources of uncertainty.

Aside from the AmLi neutron emission rate, the main secondary contribution is statistical uncertainty, where the values here were taken from the average uncertainty from the measurements of the A1 and A2 fuel assemblies using 30×30 second cycles in active mode and 15×30 second cycles in passive mode (total 22.5 minutes or approximately 25 minutes including the transition from passive to active mode). In principle longer measurements could be taken to reduce this, however the AmLi emission rate will remain the dominate source of uncertainty.

Component	Estimated uncertainty (1σ)
Statistical (includes passive and active)	0.76%
Fuel assembly position	0.20%
Fuel assembly length	0.20%
AmLi neutron emission rate	1.13%
Overall uncertainty	1.39%

Table 13. Experimental uncertainty estimate for active net Doubles (note: calculated U-235 linear density also includes correction factor uncertainties)

Two additional sources of uncertainty not assessed here include the effect of room background on measurement uncertainty, and the directional variation in emissions from AmLi sources. Non-isotropic emissions have been shown to have just under 1.5% effect on the Singles count rate, however this may not correspond to an equivalent degree of Doubles variation and is also likely to be source dependent (Looman et al. 2001). For measurements in Brazil this has been mitigated by marking the AmLi source so that it is always in the same position within the source holder, however in simulations the source emissions are approximated as being isotropic. This should effectively give an average of the emission rates across all angles and is very roughly estimated to effect the simulated signal by ~0.5-0.75%.

All uncertainties described correspond to the Doubles rates, however during verification measurements the measured observable (Doubles) is input into the inverted calibration curve to determine the ^{235}U linear density. In this case the uncertainty in the calibration curve and the correction factors discussed in the following section need to be considered to understand the uncertainty in the quantity of interest. However, for verification measurements of commercial Angra fuel assemblies containing Gd rods error in the calculated ^{235}U linear density is often >6σ using the overall uncertainty value of 1.39% in Table 13. For this reason updated coefficients for the poison rod correction are being considered.

References

[Awschalom and Sanna 1985]
M. Awschalom and R.S. Sanna, Applications of Bonner sphere detectors in neutron field dosimetry, Radiat Prot Dosim 10(1-4) 89-101(1985).

[Bairiot et al. 1995]
H. Bairiot, P. Chantoin, N.Z. Cho, A. Delbrassine, D. Farrant, G, Gündüz, M. Hron, V.D. Onufriev, V. Proselkov, B. Roulier, G. Sukhanov, M. Toba. Characteristics and use of uraniua-gadolinia fuels, Vienna, Austria, IAEA-TECDOC-844, 1995.

[Sources99]
D.H. Beddingfield, "Application of the Sources Code in Nuclear Safeguards" Proceedings of American Nuclear Society 12th Biennial Topical Meeting of the Radiation Protection and Shielding Division, Santa Fe, NM, 2002.

[3-micron (DHB); 5-micron (DHB); SGTS1; SGTS2]
D.H. Beddingfield, AmLi spectra (3-micron, 5-micron, SGTS1, SGTS2), Private Communication, July 14th 2016.

[Birch]
R. Birch, L.H.J. Peaple, H.J. Delafield. Measurement of Neutron Spectra with Hydrogen Proportional Counters Part 1. Spectrometry System and Calibration United Kingdom Atomic Energy Authority Harwell Report, AERE-R 11397, 1984.

[Chadwick et al. 2006]
M.B. Chadwick, et al., "ENDF/B-VII.0: Next Generation Evaluated Nuclear Data Library for Nuclear Science and Technology", Nuclear Data Sheets, Vol. 107, Number 12, Dec 2006, UCRL-JRNL-225066 (2006).

[Croft 2018]
S. Croft, Yield of MRC-95 notes comparing HOM, NIST, JRC/NPL measured MRC-95 yields, Priv. Commun. Aug. 22 2018.

[Croft et al. 2011]
S. Croft, A. Favalli, M.T. Swinhoe, C.D. Rael, State of the Art Monte Carlo modeling of active collar measurements and comparison with experiment, Proc. 52nd Annual INMM Meeting, July 2011 Palm Desert, CA, USA.

[da Silva et al. 2011]
C.A.M. da Silva, R.B. de Faria, C. Pereria, A.L. Costa, A.F. Veloso, J.A.D. Salome, An evaluation of PWR cycle including burnable absorbers using MCNP –steady-state core simulation, 2011 International Nuclear Atlantic Conference –INAC 2011, Belo Horizonte, MG, Brazil, October 24-28, 2011.

[Delafield and Birch]
H.J. Delfield and R. Birch, Neutron Spectrometry Measurements with Large Volume Cylindrical Proton Recoil Counters Developed for Use in Radiological Protection United Kingdom Atomic Energy Authority Harwell report AERE-R 13103, 1989.

[Everaldo 2017]
Everaldo, National Nuclear Energy Commission (CNEN), Technical drawing of EC CURTO: EC ANG2 REDUZIDO CNEN-Collar Neutrons, Design Number: INB-DP-394.01, 28/11/2017.

[Favalli et al. 2018]
A. Favalli, M. Browne, S. Croft, M.S. Grund, G. Renha, An Example of International Collaboration: the Evolution of Active Neutron Interrogation Collar Methods for Modern Fresh Fuel Assemblies, IAEA Symposium on International Safeguards, November 2018 Vienna, Austria.

[Geiger and van der Zwan]
K.W. Geiger, L. van der Zwan, The neutron spectra and the resulting fluence-kerma conversions for AmLi and PoLi sources. Health Phys., 21 (1971), pp.120-123

[Grady et al. 2017]
D. Grady, E. Smith, K. Chand, M. Swinhoe, and J. Kulisek, "U-235/U-234 Ratio Behavior in Gas Centrifuge Enrichment Plants and Implications for Unattended Verification of UF6 Cylinders by Safeguards Inspectorates", Lawrence Livermore National Laboratory report: LLNL-TR-739009 (Livermore CA), 2017.

[IAEA 1995]
Characteristics and use of uraniua-gadolinia fuels, IAEA-TECDOC-844; Vienna, Austria; International Atomic Energy Agency, 1995.

[IAEA 1995]
HEU to LEU conversion and blending facility uf6 blending alternative to produce LEU UF6 for commercial use (1995) https://inis.iaea.org/collection/NCLCollectionStore/_Public/28/036/28036782.pdf

[Ing et al. 1981]
H. Ing, J.W. Cross, and J.B. Tymons, The spectrum of neutrons from a Pu-Li source Health Physics 40, 345-350 (1981).

[Jacobs and Liskien 1983]
G.J. Jacobs, and H. Liskien, Energy spectra of neutrons produced by α particles in thick targets of light elements, Ann. Nucl Energy, 10(10) 531-552, 1983.

[Madland et al. 1999]
D.G. Madland, E.D. Arthur, G.P. Estes, J.E. Stewart, M. Bozoian, R.T. Perry, T.A. Parish, T.H. Brown, T.R. England, W.B. Wilson, and W.S. Charlton. SOURCES 4A: A Code for Calculating (alpha,n), Spontaneous Fission, and Delayed Neutron Sources and Spectra. Los Alamos National Laboratory report: LA-13639-MS (1999).

[Menlove et al. 1985]
H.O. Menlove, M.A.S. Marzo, S.G. de Almeida, M.C. de Almeida, L.P.M. Moitta, L.F. Conti, J.R.T. de Paiva. In-Plant Test and Evaluation of the Neutron Collar for Verification of PWR Fuel Assemblies at Resende, Brazil. Los Alamos National Laboratory report: LA-10562-MS. Los Alamos, NM. 1985.

[Menlove et al. 1990]
H.O. Menlove, J.E. Stewart, S.Z. Qiao, T.R. Wenz, G.P.D. Verrecchia. Neutron collar calibration and evaluation for assay of LWR fuel assemblies containing burnable neutron absorbers. Los Alamos National Laboratory report: LA11965-MS (1990).

[Owens 0.1 and 5 Ci]
J.G. Owen, D.R. Weaver and J. Walker, Neutron Spectra from Am/f and Am/Li sources. Nuclear Data for Science and Technology Proc. Of the International Conf. on Nucl Data for Science and Technol., Antwerp, 6-10 Sept 1982. pp492-494

[Ravazzani et al. 2001]
A. Ravazzani, R. Jaime, M. Looman. B. Pedersen, P. Peerani, P. Schillebeeckx, M. Thornton, A. Foglio Para, V. Maiorov, Characterization of neutron sources by NDA. Proc. 23th Annual Symp. on Safeguards and Nuclear Material Management, Bruges, Belgium. ESARDA, Rep. EUR 1944 EN, ed. C. Foggi, JRC Ispra, Italy, 2001, pp. 181-191.

[Rinard and Menlove 1998]
P.M. Rinard, and H.O. Menlove, "Calibration of the IAEA Active Well Coincidence Counter for Measurements of the Bruce 'A' Unirradiated Booster Rods" Los Alamos National Laboratory Report: LA-UR-98-4362, 1998.

[Rinard 2011]
P.M. Rinard, Obninsk Russia IPPE, Priv. Comm. to Stephen Croft, 1st June 2011

[Tagziria2003]
H. Tagziria, N.J. Roberts, D.J. Thomas, "Measurement of the 241Am–Li radionuclide neutron source spectrum", Nucl. Instrum. Methods Phys. Res. A, 510 (3) (2003), pp. 346–356

[Tagziria2004]
H. Tagziria, H. Klein, B. Wiegel, B. Knauf, J. Wittstock, J. Zimbal, "Measurement and Monte Carlo Modelling of the JRC 241AmLi(α,n) source spectrum", Radiat. Prot. Dosim., 110 (1-4) (2004), pp. 129–134

[Tagziria 2012]
H. Tagziria, and M. Looman, "The Ideal Neutron Energy Spectrum of AmLi sources", Applied Radiation and Isotopes 2012.

[Trellue and Little 2008]
H.R. Trellue, R.C. Little. Release of New MCNP S(α, β) Library ENDF70SAB Based on ENDF/B-VII.0. memorandum - LA-UR-08-3628, 2008. [https://mcnp.lanl.gov/BUGS/la-ur-08-3628_endf70sab.pdf]

[Trykov2mm; Trykov4mm]
L.A.Trykov, V.A. Chernov, S.V. Rabochy. Investigations of AmO2–LiH neutron sources characteristics. Private Commun. 1997.

[Weinmann-Smith et al. 2017]
R. Weinmann-Smith, D.H. Beddingfield, A. Enqvist, M.T. Swinhoe. Variations in AmLi Source Spectra and Their Estimation Utilizing the 5 Ring Multiplicity Counter. Nuclear Instruments and Methods in Physics Research Section A, 2017. DOI: 10.1016/j.nima.2017.02.083

[Werle]
H. Werle. Spectrum measurements of Radioactive Neutron sources in the 10 keV to 10 MeV energy region with proton recoil proportional counters. Karlsruhe Report: KFK-INR-4/70-25, ORNL-tr-2415 English translation (1970).

[Werner et al. 2017]
C.J. Werner (editor), "MCNP User's Manual - Code Version 6.2", LA-UR-17-29981 (2017).

Part II - Evaluation of UNCL ^{235}U linear density calibration and BP correction for commercial Angra reactor fuel

2.1 General description of correction factor application

The ABACC, the IAEA and EURATOM all verify ^{235}U content in fresh fuel non-destructively using active neutron coincidence counting measurements. These measurements traditionally have used an AmLi source placed within a neutron collar (UNCL) in order to induce fissions in ^{235}U, producing neutrons in coincidence that are then moderating and detected by an array of polyethylene moderated ^{3}He detectors. The ^{235}U linear density [g/cm] is extracted from the coincidence neutron count rate, Doubles, by carefully correcting the measured count rate back to the reference calibration curve created for a designated collar-AmLi source combination (LANL-3 with MRC-95) and a fuel assembly free of burnable poison (BP) rods.

The main resource for these corrections is the report of Menlove et al. (1990), which contains relative detector coincidence efficiencies for each neutron collar, and AmLi emission rates for the sources used globally with UNCL's. While the general calibration makes distinctions between PWR and BWR fuel, beyond that all corrections aside from the heavy metal correction are applied independent of fuel type. Here the calibrations and correction factors are evaluated specifically for the commercially used Angra reactor fuel in order to assess performance and potentially improve verification measurements conducted in Brazil. This also allows limitations of the analysis of Menlove et al. (1990) to be explored further.

The simulations first compare response for fuel assemblies with uniform enrichment over the full enrichment range of 1.9%-4.95% relative to the initial calibration based on measurements with various combinations of DU and 3.2% fuel rods to approximate uniform fuel assemblies at various enrichments. These results are analyzed to consider whether alternative fits might improve the Doubles-^{235}U linear density relation. Modern fuel assemblies often contain higher enrichment and Gd_2O_3 content than was common in the 1980s when the original correction factors were optimized to enable increased fuel burn-up. Accurate assay of ^{235}U linear density in assemblies with poison rods has become one of the main challenges in verification measurements for modern Angra II fuel in Brazil. To address this the focus of this section on the analysis of a set of simulated cases with BP rods, which used to first optimize the correction factor coefficients and then compare the reference and optimized coefficients when applied to experimental measurements.

The corrections are applied to relate the measured Doubles rate to the ^{235}U linear density as

$$D_{corr} = \prod_{0}^{5} k_i D_{meas} = \frac{a \cdot m_{235}}{1 + b \cdot m_{235}}$$

Where m_{235} is the ^{235}U linear density in g/cm, a and b are the coefficients fit to the reference fuel assembly measurements with a range of ^{235}U linear densities. The individual correction

factors k_0 through k_5 respectively account for neutron source strength, electronic drift, the efficiency of a given collar/source-sample coupling, effects of burnable poison rods (Gd_2O_3) effects of heavy metal loading (U g/cm), and other conditions (e.g. perturbations from a bag covering the fuel assembly). The correction factors will be further described by giving an explanation of the values used here.

The correction for AmLi source strength, k_0, accounts for the difference between the neutron emission rates for a given AmLi source relative to the reference MRC-95 source at the date the ^{235}U linear density calibration. After taking into account that the original MRC-95 neutron emission rates of Menlove et al. (1990) were found to be 17% too high (Ravazzani et al 2001), the reference MRC-95 emission rates of 32737 ± 1.12% nps (neutrons per second) on 14 February 2014. The analysis here corresponds to measurements using the MRC-118 AmLi source located at the National Nuclear Energy Commission (CNEN) fuel fabrication facility near Rio de Janeiro, Brazil. The emission ratio, $\frac{MRC118}{MRC95} = 1.2207 \pm 0.0017$, is applied to obtain the emission rate of MRC-118 as 39962 ± 1.13% nps on 14 February 2014 (Croft 2018). The MRC-118 activity was then decayed to the March 2018 activity of 39707 ± 1.13% nps, which corresponds to the activity when experimental measurements at CNEN were conducted for validating the MCNP model in use here. The term k_0 used to correct both the measured and simulated count rates back to the MRC-95 emission rate in November 1989 was determined as

$$k_0 = \frac{1}{1.2207}\left[e^{\left[\frac{ln2}{432\ years}\left(2018+\frac{3}{12}-\left(1989+\frac{10}{12}\right)\right)\right]}\right]$$

where the exponential term accounts for the decay since the reference calibration in October 1989 and the leading term accounts for the relative emission rate of MRC95 to MRC118.

The corrections for electronic drift, k_1, is traditionally set to 1 except in cases where a significant failure occurs. The variation in detector efficiency and source sample coupling, k_2, for the CNEN collar, LANL-1, is accounted for by setting $k_2 = 1.520 \pm 0.0220$ to correct for the differences between the reference LANL-3 collar and the LANL-1 collar analyzed here. This value of 1.520 was determined as the product of the MRC-118:MRC-95 emission ratio, 1.2207 (Croft 2018), and the error weighted mean of k_2 estimates, 1.2634 ± 1.16% and 1.2154 ± 1.51%. These estimates were respectively determined by averaging the k_2 term isolated for 65 historical fuel assembly measurements taken in the fuel fabrication facility near Resende, Brazil as reported by Menlove et al. (1985); and by relative normalization of collars LANL-1,2 and 3, AmLi emission ratio and accounting for the fact that the relative collar measurements were made with the fuel assembly touching the front face of the collar instead of being 1 cm back.

The semi-empirical poison rod correction, k_3, was determined based on a limited BWR dataset and is one of the main factors being considered here. Uncertainty is not reported for individual coefficients or overall for the k_3 term. The BP rod correction factor for both PWR and BWR fuel assemblies is

$$k_3 = 1 + n\left(\frac{204}{N}\right) \cdot (corr./rod) \cdot \delta$$

where n and N are respectively the number of BP rods and total rods (BP and fuel), with 204 corresponding to the number of fuel rods in the reference assembly. The correction per poison rod is (Menlove et al. 1990)

$$(corr./rod) = (1 - e^{-0.647 \cdot Gd}) \cdot 0.0213$$

where Gd refers to the weight percent of Gadolinium in the poison rods, determined here using the ratio of Gd_2O_2 mass to total fuel pin mass as

$$Gd\ wt\% = \frac{m(Gd_2O_3)}{m(Gd_2O_3) + m(UO_2)}$$

though the definition of Gd weight percent is not explicitly stated in the original report. The delta term, δ, accounts for spectral hardening due to absorption of thermal neutrons by ^{235}U, which varies proportional to the average enrichment of the assembly, E_n.

$$\delta = (2.27 - 0.40 \cdot E_n)$$

A more precise indication of ^{235}U content would be given by the ^{235}U linear density, however the difference is likely to be marginal. Without combining coefficients the full BP rod correction factor is

$$k_3 = 1 + n\left(\frac{204}{N}\right)[(1 - e^{-0.647 * Gd}) \cdot 0.0213](2.27 - 0.40 \cdot E_n)$$

The heavy metal correction, k_4, is a semi-empirical correction applied to account for the change in the Doubles rate resulting from variations in the linear U density [g/cm] mainly due to moderation from inelastic scatter reactions in the fuel. The heavy metal correction is applied as

$$k_4 = 1 + 3.89 \cdot 10^{-4}(1215 - \frac{m_U}{L_{fuel}})$$

where m_U is the total U mass and L_{fuel} the active length of the fuel and 1215 g/cm corresponds to the linear U density in the reference PWR assembly (coefficients of k_4 specific to PWR or BWR fuel). The relative error in k_4 is 0.225%.

2.2 Simulated Uranium isotopics

The first set of simulations focus on variations in enrichment over the DU (0.2%) to 4.95% range without BP rods. For the enrichments 1.9025% and 3.1995% the SGAS-NML Reference: 9672 sample measurements corresponding respectively to Batches 1 and 2 as reported by Amaraggi (2013). At other enrichments the ^{234}U content was determined using the following relation:

$$^{234}U\ wt\% \ = \ 0.01259 \cdot \left(^{235}U\ wt\%\right)^{1.101161}$$

where the weight percent values correspond to the fraction of the total U mass. The coefficient values in the ^{234}U equation were optimized from the general equation of Bownam and Hermann (1995)

$$^{234}U\ wt\% \ = \ 0.007731 \cdot \left(^{235}U\ wt\%\right)^{1.0837}$$

using the known ^{235}U-to-^{234}U ratios of 130, 115.51 and 114.62 from samples at 0.72% (NU), 1.9025% and 3.1995%. The NU ratio from Grady et al. (2017), is considered reasonable as it is consistent with the ^{235}U-to-^{234}U ratio of 128 ± 10% calculated using the following relation recommended by Kimball (2007)

$$\frac{^{235}U}{^{234}U} = \frac{157.72237 - 155.6896\left(^{235}U\ wt\%\right)^{0.5}}{1 - 0.95152907\left(^{235}U\ wt\%\right)^{0.5}}$$

Using the optimized $^{234}U\ wt\%$ relation along with set of declared isotopics, simulations were conducted at enrichments of 1.9025%, 2.5%, 3.1995%, 3.5%, 4%, 4.5% and 4.95% to cover the cover startup fuel and extend to the maximum possible LEU enrichment, which extends well beyond the current licensing limit for Angra reactors of 4.25% (Campolina et al. 2018). As a test case outside of the standard bounds a DU (0.2%) fuel assembly was also simulated using the isotopics reported by the Y-12 Nuclear Materials Disposition Program Office (1995).

2.3 Evaluation of Doubles-^{235}U linear density calibrations

The resulting Doubles as a function of linear ^{235}U density from a standard shift register style coincidence tally with a predelay of 4.5 μs and gate width of 64 μs are reported in Table 1 and shown with the traditional calibration overlaid in Fig. 1 (k_0, k_4 and k_5 were applied to the simulated rates to match the scale of the traditional calibration). Although fuel was simulated here with varying density corresponding to the U molar mass variations the effects on U linear density can be considered as negligible as they correspond to a change of only 0.025% in the heavy metal correction factor. The simulated set of Doubles rates shows reasonable consistency with the reference Padé curve fit of Menlove et al. (1990), however a clear trend is seen in Fig. 1 (b) where the 3.1995% enriched fuel assembly has the greatest deviation from the reference calibration curve, with assemblies at higher and lower enrichments all having better agreement. The most significant difference between the reference calibration and the current study is the number and type of fuel rods; here 236 fuel rods based on those used commercially in Angra II and III reactors are simulated, whereas the original study used 204 fuel rods of a type no longer used in reactors. The original experimental measurements also approximated fuel assemblies with uniform enrichment by using a combination of DU and 3.19% fuel rods, which has been show to result in variations in the range of ±2-3% in a previous simulation study (Looman et al. 2001). This makes the disagreement for the assembly at 3.1995% enrichment (~45 g/cm) concerning as this is the case where the original calibration would have had the best comparative

measurement. It is possible that the original calibration was perturbed by the combination of DU and 3.19% fuel rods due in part to the differences in density, but the most likely cause appears to be variations in local multiplication.

^{235}U wt %	Fuel Density [g/cm^3]	^{235}U [g/cm]	U [g/cm]	Simulated Doubles [cps]	Corrected Doubles [cps]
0.20	10.274	2.787	1393.234	24.409	29.606
1.9025	10.272	26.500	1392.895	124.247	150.722
2.5	10.271	34.819	1392.776	143.271	173.809
3.1995	10.270	44.557	1392.636	161.188	195.557
3.5	10.270	48.740	1392.576	168.144	204.001
4	10.269	55.699	1392.476	178.427	216.485
4.1819	10.269	58.231	1392.440	181.967	220.784
4.5	10.269	62.657	1392.377	187.727	227.779
4.95	10.268	68.918	1392.287	195.355	237.043

Table 1. Fuel characteristics and results from calibration curve (Doubles correspond to AmLi emission normalized to reference MRC-95 emissions)

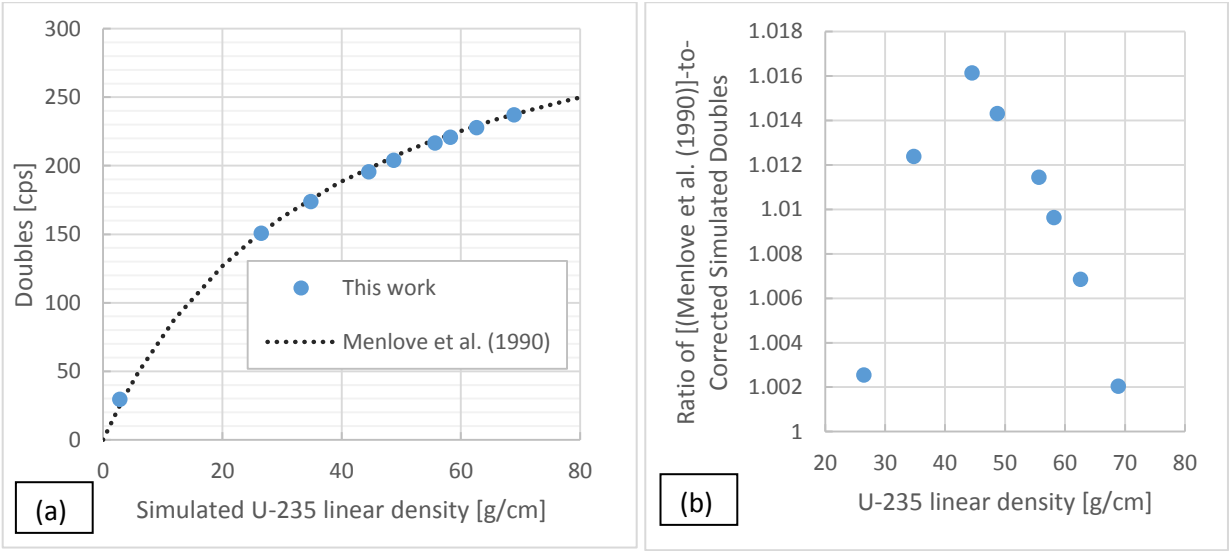

Figure 1. (a) Corrected simulated Doubles for fuel assemblies over the DU (0.2%) to 4.95% ^{235}U enrichment range with dashed line indicating the ideal semi-empirical relation; and **(b)** relative to the Doubles rate from reference calibration

The original work of Menlove et al. (1990) assumes that the shape of the calibration curve is equivalent for all collars and that by normalizing Doubles rates measurements of any fuel assembly with any AmLi source can be made to follow the reference curve. Here a comparison of several calibration curves applied to the simulated data set are summarized in Table 2 and Fig. 2. Note that the optimizations performed here were for the inverted Padé equation and polynomials both arranged as ^{235}U linear density as a function of Doubles (note that a simple inversion of a fit of the Doubles as a function of ^{235}U linear density is not equivalent to the fit of

the ^{235}U linear density as a function of Doubles, as demonstrated on p.127 of Andreon and Weaver 2015).

The new calibration curve fits are optimized to a specific type of fuel assembly, and these may not necessarily improve results for UNCL measurements in general, if at all. Since this assembly is 16x16, whereas the original reference PWR calibration curve was created with a 17x17 differences in fit may indicate that either the use of a universal calibration is non-ideal or the linear heavy metal correction factor, k_4, determined by Menlove et al. (1990) could be improved upon. This is not done here, but could be evaluated by simulating a range of fuel enrichments similar to what is shown in Fig. 1 for PWR assemblies over the range 14x14 to 18x18. Variations in the Doubles-^{235}U linear density relation could then be compared using the current heavy metal correction as well as an optimized value. Depending on results it might be preferential to use an array size-based calibration. With the data of this study it is difficult to determine which of these factors is dominant, however the current combination of universal fit and correction factor are not ideal for the simulated data set.

When the absolute simulated rates are corrected and used directly the conventionally used Padé curve fit of Menlove et al. (1990) appears to be biased high. However even when the coefficients are optimized it clearly overestimates ^{235}U mass for assemblies in the 45 g ^{235}U/cm range and underestimates for assemblies with linear densities both higher and lower than this. As an additional test the original coefficients were applied with a scaling factor applied to the simulated Doubles which was optimized to minimize the relative standard deviation. As this only reduced σ_R from 6.94% to 6.91% this demonstrates that this is not simply an issue that can be solved by simulation normalization (the normalization factor was trivial at just 1.0027). The addition of the constant c to the Padé offers a further slight improvement. By fitting the data with a 2nd order polynomial inverts this trend, and increasing the polynomial to a 3rd appears to fit the simulated data exceptionally well, but with 4 coefficients used, and loss of physics information that were in the Padé shape (saturation for higher increasing the linear density m).

Calibration type	σ_R	a	b	c	d
Padé from Menlove et al. (1990) $(D = \frac{am}{1+bm})$	6.94%	9.646	0.0261	-	-
Padé with updated coefficients: $(D = \frac{am}{1+bm})$	1.05%	9.436	0.0255	-	-
Padé + c $(D = \frac{am}{1+bm} + c)$	0.91%	8.944	0.0238	-6.659	
2nd order poly. $(m = aD^2 + bD + c)$	1.12%	0.001396	-0.05934	3.320	-
3rd order poly. $(m = aD^3 + bD^2 + cD + d)$	0.09%	0.000004543	-0.0004752	0.1542	-1.481

Table 2. Relative standard deviation, σ_R, for ^{235}U linear density from calibrations fit to assemblies with enrichments ranging 1.9-4.95% (note: Padé + c and polynomial functions were optimized including the DU fuel to produce the expected curve shape)

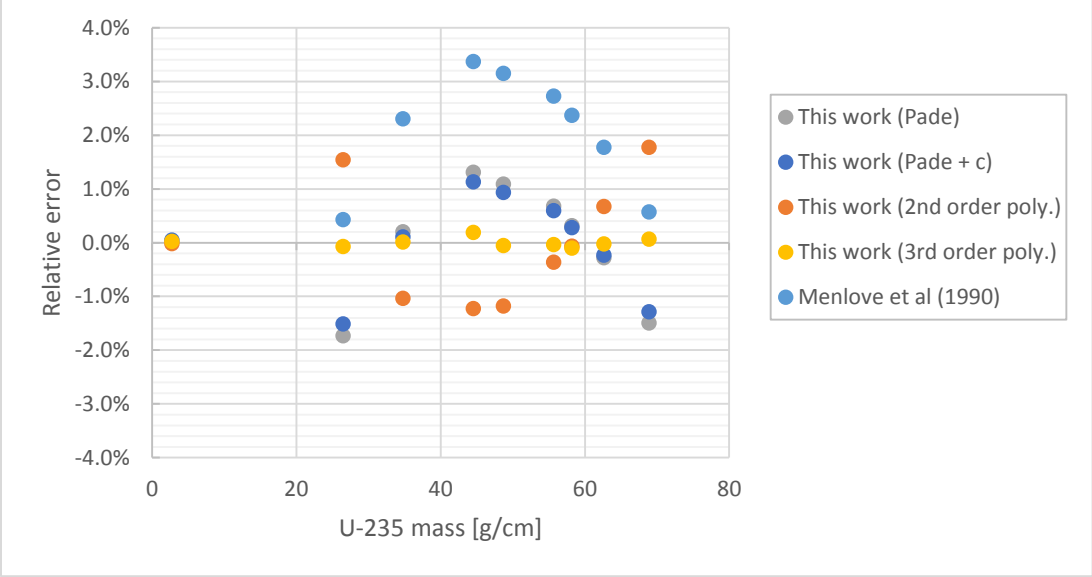

Figure 2. Relative error in the calculated ^{235}U linear density as a function of linear density

When the calibrations fit to the simulations rates are applied to experimental rates in Fig. 3 the original calibration performs better. While not ideal, the relative error for the calibrations peaks around 45 g/cm ^{235}U where the 3.1995% fuel assembly falls so this may be the weakest point in the simulated calibrations. Also, the simulated Doubles rate differs from the experimental rate by 1.33% which likely contributes to the higher relative error. The calibrations generated here do somewhat reduce error for the fuel assemblies with BP rods, however in all cases the relative error remains high, suggesting that the BP rod correction factor could likely be improved.

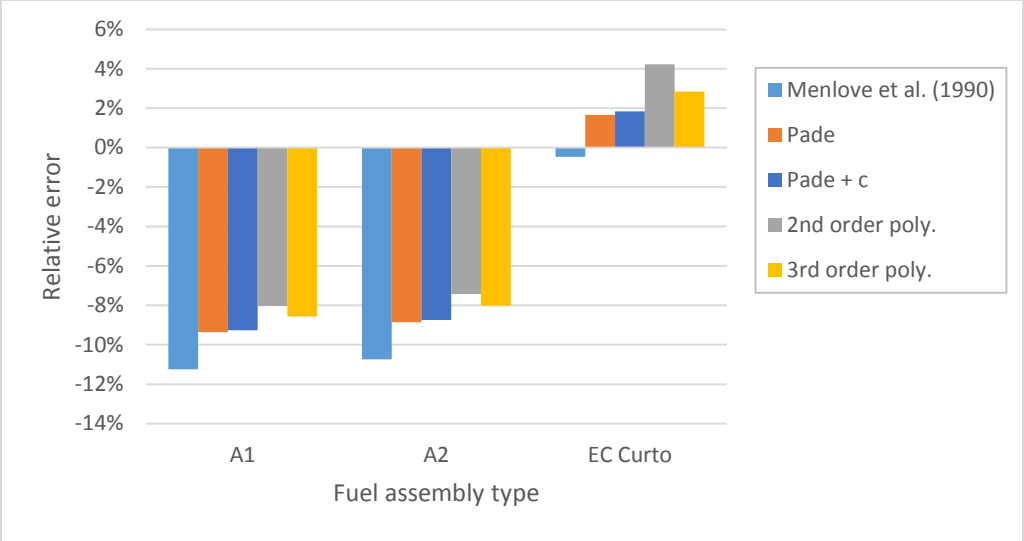

Figure 3. Assessing calibration curve performance for experimental measurements

2.4 Die-away as a function of enrichment

It is possible that the time dependent distribution in the coincidence detection profile could be used to replace or augment the traditional calculation using only the net active Doubles rate to indicate ^{235}U content. The coincidence profile is represented by the 1-D Rossi-alpha distribution (RAD) generated using a series of coincidence tallies with 5 μs gate widths and predelay values increasing incrementally by 5 μs over the range 4.5-204.5 μs. The resulting RADs for the active AmLi simulations are shown both as absolute count rates and normalized in Figs. 4 (a) and (b). Although these curves can be distinguished on an absolute scale, the relative scale shows that within the operational enrichment range (~1.9%-4.95%) the die-away characteristics of the UNCL do not vary dramatically. The assembly consisting of DU fuel does have a noticeably smaller die-away relative to LEU fuel, which is expected due to the significantly lower fissile material. By fitting exponentials to the RAD the die-away time may make it possible to extract information that is not apparent qualitatively.

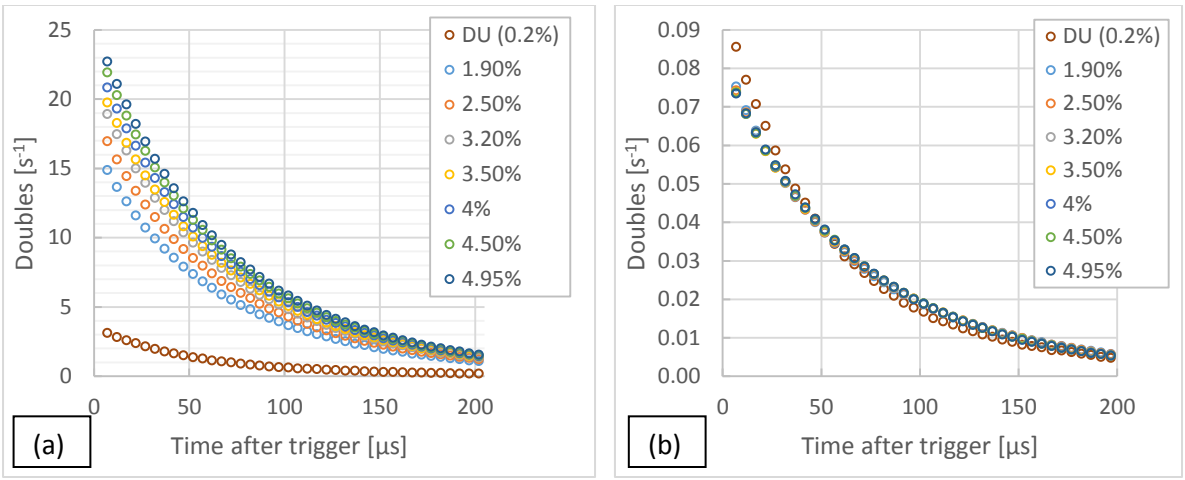

Figure 4. (a) Absolute and **(b)** normalized active Doubles counts as a function of time after the initial trigger (time after trigger corresponds to the middle of the 5 µs gate)

These distributions were analyzed for patterns in the die-away over several different time periods, where die-away, τ, is was determined from the RAD based on

$$D(t) = D_0 e^{-\frac{t}{\tau}}$$

The die-away over a given range of times after the initial trigger is found by taking the inverse of the exponential curve fit to the RAD. The die-away curves were analyzed over three different time ranges: full (4.5-204.5 µs), early (4.5-44.5 µs) and late (99.5-204.5 µs). Use of different time regions can be beneficial as the overall die-away curve is a combination of the source (fission chain) and detector (moderation) die-away curves.

The resulting die-away times are shown in Fig. 5 (a), along with the ratio of the early-to-late die-away times in Fig. 5 (b). These results demonstrate that die-away does appear to provide a good indication of linear ^{235}U density in the absence of BP rods. This shows a basic proof-of-concept, however since measurement of fuel without burnable poison are currently conducted with acceptable accuracy using the net Doubles rate this is not likely to be applied. The main benefit of the RAD would be if it provided a method for independently verifying the presence of poison rods, which should quench multiplication more rapidly, potentially making it possible to resolve fuel with and without poison rods based on the RAD. This is considered along with other alternative signals and optimization of the traditional poison rod correction in the following section.

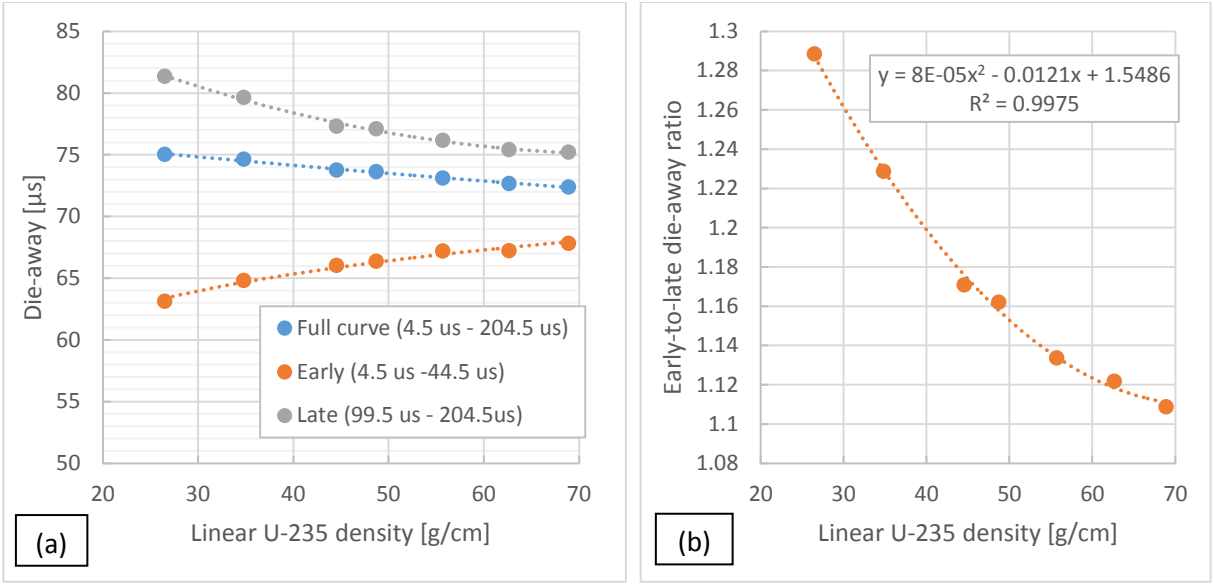

Figure 5. (a) Die-away as a function of enrichment for various time ranges; and **(b)** the ratio of the early-to-late die-away times as a function of enrichment

2.5 Assessing Burnable poison rod corrections

When fuel assemblies containing burnable poison rods are measured the Doubles rate is reduced by the capture of thermal neutrons in the Gd poison used to reduce the initial fuel reactivity to allow for increased ^{235}U loading and burnup. This is accounted for by applying a correction based on a combination of early experimental (Menlove et al. 1990) and Monte Carlo work (Swinhoe 1988). The correction converts the measured response to the expected response from an assembly free of Gd poison with the equivalent ^{235}U loading. This does not appear to directly confirm the declaration as the verification uses a synthetic response generated based on the Gd poison rod declaration, which is not independently verified. In the report of Menlove et al. (1990) limitations of the BP correction are recognized. Specifically, the correction is based on

> …the assumption that the BP rods do not interact with each other (shadow shielding) and that the fractional neutron absorption in the BP rods is independent of the average uranium enrichment. The first assumption is valid for… n <=20 [less than 20 BP rods] for PWR assemblies; however, the second assumption is not true for a wide range of enrichments (Menlove et al. 1990).

While the range of enrichments over which the assumption is valid is not specified, experimental measurements were only done for assemblies consisting of mixtures of DU and LEU pins having average overall enrichments of 3.19%, 2.26% and 1.36%. By analyzing a larger set of simulated cases it may be possible to assess the assumptions of the original report.

The response of the UNCL is mainly dependent on the ^{235}U linear density and the burnable poison (Gd) content within the assembly. The variation as a function Gd wt% here refers to $Gd_2O_3/(Gd_2O_3+UO_2)$, where UO_2 isotopics follow the description given previously and Gd

follows the natural isotopic composition (NIDC 2015). It is unclear whether Gd wt% was originally intended to be calculated as $\frac{Gd}{Gd_2O_3+UO_2}$, $\frac{Gd_2O_3}{Gd_2O_3+UO_2}$ or $\frac{Gd}{UO_2}$. Although Table V of Menlove et al. (1990) appears to use the definition $\frac{Gd}{UO_2}$, the definition $\frac{Gd_2O_3}{Gd_2O_3+UO_2}$ was used exclusively here as it follows Gd declaration conventions in Brazil and was found marginally improve results (σ_R was reduced by ~0.1% for the simulated set of 40 fuel assemblies containing Gd rods).

While the analysis in the previous section demonstrated that variations in response are reasonably well characterized for fuel assemblies without burnable poisons, when poison rods are present the response becomes more complex. Here a series of 8 fuel assembly geometries are simulated with two types of Gd poison rods to cover a wide range of conditions. The simulated geometries are shown in Fig. 6, where it is noted that the current Angra II reactors only use the loading pattern shown with 12 Gd rods. The simulated conditions go well above and below this to understand patterns and in the variation of measurable quantities to understand how the correction might be optimized to improve calculations in general. The effect of poison rod placement was also assessed by simulating two geometries for the fuel assemblies with 8 and 20 rods in order to assess the validity of the assumption that response is approximately independent of Gd rod placement.

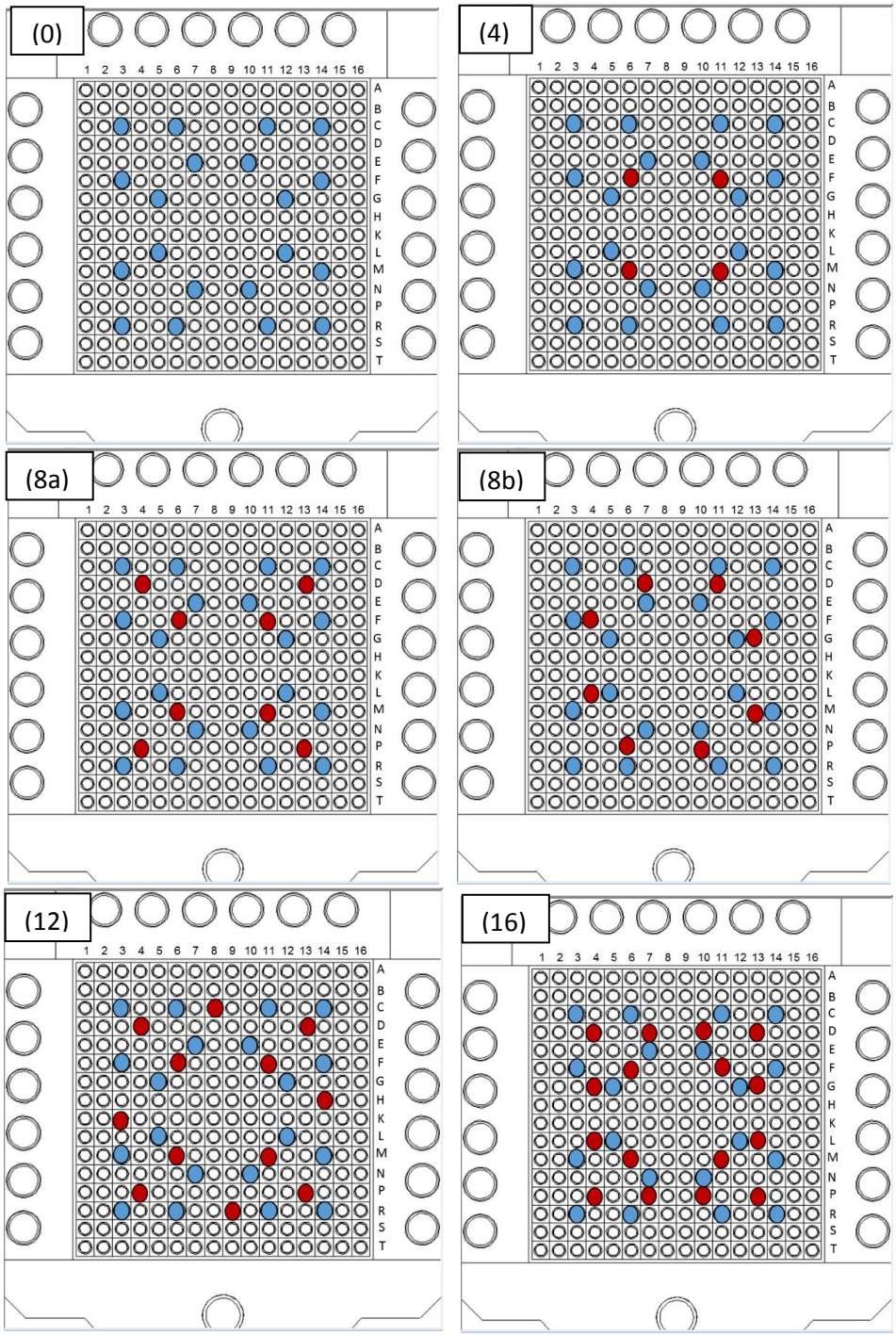

Fig. 6 ***continues on next page***

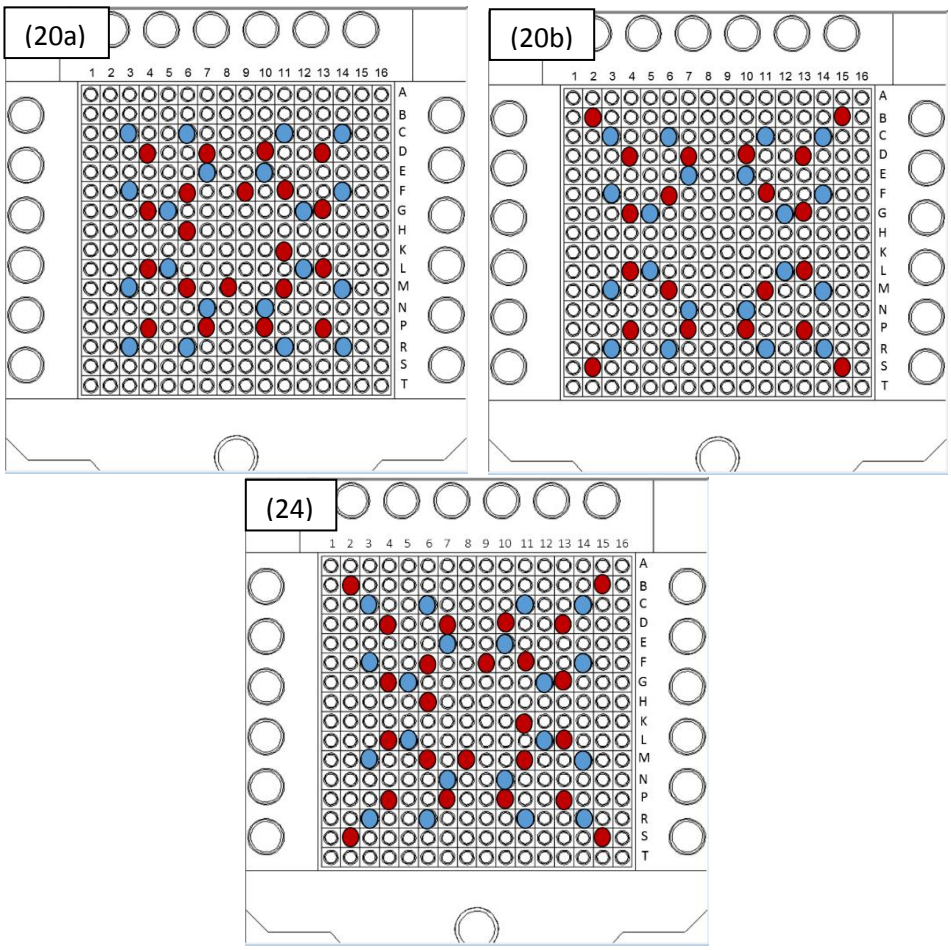

Figure 6. Illustration of simulated burnable poison geometries labelled by the number of Gd_2O_3 burnable poison rods (BP rods shown in red, guide tubes shown in blue, fuel shown in white)

Simulations were conducted for each of the descriptions given in Table 3. All simulated cases maintain a constant ^{235}U linear density to isolate effects from the number of poison rods and the Gd wt% on variations in count rates, and on the die-away profile of the RAD. The average enrichment values in Table 3 were calculated as

$$E_{235_{ave}} = \frac{[(fuel\ rod\ E_{235}) \cdot (number\ of\ fuel\ rods) + (Gd\ rod\ E_{235}) \cdot (number\ of\ Gd\ rods)]}{Total\ number\ of\ fuel\ +\ Gd\ rods}$$

Comparison of the average enrichment values makes it is clear that as Gd_2O_3 wt% and the number of Gd rods increases the ^{235}U enrichment, $^{235}U/(^{Total}U$ mass), becomes an increasingly less accurate indication of ^{235}U linear density. This difference may not have been appreciated historically as in the past fewer BP rods with lower Gd content were used relative to modern fuel assemblies. This could be avoided by using the mean enrichment within the non-BP fuel pins, which is appropriate if the BP rods can be considered as black to the thermal neutrons since thermal neutron absorption within BP pins is dominated by (n,γ) reactions in ^{155}Gd and ^{157}Gd. This assumption neglects fast leakage multiplication from ^{235}U and ^{238}U in the poison rods as the

effect is minor relative to the total Doubles response. It could be explicitly tested whether the uncertainty from this approximation is less than the uncertainty from taking the average enrichment of the assembly as the simple mean of the BP rods and fuel by looking at a wider range of ^{235}U enrichments in the BP. Further investigation of a wider range of BP rod enrichments also appears useful based on CNEN Angra II fuel studies which have included NU in BP rods (de Faria et al. 2013). Alternatively, effects of BP rods can be de-emphasized by using fast mode with the Cd liner, but this comes with the drawback of a significantly increased measurement time.

Performance of the standard BP correction factors was already demonstrated to be less than ideal when applied experimentally in Fig. 3. In Fig. 7 the corrected Doubles rates are shown for each of the 3 experimentally measured fuel assemblies, the 10 assemblies simulated without BP rods, and the 40 assemblies simulated with BP rods at 59.2 g/cm ^{235}U. The scatter in the corrected Doubles for the BP rod cases illustrates the limitations of the current BP rod correction factors.

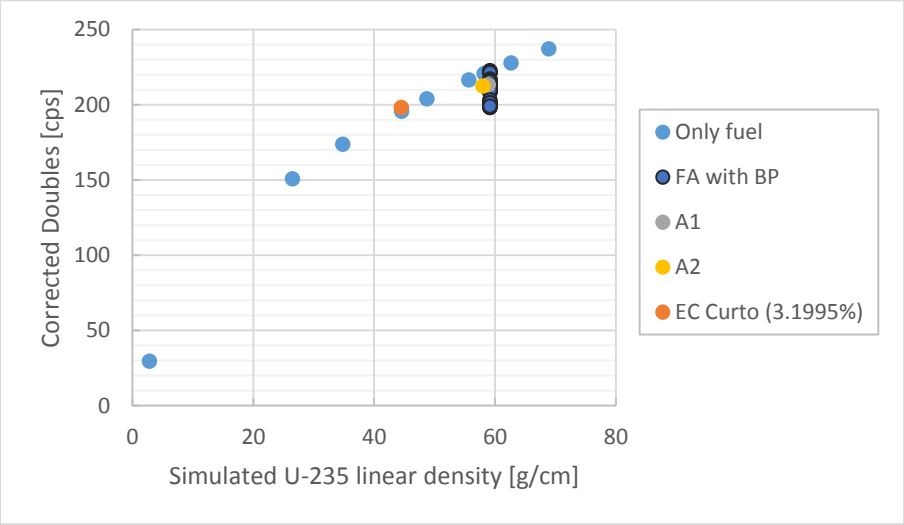

Figure 7. Summary of all simulated results along with a dashed line indicating the reference Doubles variation with ^{235}U linear density

Poison rods				Fuel			Fuel assembly averages	
Gd rods	Gd_2O_3 [wt.%]	E_{235} [%]	^{235}U weight fraction [%]	# of fuel rods	E_{235} [%]	^{235}U weight fraction [%]	E_{235} [%]	^{235}U [g/cm]
0	-	-	-	236	4.250	3.75	4.250	59.173
4	2	4.25	3.67	232	4.254	3.75	4.254	59.173
4	2	2.50	2.16	232	4.282	3.77	4.252	59.173
4	5	2.50	2.09	232	4.284	3.78	4.254	59.173
4	8	2.50	2.03	232	4.286	3.78	4.255	59.173
4	11	2.50	1.96	232	4.287	3.78	4.257	59.173
8	2	4.25	3.67	228	4.258	3.75	4.257	59.173
8	2	2.50	2.16	228	4.316	3.80	4.254	59.173
8	5	2.50	2.09	228	4.319	3.81	4.258	59.173
8	8	2.50	2.03	228	4.323	3.81	4.261	59.173
8	11	2.50	1.96	228	4.326	3.81	4.264	59.173
12	2	4.25	3.67	224	4.262	3.76	4.261	59.173
12	2	2.50	2.16	224	4.351	3.83	4.257	59.173
12	5	2.50	2.09	224	4.356	3.84	4.261	59.173
12	8	2.50	2.03	224	4.361	3.84	4.266	59.173
12	11	2.50	1.96	224	4.366	3.85	4.271	59.173
16	2	4.25	3.67	220	4.266	3.76	4.265	59.173
16	2	2.50	2.16	220	4.387	3.87	4.259	59.173
16	5	2.50	2.09	220	4.394	3.87	4.265	59.173
16	8	2.50	2.03	220	4.400	3.88	4.271	59.173
16	11	2.50	1.96	220	4.407	3.88	4.278	59.173
20	2	4.25	3.67	216	4.270	3.76	4.268	59.173
20	2	2.50	2.16	216	4.424	3.90	4.261	59.173
20	5	2.50	2.09	216	4.433	3.91	4.269	59.173
20	8	2.50	2.03	216	4.441	3.91	4.277	59.173
20	11	2.50	1.96	216	4.450	3.92	4.285	59.173
24	2	4.25	3.67	212	4.275	3.77	4.272	59.173
24	2	2.50	2.16	212	4.463	3.93	4.263	59.173
24	5	2.50	2.09	212	4.473	3.94	4.273	59.173
24	8	2.50	2.03	212	4.484	3.95	4.282	59.173
24	11	2.50	1.96	212	4.494	3.96	4.292	59.173

Table 3. Summary of parameters used in simulated cases varying the number and concentration of Gd poison rods

The relative error in the calculated ^{235}U linear density for the BP rod cases is shown in Fig. 8. The variation appears to be proportional to the number of BP rods up to 12 rods, after which geometry may be more important to consider (this may also be an outcome of the specific cases simulated). Although the BP rods were simulated in two geometries for both the cases of 8 BP and 20 BP it is seen only to cause a major difference in the case of 20 BP rods. The position of

only 4 rods distinguishes geometries 20 (a) and 20 (b), where the four BP rods were varied to be nearer to the center of the fuel assembly and nearer to the corners, respectively. This is a fairly extreme examples of a geometric effect that demonstrates BP rod position can be important. Due to the much higher flux around the middle of the fuel assembly a BP rod positioned there has a greater effect than the equivalent BP rod positioned towards the exterior of the assembly. This shows that the effect of the BP rod loading pattern cannot always be neglected, a small but significant difference from the conclusion of Looman et al. (2001). The different conclusions likely result from differences between the sets of simulated cases as position dependence appears much less variable based on the two geometries with 8 BP rods than with 20 BP rods. BP rod position dependent corrections are a potential solution to this that may be considered in the future.

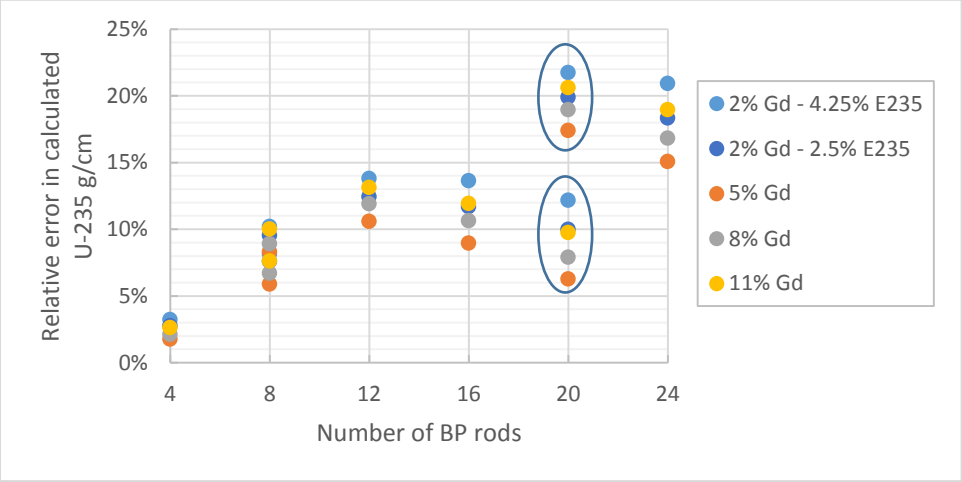

Figure 8. Relative error in the Calculated ^{235}U linear density for fuel assemblies with varying numbers of BP rods (the upper and lower circled groups of points respectively correspond to 20 (a) and 20 (b))

2.6 Relative effect of Gadolinium varying Gd weight percent and number of BP pins

In this section the relative effects from changes in Gd wt% and the number of BP pin are considered. The change in the Doubles is shown in Fig. 9 relative to an assembly with 2 wt% Gd_2O_3 for each simulated number of poison rods. The fits are reasonably good when constrained to pass through (0,0) in Fig. 9 (a) and improve significantly when unconstrained in Fig. 9 (b). Overall this shows that the Doubles variation is directly proportional to the Gd_2O_3 weight percent. To give context to the absolute magnitude of these variations the difference between the Doubles rate for 2% Gd_2O_3 vs. 11% Gd_2O_3 for fuel assemblies with 4, 8 (a), 8 (b), 12, 16, 20 (a), 20 (b), and 24 poison rods are respectively 2.0, 3.9, 4.2, 5.8, 6.7, 7.8, 7.5, and 8.6 counts per second.

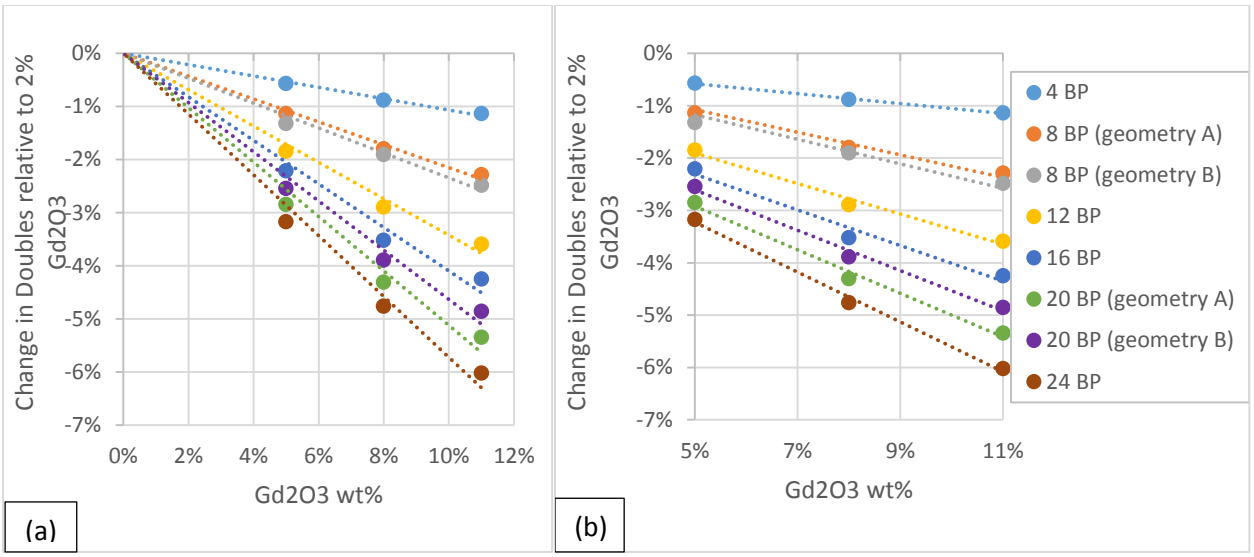

Figure 9. Variation in Doubles relative to fuel assemble with 2% Gd_2O_3, both figures show the same data, the best fit lines of **(a)** cross at (0,0) and best fit lines of **(b)** are unconstrained

These variations can also be compared by normalizing the change in the Doubles rate per poison rod as shown in Fig. 10. The slight decrease in the effect on the Doubles per rod for some of the assemblies with higher numbers of poison rods suggests self-shielding may occur due to the very high thermal capture cross section of Gd. From Fig. 11 it is seen that although the change is not constant as a function of the number of BP rods and the position of the BP rods plays a role in determining the relative weight of a given BP rod the self-shielding effect is relatively minor. This is most evident for the cases 20(a) and 20(b) where the relative weight per BP of 20(a) is consistent with the other cases, but 20(b) has a notably reduced weight per rod due to the change in position for only 4 BP rods. This suggests a considerable difference in the relative effect on the Doubles from the positioning of these 4 individual rods. In the case with 24 BP rods the weight of a given rod is the average of 20 (a) and (b) as expected based on the BP rod positions being a combination of the two cases. Considering these factors together the weight of a given rod is dependent on its position as well as the number of BP rods in the assembly.

The worth or neutronic weight of a given rod will vary proportional to the thermal flux at the given position within the assembly. This could be evaluated by comparing the relative effect of a single BP rod at various positions throughout an assembly to create a BP rod weight map and consider whether it is consistent with observations seen here. The difference between the summation of individual BP rod effects and the assembly with the full set of BP rods would indicate the degree of self-shielding. If self-shielding is significant the notion of producing a general relation for weighting a given rod based on its position will not be possible.

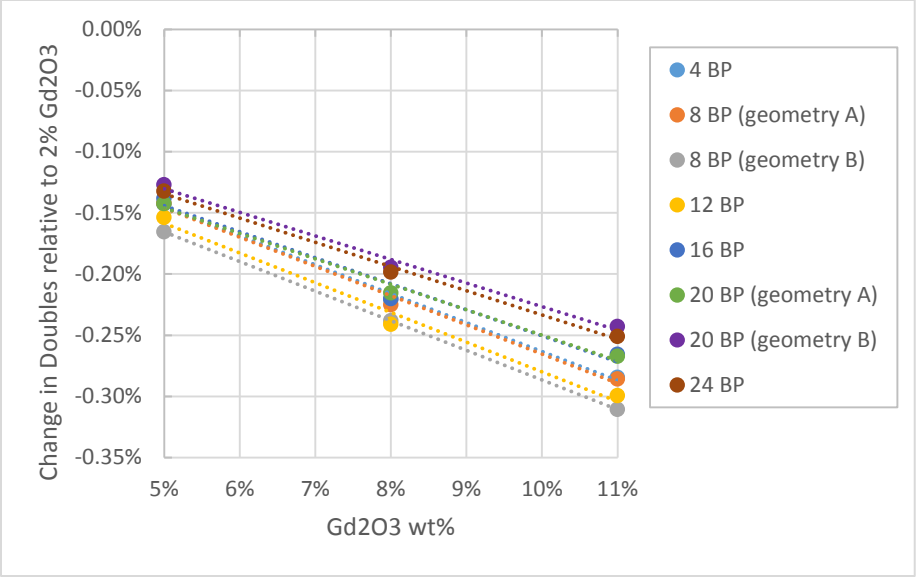

Figure 10. Variation in Doubles relative to fuel assemble with 2% Gd_2O_3 normalized per BP rod

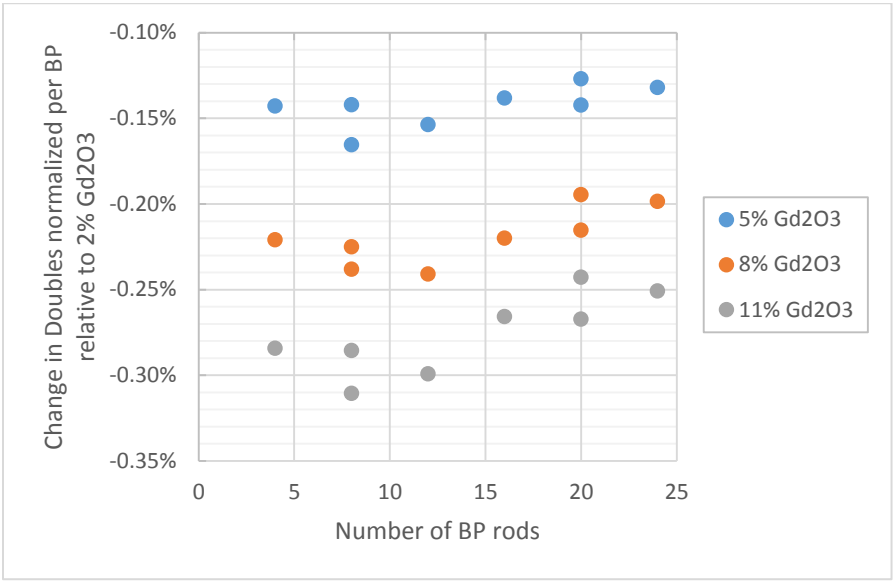

Figure 11. Evaluating change in Doubles normalized by the number of BP rods relative to the assembly with 2% Gd_2O_3

2.7 Alternative sources of BP rod information

2.7.1 *Singles from AmLi transmission*

It is of interest whether more information could be obtained if the ^{3}He tubes were recorded individually and not only in summation. This is something that is currently only feasible in simulation space as the physical pre-amplifiers are all summed together in the current system, however for R&D purposes it would be useful to break this restriction as well as the limitation to

measurement of Singles and Doubles. One potential use in the case of poison rods would be to consider whether the Singles in the 6 ^{3}He tubes directly across from the AmLi source would provide an indication of neutron transmission proportional to either the number of BP rods or the overall Gd_2O_3 content of a given assembly.

In Fig. 12 it is seen that the Singles rate for the pod directly across from the AmLi source does vary proportional to the number of the poison rods. From this the number of BP rods could be approximately verified based on the Singles transmission rate falling within a given range. Since there is overlapping between assemblies with different numbers of BP rods, this is somewhat dependent on BP rod positioning within the assembly making uncertainty in calculated number of BP rods likely as high as ±4-8 rods. Still, this appears to be a simple independent check for verifying the declared number of BP rods, especially in cases where the expected response for a given type of fuel assembly is known based on previous verification measurements. A basis on previous measurements is likely the best immediate solution as BP rod position is likely to remain consistent and BP rod position is not explicitly known in all cases as it is not part of the declaration.

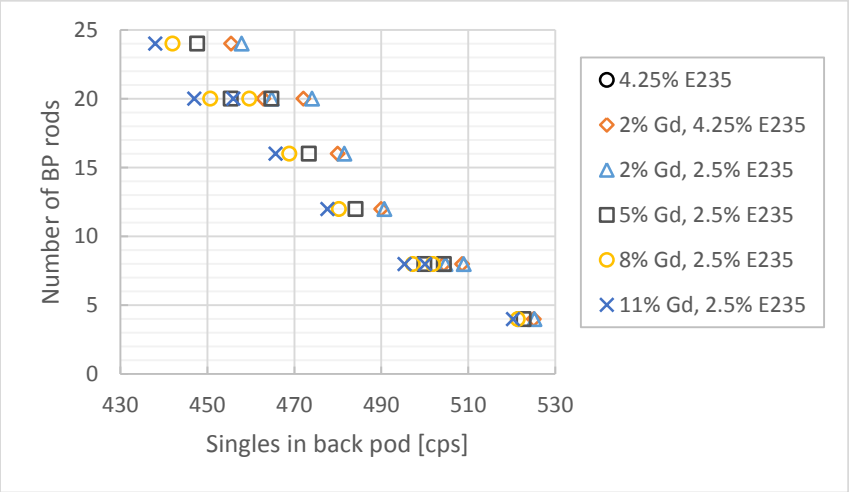

Figure 12. Number of BP rods as a function of Singles in pod directly opposite the AmLi source, with subsets based on BP rod characteristics

In Fig. 13 results are presented for the Singles transmission variation as Gd_2O_3 wt% is varied. This signal shows significant dependence on both the number of BP rods and geometry, suggesting that this is not likely to be useful for determining the Gd_2O_3 wt% without use of the declared number of BP rods.

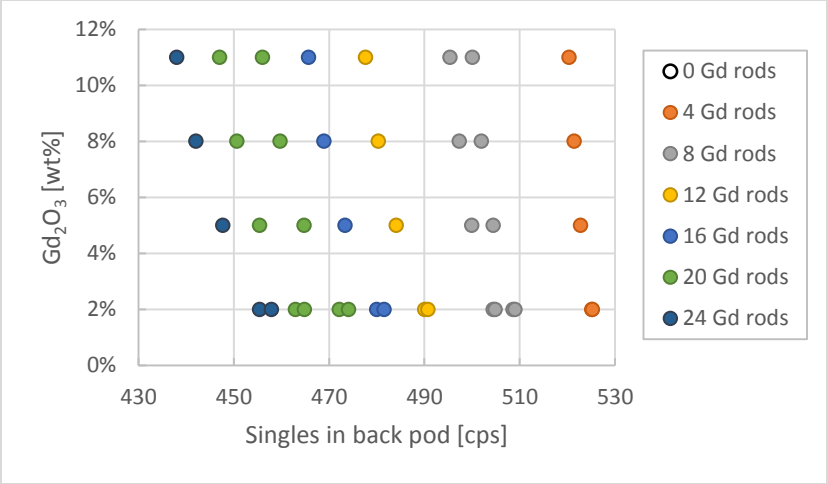

Figure 13. Gd_2O_3 wt% as a function of Singles in pod directly opposite the AmLi source, with subsets based on the number of BP rods

2.7.2 *Rossi-alpha distribution*

Since BP rods serve to decrease fuel reactivity it is expected that the RAD will be quenched to a degree that is proportional to the Gd content of the fuel. From Figs. 14 (a) and (b) it is seen that there is a minor qualitative change in the RAD as the Gd_2O_3 wt% is varied for a fixed ^{235}U enrichment and linear density that does not become more apparent by comparing die-away times. This suggests that even at 2% Gd_2O_3 time varying effects are nearly saturated.

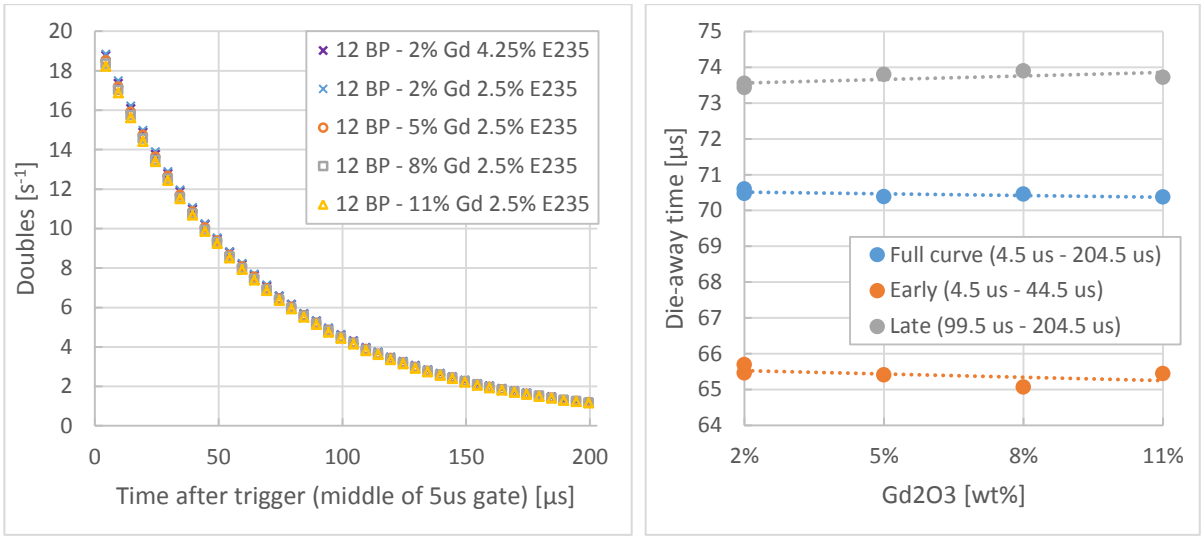

Figure 14. (a) Rossi-alpha distributions when varying enrichment or Gd_2O_3 wt% for fuel assemblies with 12 BP rods; and **(b)** corresponding die-away times

The decay characteristics are compared as a function of the number of BP rods in Fig. 15 (a) and (b), where it is seen that the die-away time may offer the potential for verifying the number of BP rods present within an assembly. The ability to discern between 4 and 8 BP rods, but not

between different Gd wt% values shows that the RAD is only useful for indicating large deviations from the declaration. The variation in UNCL die-away times for the two geometries simulated with 20 BP rods again suggests that there is positional dependence that could benefit from further assessment. A comparable analysis of the fast mode (with Cd liner) RAD would also be of interest.

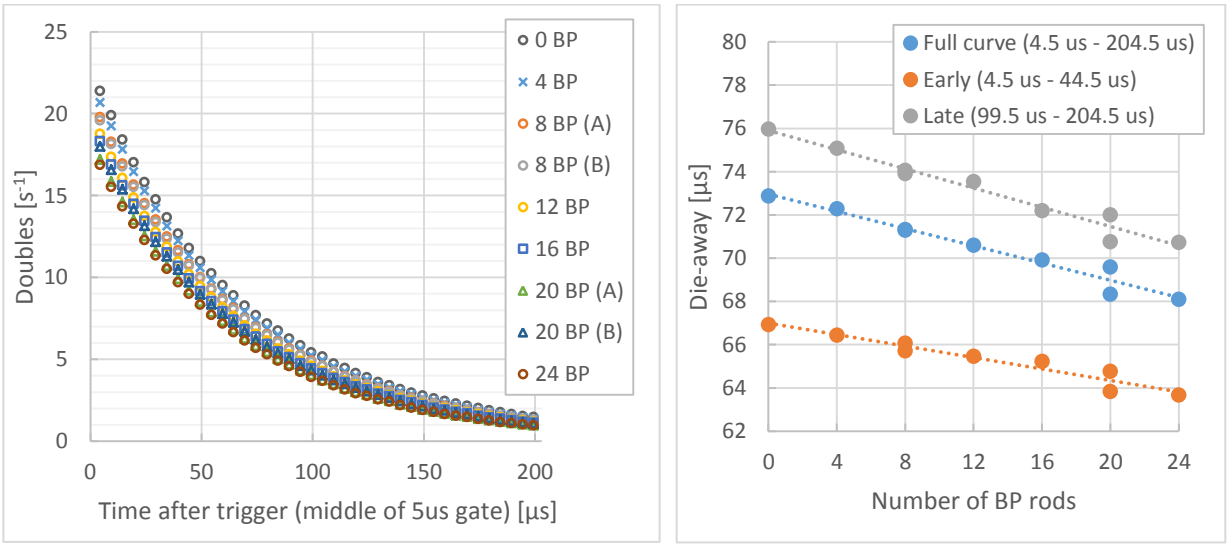

Figure 15. (a) Rossi-alpha distributions for varying numbers of a given type of BP rod (2% Gd_2O_3 4.25% E_{235}); and **(b)** corresponding die-away times

The die-away variation as a function of the number of BP rods is shown more generally in Fig. 16 which includes all 40 BP rod cases and the corresponding simulation without BP rods. It is also interesting that patterns in the die-away times overall appear independent of the time range for the three ranges analyzed here.

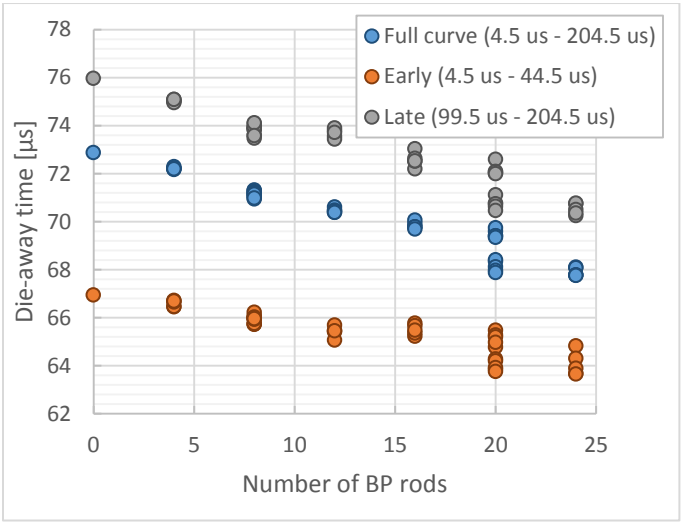

Figure 16. Die-away time corresponding to the Rossi-alpha distributions when varying the number of BP rods including all simulated Gd_2O_3 wt% values

2.8 Optimization of BP rod correction factors

The two main components of the BP rod correction factor are the correction per rod and the modified correction per rod based on the spectral hardening by ^{235}U. The spectral hardening is accounted for by

$$\delta = (c_1 - c_2 \cdot E_n)$$

The original values may be less than ideal for this due to the approximation of mixed DU-LEU fuel assemblies as uniform enrichments, but considering the average enrichment for the simulations here only cover the range of 4.25% to 4.292% this is insufficient for optimization of the delta coefficient values. Here the tradition enrichment dependence is maintained and only the coefficients c_3 and c_4 of the correction per rod are revised

$$(corr./rod) = (1 - e^{-c_3 \cdot Gd})c_4$$

The original BP rod correction factor coefficients of Menlove et al. (1990) were based on a limited set of measurements of with BWR rods. These factors are likely the cause of the relatively poor performance observed during experimental verification measurements of PWR Angra fuel assemblies with BP rods. It is possible that the difference in dimensions between PWR and BWR fuel affects reactivity to the point where distinct correction coefficients are necessary, as is the case for the heavy metal correction.

Here the coefficients were optimized to minimize σ_R for the calculated ^{235}U linear density over all BP rod simulations, where the original and new coefficients are reported in Table 4 along with the coefficients determined for a simulated study of Looman et al. (2001) based on a 17×17 PWR fuel assembly. The new values indicate a lower saturating Gd_2O_3 wt% and a greater weight for each individual BP rod relative to the original coefficients. The increased weight per BP rod differs from the conclusion of Looman et al. (2001), however in that study coefficients c_1 and c_2 of the δ term show a greater dependence on the fuel assembly enrichment.

As a test a shadow-shielding factor, $(1 - c_5 n)$ where n is the number of BP rods, was also added to determine whether reducing the weight per BP rod might further improve results. The shadow-shielding factor was added in the form

$$(corr./rod) = (1 - e^{-c_3 \cdot Gd})c_4(1 - c_5 n)$$

The extremely small value of the c_5 coefficient suggests that it is negligible or takes a more complex form. The results in Fig. 11 show including the shadow shielding factor has no qualitative effect on results.

The same is true quantitatively as the overall σ_R values in the calculated ^{235}U linear density using the standard correction, optimized correction and optimized correction with the additional BP rod weighting factor were respectively 15.70%, 4.07% and 4.07%. The 0.0007% improvement resulting from the additional shadow shielding factor shows that it is unnecessary. This summary

does not capture the significant effect of BP pin position that can clearly be seen to be a dominant effect in the optimization when looking at the relative error as a function of the number of BP rods in Fig. 17.

Parameter		This work	Looman et al. (2001)	Menlove et al. (1990)
Type		PWR	PWR	PWR
Rod lattice		16×16	17×17	15×15
n/N_{ref}		236/204	264/264	204/204
BP correction (spectral hardening)	c_1	Menlove et al. (1990)	1.64	2.27
	c_2	Menlove et al. (1990)	0.21	0.40
BP correction (corr./rod)	c_3	0.91955	1.08	0.647
	c_4	0.02901	0.01755	0.0213
	c_5*	9.085×10^{-5}	-	-

Table 4. Comparison of experimental ^{235}U linear density using the original and optimized coefficients (*values of c_3 and c_4 are unchanged if c_5 is omitted)

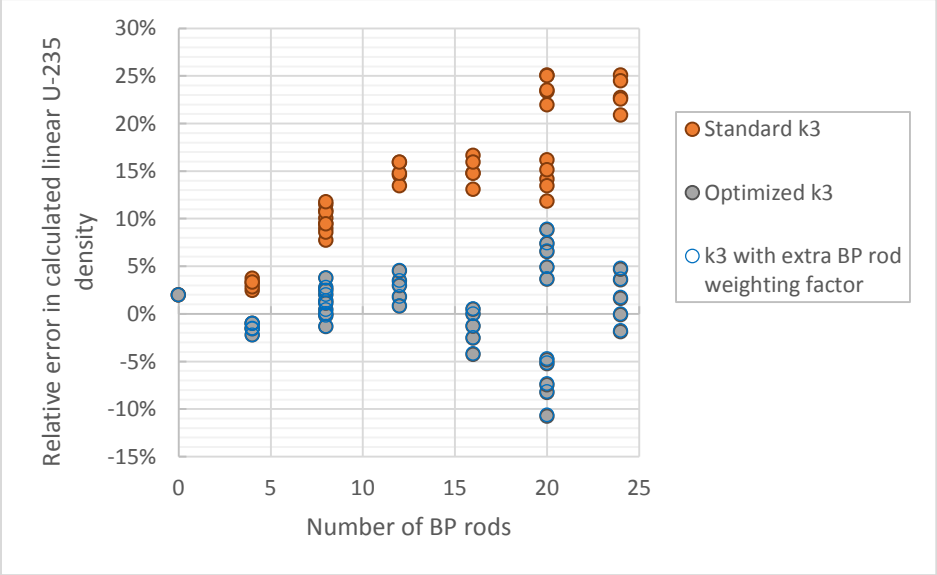

Figure 17. Relative error in the Calculated ^{235}U linear density for fuel assemblies with varying numbers of BP rods for the standard and optimized BP rod correction factors (k_3)

2.9 Benchmark Measurements of September 2017 at Resende Nuclear Fuel Factory (FCN)

In September 2017 CNEN, ORNL and LANL personnel carefully conducted measurements of two types of fuel assemblies with BP rods at the FCN in Resende. The accuracy of the verification results in Table 5 shows that using those coefficients updated with Angra-specific simulations in place of the original coefficients (c_3 and c_4) improves the accuracy of the

calculated ^{235}U linear density by a factor of 10. These results also reaffirm that the original form of the equation is reasonable and that shadow shielding does not need to be accounted for.

	Relative accuracy of calculated ^{235}U linear density		
Fuel assembly	Menlove (1990) k_3	Optimized k_3	Optimized k_3 with shadow shielding factor
A1	11.24%	0.330%	0.333%
A2	10.74%	1.13%	1.13%

Table 5. Comparison of experimental ^{235}U linear density using the original and optimized coefficients

2.10 Benchmark Measurements of February 2019 at Resende Nuclear Fuel Factory (FCN)

After the initial optimization and testing of the coefficients on the carefully conducted reference measurements they were provided to our collaborators at CNEN to independently conduct measurements as they normally would. The standard INCC analysis was used, updating only the two k_3 coefficients c_3 and c_4. The fuel assembly descriptions and corresponding measurement errors are given in Table 6, which reiterates that the Angra specific k_3 coefficients show very good performance on real fuel assemblies with an average absolute relative error of 1.9%. This is well within the ~5% uncertainty that includes both statistical uncertainty and uncertainty in all standard correction factors input into INCC except for the BP rod correction factor (this uncertainty may be estimated and included following more extensive experimental testing). One difference between the B-type fuel assemblies in Table 6 and the A-type measured in Table 5 is the length of the Gd zone, which was 330 cm for A-type assemblies in Table 5 and is 320 cm for B-type assemblies in Table 6. The localized nature of collar measurements makes this difference inconsequential.

Fuel assembly / measurement number	BP rods (#)	Gd_2O_3 (wt%)	Bias in calculated ^{235}U linear density*
B6 / 1	12	2%	0.24% ± 4.8%
B6 / 2	12	2%	-3.94% ± 5.1%
B2 / 1	12	7%	-1.61% ± 4.9%
B3 / 1	12	7%	-3.00% ± 5.0%
B3 / 2	12	7%	-0.52% ± 4.7%

Table 6. Validation of Angra specific k_3 values from independent measurements on commercial fuel assemblies (measurements 1 and 2 correspond to measurement of the same fuel assembly in the same geometry taken sequentially without removing the UNCL, *uncertainty as reported in INCC)

2.11 Summary and potential future work

The main purpose of this study was to evaluate whether the current BP rod correction factor (k_3) could be improved by optimizing the coefficients using a well-controlled set of simulations

covering a much broader range than would be measurable experimentally. This was achieved with the updated coefficients showing an improvement from >10% to <4% accuracy in ^{235}U linear density relative to the existing coefficients. By updating the coefficients without changing the form of the correction factor expression these can immediately be applied for measurement in existing INCC programs which by default asks the user confirm correction factor coefficients with the option to enter custom values. To reach that point the model was validated with experimental measurements, a number of parameters were also assessed in a Monte Carlo sensitivity analysis and additional signals were considered that could be the expanded upon in future studies.

This simulation study began with precise modelling of the reference EC Curto fuel assembly based on the engineering drawings, followed by modelling of the central region of fuel assemblies with BP rods. In each of these three cases the simulated net Doubles was within 2σ of the experimental value, where 2σ~2.5% corresponds to experimental statistical uncertainty. These models were then used in a sensitivity analysis where uncertainty was characterized for several factors affecting simulations and experimental measurement. By simulating fuel assemblies of varying lengths it was shown that 90% of the net Doubles signal comes from fuel within the UNCL and a further 9% comes from 10 cm above and below the UNCL, equating to 99% of the signal coming from 63 cm of fuel. This is significant as it shows that a fuel assembly like EC Curto with a short active length of 80.3 cm is a reasonable surrogate for a full length fuel assembly when considering the active net Doubles rate. This is important as it has the potential to permit experimental study of the BP rod correction factor studied in simulation space here, which may further improve the k_3 coefficients.

The experimental factors of axial position of the fuel assembly within the UNCL and uncertainty in the polyethylene density were considered next. It was found that with 0.25 cm possible in any axial direction the Doubles varied by 0.50%, which is minimal as it is generally less that the statistical uncertainty of ~0.76% (for 30×30 second cycles in active mode and 15×30 second cycles in passive mode). Simulations of EC Curto within a UNCL having polyethylene ranging 0.94-0.96 g/cm^3 was found to result in up to a 2.64% variation in the Doubles count rates. This is not ideal for simulations, however, generally density variations are less than this and experimentally the relative response factor, k_2, accounts for slight differences in polyethylene density between different UNCLs.

By simulating instrument response for a set of 19 semi-empirical and theoretical AmLi spectra it was shown that the distinctive spectra resulting from factors such as the bulk density, particle size, contamination with O and Be result in a range of mean energies and expected counts per initial source neutron. The Doubles rate per source neutron varies up to 3% based on which spectra is used. This shows that the current normalization based only on neutron emission rate is imprecise as the energy dependence of the fission cross section results in the count rate with a fuel assembly present being dependent on the neutron spectrum.

Considering all analyzed sources of uncertainty together, it is estimated that the simulated net Doubles have an overall 1σ uncertainty of 1.9% for the short fuel assembly. By combining

experimentally applicable sources with the statistical uncertainty it was estimated that for the MRC-118 source and the specific UNCL, LANL-1, used by CNEN the overall 1σ experimental uncertainty in the net Doubles is 1.4%. It is noted that this is only the count rate uncertainty and does not include uncertainties in the correction factor coefficients used to correlate the measured count rates to ^{235}U linear density.

A study of the ^{235}U linear density calibration was conducted by simulating Gd-free fuel assemblies at a range of enrichments and comparing calibration curve options to the standard reference calibration. The outcome of this was that while it is possible to better fit the simulated rates the improvements are not materialized when applied to the calculation of ^{235}U linear density from the corrected experimental net Doubles rates. The reference calibration performed best in all cases, however this was reliant on the standard correction factors. Perhaps if a wider range of simulated cases was conducted a full set of correction factors could be optimized specifically for the Angra II PWR fuel to compare performance of a fully customized set of coefficients to the general coefficients.

The coefficients of the *correction per BP rod* portion of the BP rod correction factor, k_3, were optimized specifically for the Angra II fuel. A set of 40 assemblies with a range of Gd_2O_3 wt% and between 4 and 24 BP were simulated so that the coefficients could be optimized for a wide range of cases. The coefficients indicate an increased weight per BP rod and a lower saturating Gd_2O_3 wt% relative to the original coefficients. Additional signals were tallied during the simulations and it appears that it may be possible to approximately measure the number of BP rods using the Singles transmission, which corresponds to the Singles rate in the pod of detectors directly across from the AmLi source. List mode measurements may also be useful for verifying the number of BP rods as the die-away curve appears to correspond to the number of BP rods. Due to the low saturating enrichment both of these techniques do not appear useful for indicating the Gd_2O_3 wt% as the BP rods are black to thermal neutrons even at a relatively low wt%.

The optimized BP correction factor coefficients were first tested experimentally during the re-analysis of a set of measurements carefully taken in 2017 at Resende Nuclear Fuel Factory, and then were tested directly in INCC for more routine measurements in 2019. These measurements included 5 unique fuel assemblies that all show remarkable improvement in response using the new k_3 coefficients. In the future these correction factors should be assessed further on a wider set of fuel assemblies with BP rods to determine whether they result in overall improvements or if the simulation of Angra II PWR specific fuel makes them specific to this fuel design. Finally, with the improved verification uncertainty is significantly greater than the expected uncertainties of <2% for both simulations and experiments further improvement of verification results may be possible, perhaps via a more complete review of the UNCL correction factors and ideally a re-verification of the reference universal calibration curve with fuel assemblies of uniform enrichment rather than a mixture of depleted and LEU fuel pins.

References

[Amaraggi 2013]
D. Amaraggi, IAEA Department of Safeguards, Standard Pellets for In-the Field DA Calibration (COMPUCEA), Report: SG-RP-12114 (values used correspond to: SGAS-NML REFERENCE: 9672) (2013).

[Andreon and Weaver 2015]
"Chapter 8: Fitting Regression Models." *Bayesian Methods for the Physical Sciences Learning from Examples in Astronomy and Physics*, by S. Andreon and B. Weaver, Springer, 2015.

[Bowman and Hermann 1995]
S. M. Bowman, O. W. Hermann. SCALE-4 Analysis of pressurized water reactor critical configurations: volume 3 – Surry Unit 1 Cycle 2, Oak Ridge National Laboratory Report: ORNL/TM-12294/V3, 1995.

[Campolina et al. 2018]
D. Campolina, E.F. Faria, A.A.C. Santos, V. Vasconcelos, M.P.V. Franco, M.S. Dias, J.R.L. Mattos, Parametric study of enriched gadolinium in burnable neutron poison fuel rods for Angra-2, Annals of Nuclear Energy, Volume 118, P.375-380, 2018.

[Croft 2018]
S. Croft, Yield of MRC-95 notes comparing HOM, NIST, JRC/NPL measured MRC-95 yields, Priv. Commun. 22 Aug. 2018.

[de Faria et al. 2013]
R.B. de Faria, C. Pereira, R. Sousa, C.A.M. da Silva, M.A.F. Veloso, and A.L. Costa, Impact of burnable poison rods on Angra II core – a study case, International Nuclear Atlantic Conference 2013 Recife, (Brazil).

[Grady et al. 2017]
D. Grady, E. Smith, K. Chand, M. Swinhoe, and J. Kulisek, "U-235/U-234 Ratio Behavior in Gas Centrifuge Enrichment Plants and Implications for Unattended Verification of UF6 Cylinders by Safeguards Inspectorates", Lawrence Livermore National Laboratory report: LLNL-TR-739009 (Livermore CA), 2017.

[IAEA 1995]
HEU to LEU conversion and blending facility uf6 blending alternative to produce LEU UF6 for commercial use (1995) https://inis.iaea.org/collection/NCLCollectionStore/_Public/28/036/28036782.pdf

[Kimball 2007]
Recommendations of 235U/234U Ratios and Alpha-Neutron Yields for the K-25/K-27 D&D Neutron NDA Methodology. BJC/OR-2862/R0. August, 2007. K. D. Kimball

[Looman et al. 2001]
M. Looman, R. Jaime, P. Peerani, P. Schillebeeckx, S. Jung, P. Schwalbach, M.T. Swinhoe, P.J. Chare and W.F. Kloeckner, The Effect of Gadolinium Poison Rods on the Active Neutron Measurement of LEU Fuel Assemblies, ESARDA 2001, Bruges (Belgium).

[Menlove et al. 1985]
H.O. Menlove, M.A.S. Marzo, S.G. de Almeida, M.C. de Almeida, L.P.M. Moitta, L.F. Conti, J.R.T. de Paiva. In-Plant Test and Evaluation of the Neutron Collar for Verification of PWR Fuel Assemblies at Resende, Brazil. Los Alamos National Laboratory report: LA-10562-MS. Los Alamos, NM. 1985.

[Menlove et al. 1990]
H.O. Menlove, J.E. Stewart, S.Z. Qiao, T.R. Wenz, G.P.D. Verrecchia. Neutron collar calibration and evaluation for assay of LWR fuel assemblies containing burnable neutron absorbers. Los Alamos National Laboratory report: LA11965-MS (1990).

[NIDC 2015]
"Gadolinium Natural Isotopic Abundances." NIDC: Medical Radioisotopes, ORNL, www.isotopes.gov/catalog/product.php?element=Gadolinium (2015).

[Ravazzani et al. 2001]
A. Ravazzani, R. Jaime, M. Looman, B. Pedersen, P. Peerani, P. Schillebeeckx, M. Thornton, A. Foglio-Para, and V. Maiorov, "Characterisation of Neutron Sources by NDA" , Proceedings of the 23rd Annual Symposium on Safeguards and Nuclear Material Management, Bruges, Belgium, 8 – 10 May 2001.

[Swinhoe 1988]
M.T. Swinhoe, "Calculation of the Effect of Enrichment and Poison Rods on Neutron Coincidence Collar Measurements of PWR Assemblies", UKAEA Safeguards R&D Report, SRDP-R151, December 1988.

[Y-12 Nuclear Materials Disposition Program Office 1995]
Y-12 Nuclear Materials Disposition Program Office. HEU to LEU Conversion and Blending Facility – UF_6 Blending Alternative to Produce LEU UF_6 for Commercial Use. Nuclear Materials Disposition Program Office; Y-12 Defense Programs. Report number Y/Es-063/R2 1995. Available: https://inis.iaea.org/collection/NCLCollectionStore/_Public/28/036/28036782.pdf

Part III – Sensitivity studies to AmLi spectrum using well counter measurements

Purpose: There is no generally accepted representation of the launch and/or emergent spectra of the Am/Li sources used in the uranium collar. There may also be differences between physical sources. One way to pick between plausible representations is to compare observed rates to predicted rates for a source inside a thermal-well as a function of the thickness of moderator placed around the source. This note summarizes an attempt to do this using the Large Volume Active Well Coincidence Counter. It was found that the approach could differentiate between spectra and variation with a relatively intense soft component were not favored. Source of well-known output would be useful to improve the power of the method. Future work could also adapt the approach to perform unfolding.

3.1 The Large Volume-Active Well Coincidence Counter (LV-AWCC)

The AWCC [1] was developed to provide penetrating, accurate assay of bulk uranium-oxide samples, highly enriched uranium (HEU) metals and alloys, light water reactor fuel pellets and uranium-bearing scrap materials. The AWCC is a ^{3}He proportional tube–based neutron coincidence well counter where Am(Li) neutron sources located in the detector end-plugs provide a source of fast interrogating neutrons. The Am(Li) neutrons induce fission in the fissile materials contained within the item of interest. The fissile mass of the item is determined from the observed neutron coincidence rate using an empirically derived calibration curve. Although the Am(Li) neutron interrogation sources are no longer readily available, the AWCC can still serve as a versatile and high-performance neutron detector for international safeguards if the isotopic neutron sources are replaced with a pulsed neutron generator.

The LV-AWCC (Figure 1) is somewhat larger than the standard AWCC, but its design was simply scaled up from the standard unit and provides similar overall performance characteristics as shown in Table 1. For these measurements the HDPE end-plug were replaced with graphite plugs to increased efficiency (34% for ^{252}Cf fission neutrons) and more linear axial response profile (Figure 2).

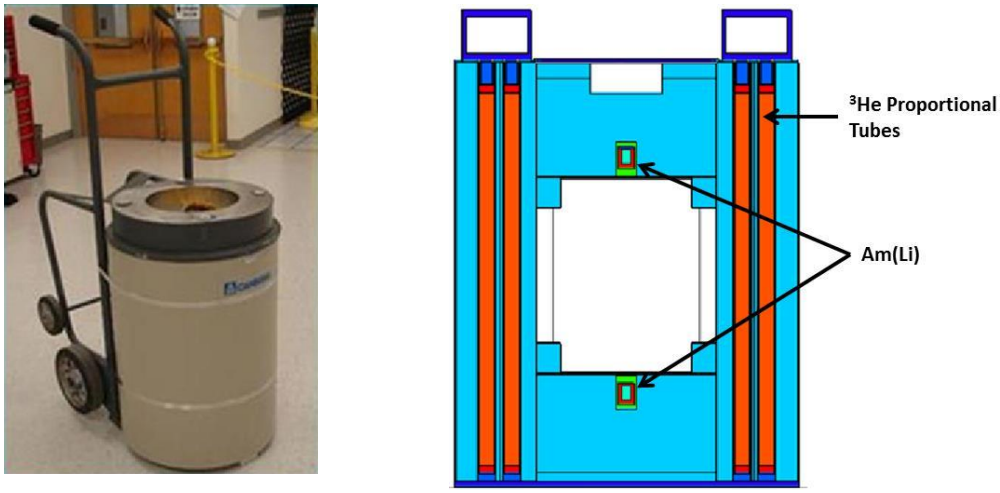

Figure 1. Photograph of the LV-AWCC (*left*) and a diagram of the LV-AWCC generated from the MCNPX input file (*right*). The LV-AWCC diagram has been adjusted to show the inner and outer ring of tubes, which are not normally visible at the same time in the vertical cross section through the counter.

Table 1. Comparison of AWCC and LV-AWCC characteristics

	AWCC	LV-AWCC	LV-AWCC/Graphite
Assay cavity (ID × OD)	20.6 × 22.9 cm	37.4 × 28.0 cm	37.4 × 28.0 cm
^{3}He proportional tubes			
Quantity	42 tubes	48 tubes	48 tubes
Active Length	50.8 cm	63.5 cm	63.5 cm
Efficiency (bare ^{252}Cf at cavity center)	26.4%	30%	34%
Die-away time	50 µs	54 µs	52 µs

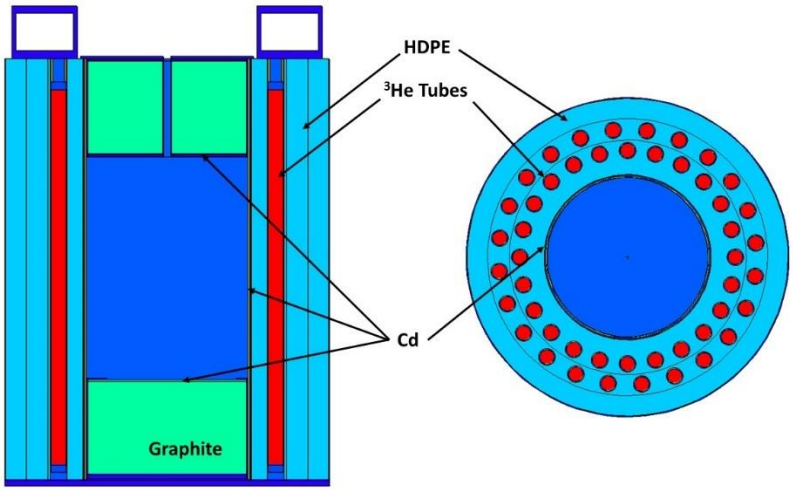

Figure 2. Diagram of the modified LV-AWCC with graphite end-plugs installed.

3.2 Measurements

Measurements were performed using the LV-AWCC of 3 neutron sources, one ^{252}Cf and two Am(Li). The ^{252}Cf source, CF1830, was characterized at NIST (Mn bath measurement) with a certified neutron yield known to +/-1%. The Am(Li) sources manufactured by Gammatron (N458 and N459) each with nominal yield of 50,000 n/s. The sources were each measured inside increasing thicknesses of High Density Polyethylene (HDPE) in spherical and cylindrical configurations. Measurements were performed using both traditional shift register electronics (JSR-15) and list mode acquisition (PTR-32). The LV-AWCC is configured to provide separate outputs from both the inner and outer rings and the summed signal for the counter. (Note: Although our intent was to record the signals from each of the three signals for each measurement, operational issues with the PTR-32 caused the loss of inner and outer ring data for several measurements such that for some configurations only the sum signal data was recorded).

Polyethylene Spheres and Cylinders

High Density Polyethylene (HDPE) moderators in both cylindrical and spherical form were used for these measurements. The poly spheres were fabricated as a set of nesting shells. The shells fit tightly together so that when assembled they can be considered as a single component. The poly cylinders were comprised of either two or four pieces (top, bottom, cap and barrel). The dimensions and masses of each component were measured multiple times, the average values for each component are provided in Tables 2 to 4.

Table 2. HDPE Spherical Shell Properties					
Shell	ID (cm)	OD (cm)	Volume (cc)	Mass (g)	Density (g/cm^3)
1	3.14	4.40	28.34	27.15	0.9579
2	4.40	7.09	142.00	133.05	0.9369
3	7.09	9.62	279.68	262.40	0.9382
4	9.62	12.33	514.80	478.10	0.9287
5	12.33	14.97	775.47	732.35	0.9444
6	14.97	17.32	963.11	919.05	0.9543

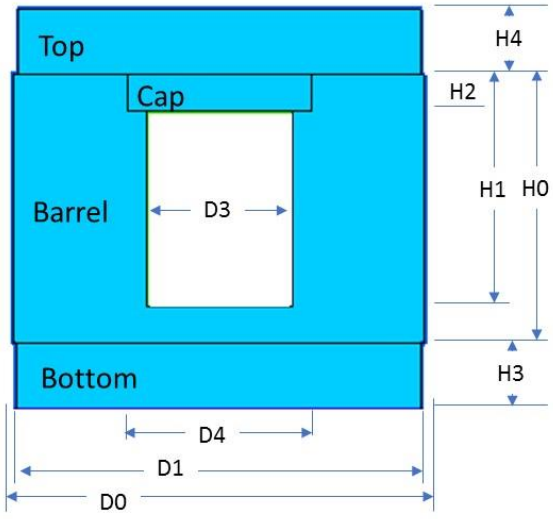

Figure 3. Sketch of a Poly Cylinder

Table 3. Properties of the poly cylinder barrel component.

Cylinder	D0	D3	D4	H0	H1	H2	Mass	Volume	Density
1	41.30	28.50	35.05	50.45	43.30	6.00	37.100	38.00	0.9763
2	54.15	28.60	35.10	50.04	43.10	6.30	80.900	85.50	0.9462
3	66.60	28.50	34.95	50.72	43.20	6.30	141.500	147.11	0.9619
4	77.40	28.55	34.95	50.95	43.20	6.33	200.700	210.05	0.9555
5	91.70	28.50	35.00	50.55	43.30	6.30	295.400	304.18	0.9711
6	104.45	28.40	34.90	50.55	43.40	6.30	390.800	403.61	0.9683
7	117.00	28.50	34.90	50.60	43.30	6.20	491.200	514.42	0.9549
8	130.00	28.80	35.00	50.80	43.50	5.90	608.700	644.11	0.9450
9	155.45	28.00	34.70	50.75	43.30	6.20	885.100	934.47	0.9472

Table 4. Properties of the poly cylinder top and bottom disk components.

	Disk 1					Disk 2				
Cylinder	D1	H3	Mass	Volume	Density	D1	H4	Mass	Volume	Density
1	---	---	---	---	---	---	---	---	---	---
2	---	---	---	---	---	---	---	---	---	---
3	63.55	6.20	19.30	19.67	0.9814	63.40	6.25	19.30	19.7	0.9782
4	76.10	12.60	55.40	57.31	0.9667	75.95	12.60	55.10	57.1	0.9652
5	88.70	18.88	111.90	116.66	0.9592	88.70	18.90	113.10	116.8	0.9684
6	101.65	25.40	196.50	206.13	0.9533	101.65	25.35	196.20	205.7	0.9537
7	114.20	31.60	310.50	323.68	0.9593	114.10	31.60	310.00	323.1	0.9594
8	127.80	38.05	460.90	488.10	0.9443	128.00	38.00	460.10	489.0	0.9409
9	152.20	50.85	885.10	925.15	0.9567	152.20	50.80	883.80	924.2	0.9562

Cylinders 1 and 2 did not have an associated top or bottom disk.

^{252}Cf Measurements

The ^{252}Cf source was measured first by itself centered in the LV-AWCC assay cavity using a standard lab jack. The source was then placed inside each of the poly cylinders, centered in the central void using a low-density plastic foam. The height of the lab jack was adjusted for each measurement to position the ^{252}Cf source in the center of the assay cavity. The measurements were performed using a JSR-15 shift register with pre-delay of 4.5 µs and gate width setting of 64 µs. The inner and outer ring signals were recorded through the Aux Scaler inputs and the sum signal provided both singles and doubles rates for the source. The rates were corrected for background and deadtime. The corrected rates are presented in Table 5. Measurements were then performed placing the ^{252}Cf source within the nested spherical shells. The inner diameter of the sphere was 3.14 cm for each of the configurations. The results are presented in Table 6.

Table 5. Net rates for ^{252}Cf source CF1830 located within the collection of poly cylinders.

Measured Rates: Cf-Source in Poly Cylinders (8/19/2015)					n/s = 489936 ± 4899						
MCNP Configuration	Cylinder OD	Inner Ring		Outer Ring		Sum Signal		Sum Doubles		Singles Ring Ratio	
Bare 252Cf - No Poly	0.00	100710	± 59	67444	± 48	168056	± 26	59725	± 201	1.4932	± 0.0014
252Cf in HDPE cylinder	4.13	104074	± 60	65592	± 47	169492	± 24	61235	± 163	1.5867	± 0.0015
252Cf in HDPE cylinder	5.42	104665	± 60	63102	± 46	167531	± 25	59430	± 151	1.6587	± 0.0015
252Cf in HDPE cylinder	6.66	103893	± 60	59568	± 45	163306	± 26	56861	± 174	1.7441	± 0.0017
252Cf in HDPE cylinder	7.74	100845	± 59	55839	± 43	156492	± 27	52254	± 161	1.8060	± 0.0018
252Cf in HDPE cylinder	9.17	94804	± 57	50579	± 41	145309	± 23	44815	± 132	1.8744	± 0.0019
252Cf in HDPE cylinder	10.45	87806	± 55	46007	± 39	133539	± 26	37855	± 148	1.9085	± 0.0020
252Cf in HDPE cylinder	11.70	80281	± 52	41363	± 37	121368	± 24	30953	± 119	1.9409	± 0.0022
252Cf in HDPE cylinder	13.00	72547	± 50	36983	± 35	109345	± 14	25186	± 117	1.9616	± 0.0023
252Cf in HDPE cylinder	15.55	56964	± 44	28920	± 31	85722	± 20	15595	± 102	1.9697	± 0.0026

Table 6. Net rates for ^{252}Cf source CF1830 located within the poly spheres.

Measured Rates, Poly Spheres, Cf-1830 (8/7/2015)					n/s = 494173 ± 4942						
MCNP Configuration	Sphere OD	Inner Ring		Outer Ring		Sum Signal		Sum Doubles		Singles Ring Ratio	
Bare 252Cf - No Poly	0.00	101510	± 59	67992	± 48	169466	± 31	169466	± 31	1.4820	± 0.0014
252Cf in HDPE Sphere	4.40	104171	± 60	66572	± 47	170687	± 18	170687	± 18	1.5519	± 0.0014
252Cf in HDPE Sphere	7.00	105150	± 60	60599	± 45	165772	± 38	165772	± 38	1.7183	± 0.0016
252Cf in HDPE Sphere	9.70	98031	± 58	53060	± 42	150760	± 28	150760	± 28	1.8293	± 0.0018
252Cf in HDPE Sphere	12.20	85031	± 54	44228	± 39	129021	± 19	129021	± 19	1.9053	± 0.0021
252Cf in HDPE Sphere	15.00	70079	± 49	35800	± 35	105660	± 17	105660	± 17	1.9426	± 0.0023
252Cf in HDPE Sphere	17.30					85063	± 22	85063	± 22		

The two Am(Li) sources were measured with and without a cadmium wrapping (1 mm thick) and the tungsten source bottles (Table 7). Each Am(Li) source contains approximately 4E10 Bq of ^{241}Am, the sources are normally placed within the tungsten source bottles to minimize gamma-ray exposure to personnel. The observed count rates for these measurements were unaffected by the presence or absence of the Cd or tungsten. This demonstrates that the gamma-ray exposure from the Am(Li) source has no impact on the measurement results. Comparison of the Cd-wrapped and bare source measurement shows that there is no significant thermal neutron emission from the sources. Table 7 also presents the observed rates obtained with the Cd wrapped Am(Li) source placed within the two smaller poly cylinders and a single poly spherical shell. Table 7 presents the only individual ring rates obtained with the Am(Li) sources during this measurement campaign.

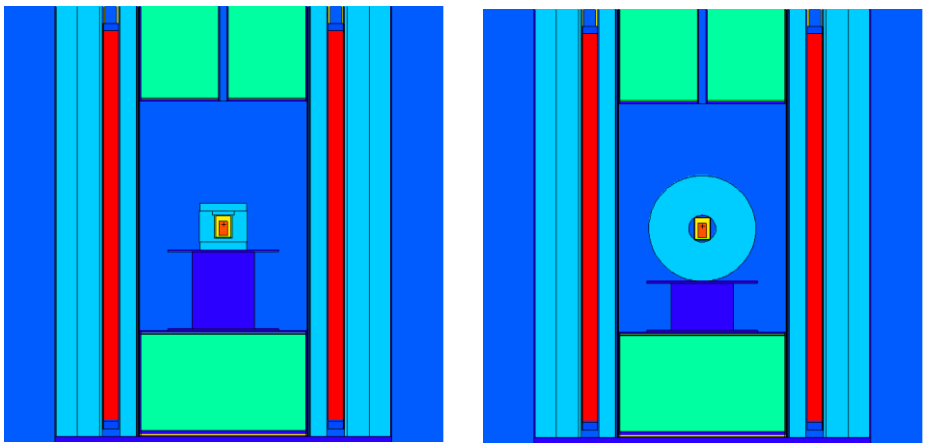

Figure 4. Illustration of the measurement arrangement of the Am(Li) sources within the poly cylinders (left) and the poly spheres (right) in the LV-AWCC.

Table 7. Net rates for the two Am(Li) sources with ring ratios in various configurations.

Am(Li) Ring Ratio Measurements - Measured Rates						
	N458 rates			N459 rates		
Measurement Configuration	Inner Ring	Outer Ring	Sum	Inner Ring	Outer Ring	Sum
AmLi Bare	13054 ± 21	6471 ± 15	19525 ± 26	13333 ± 21	6578 ± 15	19912 ± 26
Am(Li) Cd	13035 ± 21	6471 ± 15	19506 ± 25	13340 ± 21	6623 ± 15	19963 ± 26
Am(Li) in W	13081 ± 21	6467 ± 15	19548 ± 26	13345 ± 21	6652 ± 15	19997 ± 26
Am(Li) in W	13046 ± 21	6521 ± 15	19567 ± 26			
Am(Li) Cd in 1.5x2 poly cyl	13042 ± 21	5901 ± 14	18943 ± 25	13346 ± 21	6041 ± 14	19387 ± 25
Am(Li) Cd in 2x2 poly cyl	12643 ± 21	5313 ± 13	17956 ± 24	12924 ± 21	5425 ± 13	18349 ± 25
Am(Li) Cd in 9.7 cm sphere (w/o 7cm sphere)				12579 ± 20	5261 ± 13	17840 ± 24

The Am(Li) sources were too large to fit within the smallest spherical polyethylene shell. The Am(Li) source was wrapped in 1 mm cadmium (a rolled Cd cylinder and two Cd disks were fabricated for this purpose) and placed within the 4.4 cm OD poly shell and assayed, centering the sphere within the assay cavity and making every effort to maintain the Am(Li) source in a constant orientation (upright within the sphere). The observed rates (background and deadtime corrected) are shown in Table 8.

Table 8. Net rates for the Am(Li) sources within the poly spheres.

Measurement Configuration	Sphere* OD	AmL(Li) 458 Singles Rates	AmL(Li) 459 Singles Rates	AmL(Li) 458 Norm Singles Rates	AmL(Li) 459 Norm Singles Rates
Am(Li) wrapped in Cd - No Poly	0.0	19526.66 ± 10.26	19966.14 ± 8.77	1.0000 ± 0.0005	1.0000 ± 0.0004
Am(Li) wrapped in Cd in Poly Sphere	4.4				
Am(Li) wrapped in Cd in Poly Sphere	7.0	17772.41 ± 6.45	18181.06 ± 7.15	0.9102 ± 0.0003	0.9106 ± 0.0004
Am(Li) wrapped in Cd in Poly Sphere	9.7	14318.51 ± 6.22	14645.34 ± 6.20	0.7333 ± 0.0003	0.7335 ± 0.0003
Am(Li) wrapped in Cd in Poly Sphere	12.2	10311.00 ± 4.82	10519.06 ± 7.91	0.5280 ± 0.0002	0.5268 ± 0.0004
Am(Li) wrapped in Cd in Poly Sphere	15.0	6833.11 ± 4.93	7000.63 ± 5.98	0.3499 ± 0.0003	0.3506 ± 0.0003
Am(Li) wrapped in Cd in Poly Sphere	17.3	4522.50 ± 3.29	4640.08 ± 4.68	0.2316 ± 0.0002	0.2324 ± 0.0002

3.3 **MCNP Simulations**

Each measurement configuration was modeled using MCNPX and/or MCNP6 (to investigate potential issues with fission neutron energy distributions used by MCNP). Most of simulations were performed using MCNPX because the LV-AWCC model was created prior to the release of MCNP6 and the models are known to work well using the older (MCNPX) executable and libraries.

3.3.1 ^{252}CF SIMULATIONS

The ^{252}Cf spontaneous energy distribution developed by Mannhardt [INDC(NDS)-220(1989)305] was used to evaluate the base model for the LV-AWCC. The ^{252}Cf source was modeled as stainless steel cylinder with a point source located near one end of the capsule. The source was centered within the empty volume at the center of the spheres and cylinders. The resulting simulated efficiencies are given in Table 9 and the measured efficiencies are given in Table 10. A simple comparison of the measured and simulated efficiencies is provided in Figure 5 and Figure 6. From the scaling it is difficult to assess the closeness of the simulations to reality, so the data have been replotted in Figure 7 and Figure 8 showing the ratio of simulated over measured rates. From the figures it appears there is dependence on the ratio of simulated to measured efficiencies with polyethylene thickness suggesting an energy dependence and a potential short-coming in the LV-AWCC model. We note that in Figure 7 and Figure 8 the inner, outer and summed signals exhibit the same behavior where we might expect the inner and outer rings to have somewhat opposing dependences.

Table 9. MCNPX simulated detection efficiencies for the ^{252}Cf measurements in the LV-AWCC.

Geometry	Moderator	ID	OD	Inner Ring Efficiency		Outer Ring Efficiency		Summed Efficiency		Singles Ring Ratio	
Sphere	None			0.2081	± 0.0002	0.1388	± 0.0001	0.3469	± 0.0002	1.4999	± 0.0018
Sphere	HDPE	3.06	4.40	0.2130	± 0.0002	0.1356	± 0.0001	0.3486	± 0.0002	1.5706	± 0.0019
Sphere	HDPE	3.06	7.09	0.2135	± 0.0002	0.1235	± 0.0001	0.3371	± 0.0002	1.7286	± 0.0022
Sphere	HDPE	3.06	9.62	0.1964	± 0.0002	0.1059	± 0.0001	0.3022	± 0.0002	1.8551	± 0.0025
Sphere	HDPE	3.06	12.33	0.1702	± 0.0001	0.0889	± 0.0001	0.2592	± 0.0002	1.9141	± 0.0028
Sphere	HDPE	3.06	14.97	0.1372	± 0.0001	0.0703	± 0.0001	0.2074	± 0.0002	1.9519	± 0.0032
Sphere	HDPE	3.06	17.32	0.1116	± 0.0001	0.0569	± 0.0001	0.1685	± 0.0001	1.9618	± 0.0036
Cylinder	none	0	0.00	0.2081	± 0.0002	0.1388	± 0.0001	0.3469	± 0.0002	1.4999	± 0.0018
Cylinder	HDPE	2.76	4.13	0.2132	± 0.0002	0.1350	± 0.0001	0.3482	± 0.0002	1.5792	± 0.0019
Cylinder	HDPE	2.76	5.42	0.2148	± 0.0002	0.1303	± 0.0001	0.3451	± 0.0002	1.6482	± 0.0020
Cylinder	HDPE	2.76	6.66	0.2125	± 0.0002	0.1220	± 0.0001	0.3345	± 0.0002	1.7412	± 0.0022
Cylinder	HDPE	2.76	7.74	0.2058	± 0.0002	0.1141	± 0.0001	0.3199	± 0.0002	1.8033	± 0.0024
Cylinder	HDPE	2.76	9.17	0.1925	± 0.0002	0.1031	± 0.0001	0.2957	± 0.0002	1.8665	± 0.0025
Cylinder	HDPE	2.76	10.45	0.1775	± 0.0001	0.0932	± 0.0001	0.2707	± 0.0002	1.9040	± 0.0027
Cylinder	HDPE	2.76	11.70	0.1622	± 0.0001	0.0841	± 0.0001	0.2462	± 0.0002	1.9297	± 0.0029
Cylinder	HDPE	2.76	13.00	0.1468	± 0.0001	0.0753	± 0.0001	0.2221	± 0.0002	1.9498	± 0.0031
Cylinder	HDPE	2.76	15.55	0.1139	± 0.0001	0.0582	± 0.0001	0.1721	± 0.0001	1.9579	± 0.0035

Table 10. Measured detection efficiencies for the ^{252}Cf measurements in the LV-AWCC.

Geometry	Moderato	ID	OD	Inner Ring		Outer Ring		Sum Signal	
Sphere	None			0.2054	± 0.0021	0.1376	± 0.0014	0.3429	± 0.0001
Sphere	HDPE	3.06	4.40	0.2108	± 0.0021	0.1347	± 0.0014	0.3454	± 0.0000
Sphere	HDPE	3.06	7.09	0.2128	± 0.0021	0.1226	± 0.0012	0.3355	± 0.0001
Sphere	HDPE	3.06	9.62	0.1984	± 0.0020	0.1074	± 0.0011	0.3051	± 0.0001
Sphere	HDPE	3.06	12.33	0.1721	± 0.0017	0.0895	± 0.0009	0.2611	± 0.0000
Sphere	HDPE	3.06	14.97	0.1418	± 0.0014	0.0724	± 0.0007	0.2138	± 0.0000
Sphere	HDPE	3.06	17.32					0.1721	± 0.0000
Cylinder	none	0	0.00	0.2056	± 0.0021	0.1377	± 0.0014	0.3430	± 0.0034
Cylinder	HDPE	2.76	4.13	0.2124	± 0.0021	0.1339	± 0.0013	0.3459	± 0.0035
Cylinder	HDPE	2.76	5.42	0.2136	± 0.0021	0.1288	± 0.0013	0.3419	± 0.0034
Cylinder	HDPE	2.76	6.66	0.2121	± 0.0021	0.1216	± 0.0012	0.3333	± 0.0033
Cylinder	HDPE	2.76	7.74	0.2058	± 0.0021	0.1140	± 0.0011	0.3194	± 0.0032
Cylinder	HDPE	2.76	9.17	0.1935	± 0.0019	0.1032	± 0.0010	0.2966	± 0.0030
Cylinder	HDPE	2.76	10.45	0.1792	± 0.0018	0.0939	± 0.0009	0.2726	± 0.0027
Cylinder	HDPE	2.76	11.70	0.1639	± 0.0016	0.0844	± 0.0008	0.2477	± 0.0025
Cylinder	HDPE	2.76	13.00	0.1481	± 0.0015	0.0755	± 0.0008	0.2232	± 0.0022
Cylinder	HDPE	2.76	15.55	0.1163	± 0.0012	0.0590	± 0.0006	0.1750	± 0.0018

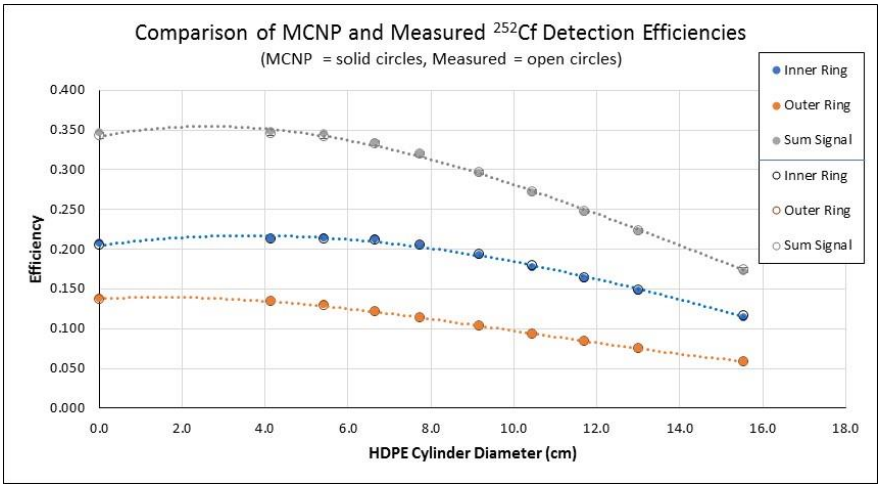

Figure 5. Comparison of the measured and predicted detection efficiency for ^{252}Cf neutrons emitted within the poly cylinders (The dashed lines represent an unweighted polynomial fit to the data and are presented as an eye guide only).

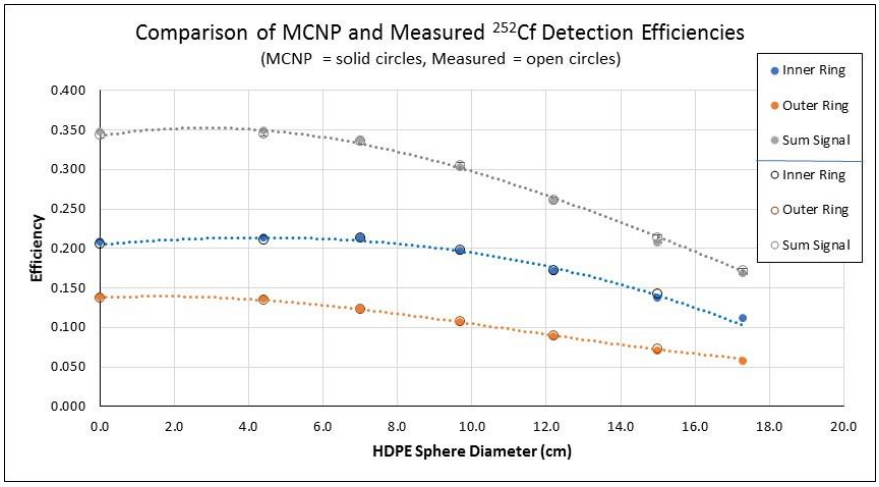

Figure 6. Comparison of the measured and predicted detection efficiency for ^{252}Cf neutrons emitted within the poly spheres (The dashed lines represent an unweighted polynomial fit to the data and are presented as an eye guide only).

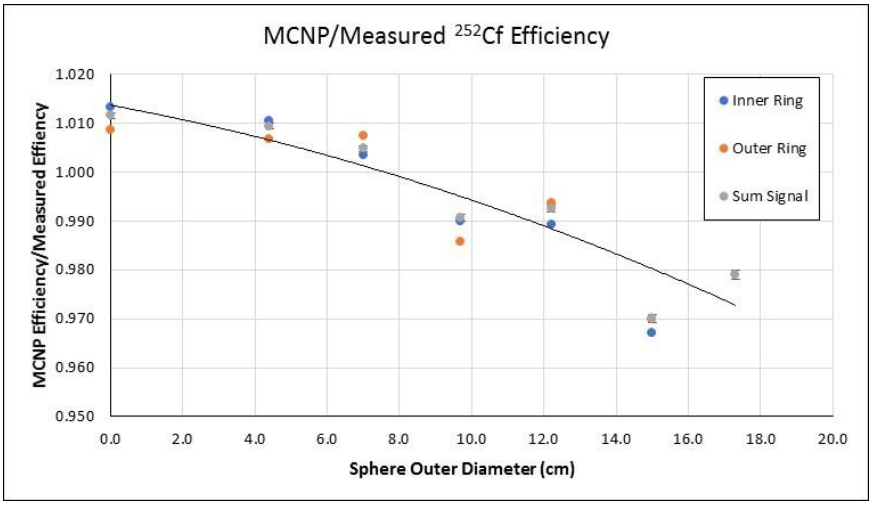

Figure 7. Ratio of the simulated and measured detection efficiencies for the ^{252}Cf source located within the poly spheres (The line represents an unweighted polynomial fit to the data and is presented as an eye guide only).

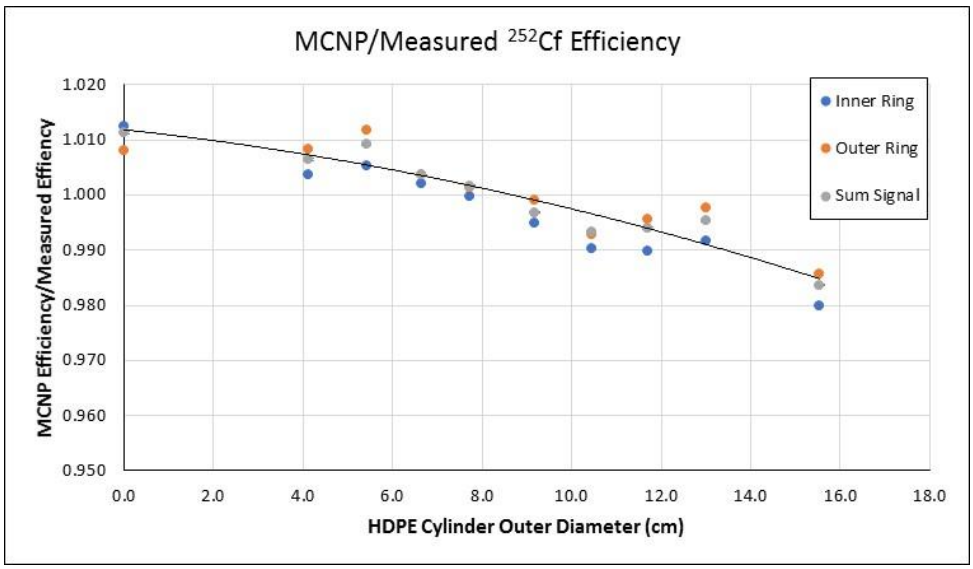

Figure 8. Ratio of the simulated and measured detection efficiencies for the ^{252}Cf source located within the poly cylinders (The line represents an unweighted polynomial fit to the data and is presented as an eye guide only).

A preliminary investigation into this behavior was performed by variation of key parameters in MCNP model. The poly sphere models were rerun after increasing the HDPE density of the counter body from 0.95 g/cc to 0.97 g/cc. The change in moderator density resulted in an increased spread between the inner and outer rings results (Figure 9) but the overall trend is the same as seen in Figure 7. Similarly decreasing the ^{3}He partial pressure (Figure 10) tended to exaggerate the overall trend. These results indicate that a drastic change in detector parameters would be required to reproduce the observed behavior. Based on this observation, it was decided to examine the impact of the poly shell material definition. Although the volumes and weights of the poly components were measured, the chemical form of the poly has some potential for ambiguity because the hydrogen to carbon ratio may not be 2:1 depending upon the specific type of polyethylene (e.g. low density polyethylene has a much higher number of branches per chain than does high density polyethylene reducing the relative number of hydrogen to carbon atoms). For a preliminary examination, simulations of the ^{252}Cf in poly spheres were tun with the modeled density of the spheres was arbitrarily reduced by 3%. The results, plotted in Figure 11, suggest that the trending seen in Figure 7 may be due to an overestimate of the hydrogen content of the poly spheres.

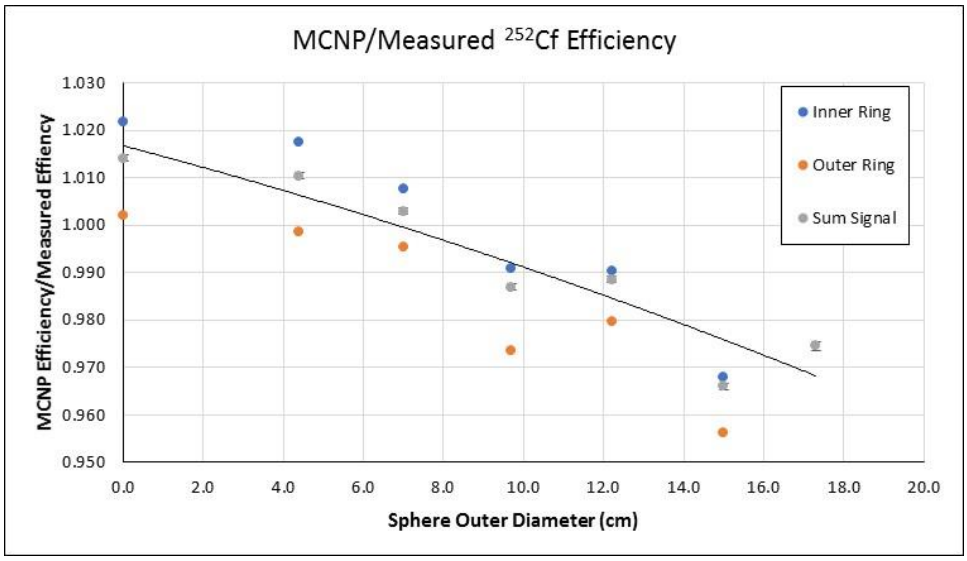

Figure 9. Ratio of the simulated and measured detection efficiencies for the ^{252}Cf source located within the poly spheres after the LV-AWCC moderator assembly density was increased to 0.97 g/cc. (Line is provided as an eye guide).

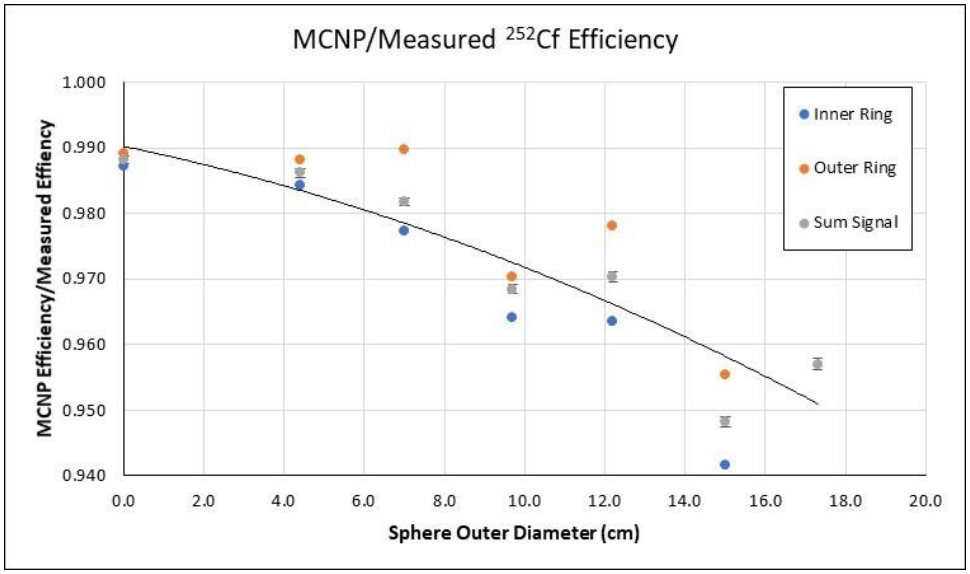

Figure 10. Ratio of the simulated and measured detection efficiencies for the ^{252}Cf source located within the poly spheres after the LV-AWCC ^{3}He partial pressure was reduced to 4 atm. (Line is provided as an eye guide).

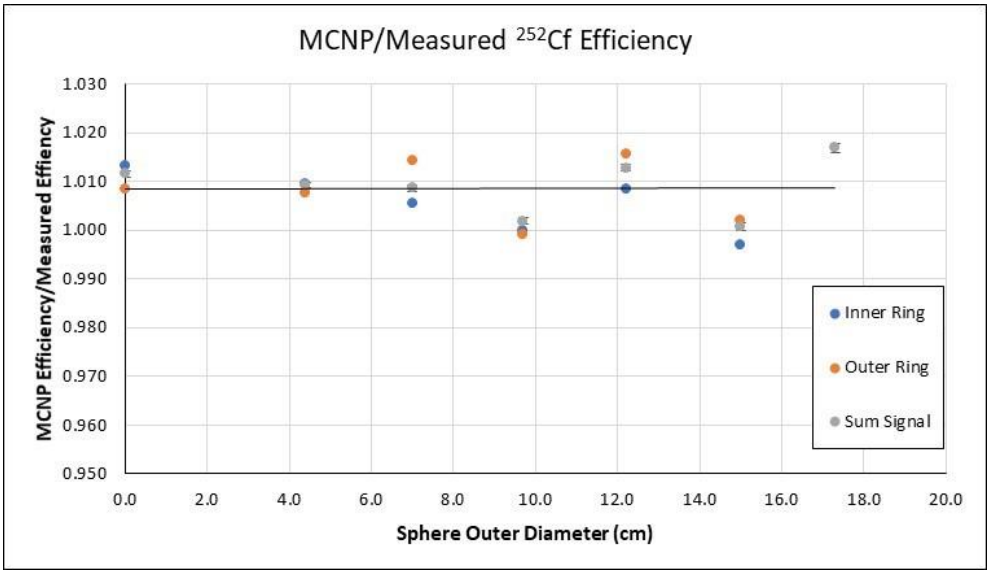

Figure 11. Ratio of the simulated and measured detection efficiencies for the ^{252}Cf source located within the poly spheres where the poly sphere density has been reduced by 3%. (Line is provided as an eye guide).

3.3.2 AM(LI) SIMULATIONS

3.3.2.1 Energy Distributions

The LV-AWCC performance was examined using seven Am(Li) neutron energy distributions. The spectra represent the more common use distributions for modeling purpose. The distributions examined in this study include:

- Sources 4C: <E> = 689 keV.
  Spectrum generated assuming the elemental composition . The spectrum was generated for 100 equal width energy bins from 0 to 4 MeV. This distribution has the greatest fraction of neutrons above Chemical composition includes AmO_2 and LiOH
  {Note: this definition of source-4C is a version elaborated by Dr.R.McElroy, different from the one we used in the part I of the report, as it contains also a high energy part of the spectrum[1]}

[1] Sources4C distribution: The Am(Li) source material was assumed to be a mixture of AmO_2 and LiOH with 3% of the total (α, n) neutron emission produced by the O(α, n) reaction and 2.3% of the total neutron spectrum were emitted with energy of 2MeV or greater. Spontaneous and induced fission events contribute less than 0.03% to the total neutron emission rate and can be ignored for the purposes of this evaluation.

- Owens: <E> = 529 keV
  DR Weaver, JG Owen and J Walker,"The neutron spectrum from a 5 Ci Am/Li neutron source", Nucl. Instrum. and Meths. 198(1982)599-602.

- Thomas: <E> = 478 keV
  This is the Tagziria emergent spectrum for the source NPL-AmLi X14 and is based on NPL's evaluation. It was provided numerically by Dr David Thomas, Prov. Comm. See Tagzirai et al, NIM in PR A510(2003)346, and Tagziria et al Radiat Prot Dosim 110(Nos. 1-4)(2004)129.

- IPPE: <E>=492 keV
  Neutron spectrum from Obninsk Russia IPPE, private communication from Phil M Rinard to S. Croft, 1st June 2011

- VDZ: <E> = 472 keV
  Neutron spectrum from Geiger and van der Zwan HP 21(July)(1971)120-123

- Werle: <E> = 433 keV
  "Spektrumsmessungen radioaktiver neutronenquellen im energiebereich von 10 keV bis 10 MeV mit protonenrückstoß-proportionalzählrohen", Kernforschungszentrum Karlsruhe, West Germany; Institut für Neutronenphysik und Reaktortechnik, Karlsruhe Nuclear Research Centre Report KFK-INR-4/70-25 Feb. 1970. In English Translation as ORNL-tr-2415/

- Trykov: <E> = 368 keV
  "Investigations of AmO2-LiH neutron sources characteristics" L.A. Trykov, V.A. Chernov and S.V. Rabochy. This work is referred to by Tagziria & Looman [ARI 70(2012)2395-2402]. The article was obtained by the present authors from Marc Looman via Priv. Comm. and does not have a a formal citation that we know of.

A comparison of the normalized neutron energy distributions is provided in Figure 12. The plot shows that distributions such as Trykov, IPPE and Thomas include a larger fraction of lower energy (<50 keV) than the other spectra. While the Sources 4C distribution provides the hardest neutron energy spectrum.

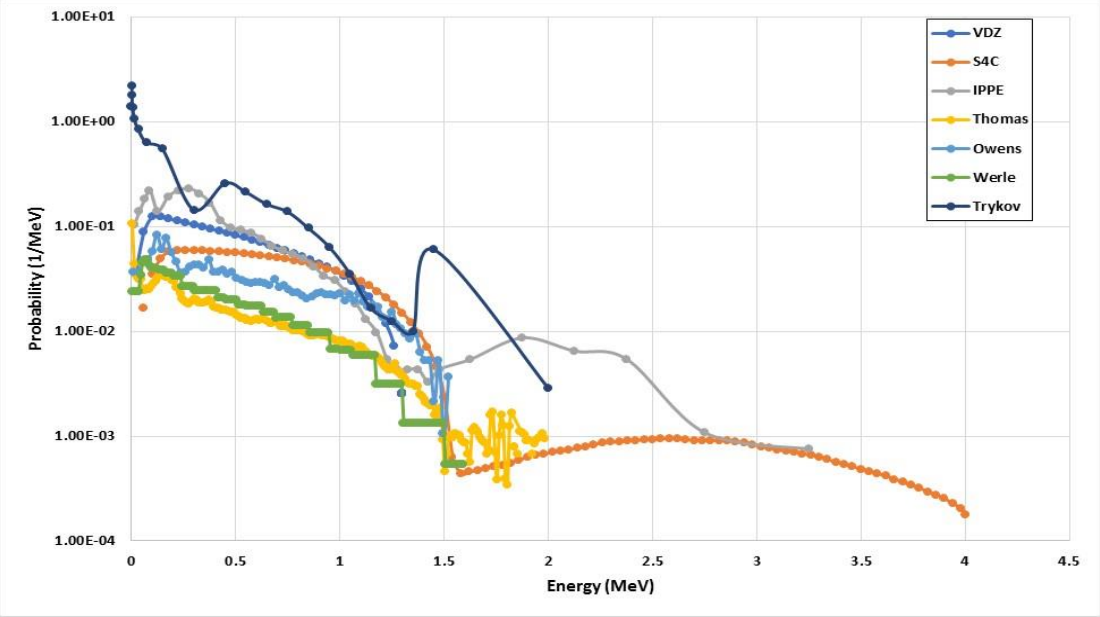

Figure 12. Comparison of the neutron energy distributions used in this study (Lines are presented as an eye guide only).

3.3.3 Am(Li) Simulated Efficiencies and Comparison to Measured Values

Each of the measured Am(Li) source/poly configuration were modeled using MCNPX. Efficiencies for the inner ring, outer ring, and sum signal were determined from the simulations. The inner and outer ring efficiencies were then used to calculated the simulated ring ratio for each configuration.

The simulated neutron detection efficiencies for the Am(Li) source ring ratio measurements are presented in Table 11 for each of the 7 neutron energy distributions. The measurement geometries for each configuration are shown in Figure 13. The measured ring ratios and the simulated results are summarized in Table 12 and the ratio of simulated to measured ring ratios are presented in Table 13. From Table 13 we see that the Geiger-Van der Swann distribution reproduces the observed ring ratios more closely than any of the other energy distributions while the Trykov and IPPE distributions provide the poorest representation of the measured values. We note that the variation of the ring ratios for each of the energy distributions about the mean value is roughly the same for each distribution. A sufficient number of particles were run for each simulation so that the statistical precision of the results were small in comparison to the measured values. The variations about the mean ring ratios may possibly be attributed to source positioning/alignment errors.

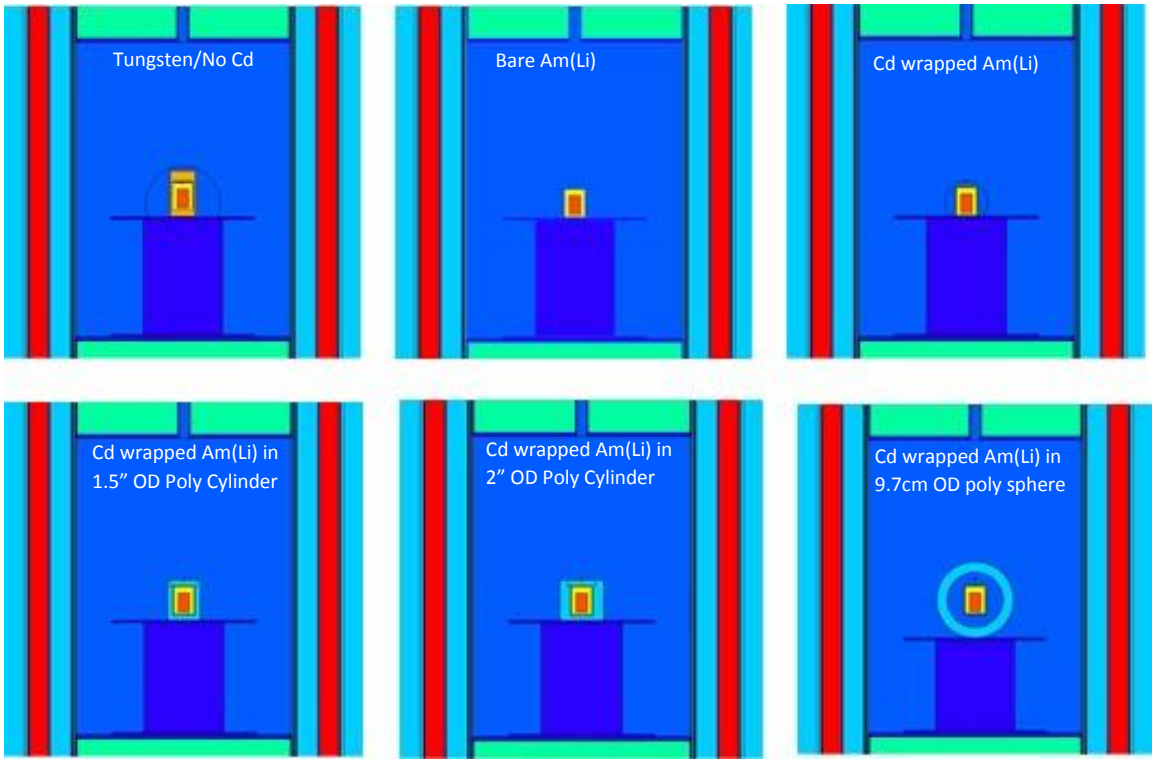

Figure 13. Illustration of the measurement geometries for the Am(Li) ring ratio measurements.

The Am(Li) sources were each placed inside a series of poly spheres on increasing thickness and measured. Each measurement was simulated using MCNPX. Unfortunately, ring ratio data were unavailable for these measurements. The measured and simulated efficiencies for each diameter poly sphere is presented in Table 14. The ratio of each simulated efficiency to its corresponding measured value is presented in Table 15 and plotted in Figure 14 and Figure 15 for each of the seven energy distributions. From Figure 14 we see that the efficiencies determined using each of the neutron energy distributions trends favorably with the measured efficiencies.

The simulated efficiencies for two of the neutron distributions, the Sources 4C and Owens agree remarkably well with the measured efficiencies. However, the uncertainty in neutron yield from the 2 Am(Li) sources is estimated to be ±3% at the 1 sigma level. A better indicator of the value of the energy distribution is the standard deviation for the collection of measurements for each distribution. A lower standard deviation indicates that the energy dependence is better represented by the neutron energy distribution, so that we consider the Sources 4C, Owens and Van der Zwan distributions to be equally valid at this stage in the analysis. (The data in Table 15 was renormalized to the source only measurement configuration and shown in Table 16 and Figure 16 to provide a clearer illustration of the response as a function poly sphere diameter.)

Table 11. MCNP generated efficiencies for the Am(Li) ring ratio measurements.

	Poly Shell									
					Am(Li) Source in tungsten bottle on lab jack centered in cavity					
Energy Distribution	ID	OD	Inner Ring Efficiency		Outer Ring Efficiency		Summed Efficiency		**Singles Ring Ratio**	
Sources 4c	0	0	0.2653	± 0.0001	0.1364	± 0.0000	0.4016	± 0.0001	1.9455	± 0.0008
Owens	0	0	0.2679	± 0.0001	0.1357	± 0.0000	0.4036	± 0.0001	1.9734	± 0.0008
Thomas	0	0	0.2697	± 0.0001	0.1299	± 0.0000	0.3997	± 0.0001	2.0758	± 0.0009
IPPE	0	0	0.2674	± 0.0001	0.1265	± 0.0000	0.3938	± 0.0001	2.1143	± 0.0009
VDZ	0	0	0.2714	± 0.0001	0.1359	± 0.0000	0.4073	± 0.0001	1.9969	± 0.0008
Werle	0	0	0.2734	± 0.0001	0.1317	± 0.0001	0.4051	± 0.0001	2.0762	± 0.0012
Trykov	0	0	0.2750	± 0.0001	0.1228	± 0.0001	0.3978	± 0.0001	2.2395	± 0.0014
	Poly Shell									
					Bare Am(Li) on lab jack centered in cavity					
Energy Distribution	ID	OD	Inner Ring Efficiency		Outer Ring Efficiency		Summed Efficiency		**Singles Ring Ratio**	
Sources 4c	0	0	0.2654	± 0.0001	0.1364	± 0.0001	0.4018	± 0.0001	1.9464	± 0.0011
Owens	0	0	0.2678	± 0.0001	0.1355	± 0.0001	0.4032	± 0.0001	1.9765	± 0.0012
Thomas	0	0	0.2702	± 0.0001	0.1298	± 0.0001	0.4000	± 0.0001	2.0817	± 0.0012
IPPE	0	0	0.2674	± 0.0001	0.1262	± 0.0001	0.3935	± 0.0001	2.1197	± 0.0013
VDZ	0	0	0.2713	± 0.0001	0.1355	± 0.0001	0.4068	± 0.0001	2.0019	± 0.0012
Werle	0	0	0.2735	± 0.0001	0.1313	± 0.0001	0.4048	± 0.0001	2.0822	± 0.0012
Trykov	0	0	0.2758	± 0.0001	0.1226	± 0.0001	0.3984	± 0.0001	2.2484	± 0.0014
	Poly Shell									
					Am(Li) wrapped in Cd on lab jack centered in cavity					
Energy Distribution	ID	OD	Inner Ring Efficiency		Outer Ring Efficiency		Summed Efficiency		**Singles Ring Ratio**	
Sources 4c	0	0	0.2651	± 0.0001	0.1357	± 0.0001	0.4008	± 0.0002	1.9528	± 0.0016
Owens	0	0	0.2676	± 0.0001	0.1354	± 0.0001	0.4029	± 0.0001	1.9769	± 0.0012
Thomas	0	0	0.2696	± 0.0002	0.1297	± 0.0001	0.3992	± 0.0002	2.0784	± 0.0025
IPPE	0	0	0.2670	± 0.0002	0.1261	± 0.0001	0.3931	± 0.0002	2.1168	± 0.0026
VDZ	0	0	0.2712	± 0.0002	0.1355	± 0.0001	0.4067	± 0.0002	2.0017	± 0.0024
Werle	0	0	0.2731	± 0.0001	0.1312	± 0.0000	0.4043	± 0.0001	2.0817	± 0.0009
Trykov	0	0	0.2751	± 0.0001	0.1225	± 0.0001	0.3976	± 0.0001	2.2461	± 0.0014
	Poly Shell									
							Am(Li) Cd in 1.5x2 poly cyl			
Energy Distribution	ID	OD	Inner Ring Efficiency		Outer Ring Efficiency		Summed Efficiency		**Singles Ring Ratio**	
Sources 4c	2.76	4.13	0.2646	± 0.0001	0.1235	± 0.0001	0.3881	± 0.0002	2.1419	± 0.0018
Owens	2.76	4.13	0.2677	± 0.0001	0.1233	± 0.0001	0.3910	± 0.0001	2.1714	± 0.0013
Thomas	2.76	4.13	0.2677	± 0.0002	0.1173	± 0.0001	0.3849	± 0.0002	2.2827	± 0.0028
IPPE	2.76	4.13	0.2649	± 0.0002	0.1134	± 0.0001	0.3783	± 0.0002	2.3368	± 0.0029
VDZ	2.76	4.13	0.2715	± 0.0002	0.1225	± 0.0001	0.3940	± 0.0002	2.2157	± 0.0027
Werle	2.76	4.13	0.2717	± 0.0001	0.1182	± 0.0000	0.3899	± 0.0001	2.2987	± 0.0010
Trykov	2.76	4.13	0.2705	± 0.0001	0.1092	± 0.0001	0.3798	± 0.0001	2.4765	± 0.0016
	Poly Shell									
							Am(Li) Cd in 2x2 poly cyl			
Energy Distribution	ID	OD	Inner Ring Efficiency		Outer Ring Efficiency		Summed Efficiency		**Singles Ring Ratio**	
Sources 4c	2.76	5.42	0.2570	± 0.0001	0.1126	± 0.0001	0.3697	± 0.0002	2.2821	± 0.0020
Owens	2.76	5.42	0.2604	± 0.0001	0.1125	± 0.0001	0.3730	± 0.0001	2.3145	± 0.0015
Thomas	2.76	5.42	0.2572	± 0.0002	0.1053	± 0.0001	0.3625	± 0.0002	2.4431	± 0.0032
IPPE	2.76	5.42	0.2545	± 0.0002	0.1013	± 0.0001	0.3558	± 0.0002	2.5108	± 0.0033
VDZ	2.76	5.42	0.2632	± 0.0002	0.1106	± 0.0001	0.3739	± 0.0002	2.3792	± 0.0030
Werle	2.76	5.42	0.2627	± 0.0001	0.1069	± 0.0000	0.3696	± 0.0001	2.4574	± 0.0011
Trykov	2.76	5.42	0.2581	± 0.0001	0.0979	± 0.0001	0.3560	± 0.0001	2.6379	± 0.0018
	Poly Shell									
							Am(Li) Cd in 9.7 cm sphere (w/o 7cm sphere)			
Energy Distribution	ID	OD	Inner Ring Efficiency		Outer Ring Efficiency		Summed Efficiency		**Singles Ring Ratio**	
Sources 4c	7.00	9.7	0.2510	± 0.0001	0.1107	± 0.0001	0.3617	± 0.0002	2.2670	± 0.0020
Owens	7.00	9.7	0.2538	± 0.0001	0.1102	± 0.0001	0.3639	± 0.0001	2.3039	± 0.0015
Thomas	7.00	9.7	0.2507	± 0.0002	0.1038	± 0.0001	0.3545	± 0.0002	2.4155	± 0.0032
IPPE	7.00	9.7	0.2481	± 0.0002	0.0997	± 0.0001	0.3477	± 0.0002	2.4884	± 0.0033
VDZ	7.00	9.7	0.2568	± 0.0002	0.1090	± 0.0001	0.3658	± 0.0002	2.3567	± 0.0030
Werle	7.00	9.7	0.2552	± 0.0001	0.1044	± 0.0000	0.3596	± 0.0001	2.4452	± 0.0011
Trykov	7.00	9.7	0.2495	± 0.0001	0.0950	± 0.0001	0.3446	± 0.0001	2.6257	± 0.0018

Table 12. Measured and Simulated Am(Li) ring ratios.

Configuration	Measured Ring Ratio		S4C		Owens		Thomas		IPPE		VDZ		Werle		Trykov	
AmLi Bare	2.022	± 0.004	1.9464	± 0.0011	1.9765	± 0.0012	2.0817	± 0.0012	2.1197	± 0.0013	2.0019	± 0.0012	2.0822	± 0.0012	2.2484	± 0.0014
Am(Li) Cd	2.014	± 0.004	1.9528	± 0.0016	1.9769	± 0.0012	2.0784	± 0.0025	2.1168	± 0.0026	2.0017	± 0.0024	2.0817	± 0.0009	2.2461	± 0.0014
Am(Li) in W	2.023	± 0.004	1.9455	± 0.0008	1.9734	± 0.0008	2.0758	± 0.0009	2.1143	± 0.0009	1.9969	± 0.0008	2.0762	± 0.0012	2.2395	± 0.0014
Am(Li) Cd in 1.5x2 poly cyl	2.210	± 0.004	2.1419	± 0.0018	2.1714	± 0.0013	2.2827	± 0.0028	2.3368	± 0.0029	2.2157	± 0.0027	2.2987	± 0.0010	2.4765	± 0.0016
Am(Li) Cd in 2x2 poly cyl	2.381	± 0.005	2.2821	± 0.0020	2.3145	± 0.0015	2.4431	± 0.0032	2.5108	± 0.0033	2.3792	± 0.0030	2.4574	± 0.0011	2.6379	± 0.0018
Am(Li) Cd in 9.7 cm sphere (w/o 7cm sphere	2.391	± 0.007	2.2670	± 0.0020	2.3039	± 0.0015	2.4155	± 0.0032	2.4884	± 0.0033	2.3567	± 0.0030	2.4452	± 0.0011	2.6257	± 0.0018

Table 13. Comparison of the Measured and Simulated Am(Li) Ring Ratios.

	Ratio of simulated to		Simulated/Measured Ring Ratio													
Configuration	Measured Ring Ratios		S4C		Owens		Thomas		IPPE		VDZ		Werle		Trykov	
AmLi Bare	1.000		0.963	± 0.002	0.977	± 0.002	1.029	± 0.002	1.048	± 0.002	0.990	± 0.002	1.030	± 0.002	1.112	± 0.002
Am(Li) Cd	1.000		0.969	± 0.002	0.981	± 0.002	1.032	± 0.002	1.051	± 0.002	0.994	± 0.002	1.033	± 0.002	1.115	± 0.002
Am(Li) in W	1.000		0.962	± 0.002	0.976	± 0.002	1.026	± 0.002	1.045	± 0.002	0.987	± 0.002	1.026	± 0.002	1.107	± 0.002
Am(Li) Cd in 1.5x2 poly cyl	1.000		0.969	± 0.002	0.983	± 0.002	1.033	± 0.002	1.057	± 0.003	1.003	± 0.002	1.040	± 0.002	1.121	± 0.002
Am(Li) Cd in 2x2 poly cyl	1.000		0.959	± 0.002	0.972	± 0.002	1.026	± 0.003	1.055	± 0.003	0.999	± 0.002	1.032	± 0.002	1.108	± 0.002
Am(Li) Cd in 9.7 cm sphere (w/o 7cm sphere	1.000		0.948	± 0.003	0.964	± 0.003	1.010	± 0.003	1.041	± 0.003	0.986	± 0.003	1.023	± 0.003	1.098	± 0.003
Average			0.962		0.975		1.026		1.050		0.993		1.031		1.110	
Standard Deviation			0.008		0.007		0.008		0.006		0.007		0.006		0.008	

Table 14. Measured and Simulated detection efficiencies for the poly spheres with Am(Li).

Am(Li) measured and modeled neutron detection efficinecies																
Sphere OD	Measured*		VDZ		S4C		IPPE		Thom		Owens		Werle		Trykov	
0.0	0.3998	+/- 0.0002	0.4067	+/- 0.0002	0.4008	+/- 0.0002	0.3931	+/- 0.0002	0.3992	+/- 0.0002	0.4029	+/- 0.0001	0.4043	+/- 0.0001	0.3976	+/- 0.0001
7.0	0.3639	+/- 0.0001	0.3592	+/- 0.0002	0.3544	+/- 0.0001	0.3403	+/- 0.0002	0.3472	+/- 0.0002	0.3574	+/- 0.0002	0.3521	+/- 0.0001	0.3359	+/- 0.0001
9.7	0.2932	+/- 0.0001	0.2827	+/- 0.0002	0.2826	+/- 0.0001	0.2609	+/- 0.0002	0.2693	+/- 0.0002	0.2838	+/- 0.0002	0.2722	+/- 0.0001	0.2505	+/- 0.0001
12.2	0.2109	+/- 0.0001	0.2083	+/- 0.0002	0.2119	+/- 0.0001	0.1876	+/- 0.0002	0.1965	+/- 0.0002	0.2114	+/- 0.0002	0.1970	+/- 0.0001	0.1758	+/- 0.0001
15.0	0.1400	+/- 0.0001	0.1330	+/- 0.0001	0.1404	+/- 0.0001	0.1174	+/- 0.0001	0.1260	+/- 0.0001	0.1384	+/- 0.0001	0.1237	+/- 0.0000	0.1074	+/- 0.0001
17.3	0.0927	+/- 0.0001	0.0873	+/- 0.0001	0.0951	+/- 0.0001	0.0766	+/- 0.0001	0.0836	+/- 0.0001	0.0931	+/- 0.0001	0.0800	+/- 0.0000	0.0684	+/- 0.0000
Cd wrapped Am(Li) source located inside HDPE sphere, each sphere is centered veritically and radially within the assay cavity.																
** includes statistical errors only*																

Table 15. Ratios of simulated to measured detection efficiencies for the Am(Li) sources in the poly spheres.

Am(Li) neutron detection efficinecy ratio of modeled to measured values.																
Sphere OD	Measured		VDZ		S4C		IPPE		Thom		Owens		Werle		Trykov	
0.0	1.0000	+/- 0.0005	1.0174	+/- 0.0008	1.0027	+/- 0.0007	0.9834	+/- 0.0008	0.9987	+/- 0.0008	1.0080	+/- 0.0006	1.0113	+/- 0.0006	0.9947	+/- 0.0006
7.0	1.0000	+/- 0.0003	0.9871	+/- 0.0007	0.9739	+/- 0.0005	0.9351	+/- 0.0007	0.9539	+/- 0.0007	0.9821	+/- 0.0007	0.9676	+/- 0.0004	0.9228	+/- 0.0004
9.7	1.0000	+/- 0.0003	0.9643	+/- 0.0008	0.9638	+/- 0.0006	0.8900	+/- 0.0007	0.9186	+/- 0.0007	0.9681	+/- 0.0008	0.9285	+/- 0.0005	0.8545	+/- 0.0005
12.2	1.0000	+/- 0.0002	0.9879	+/- 0.0009	1.0052	+/- 0.0007	0.8898	+/- 0.0008	0.9321	+/- 0.0009	1.0026	+/- 0.0009	0.9345	+/- 0.0005	0.8339	+/- 0.0005
15.0	1.0000	+/- 0.0003	0.9501	+/- 0.0011	1.0025	+/- 0.0010	0.8383	+/- 0.0011	0.9002	+/- 0.0011	0.9882	+/- 0.0012	0.8837	+/- 0.0007	0.7667	+/- 0.0007
17.3	1.0000	+/- 0.0002	0.9414	+/- 0.0013	1.0258	+/- 0.0011	0.8255	+/- 0.0012	0.9018	+/- 0.0013	1.0039	+/- 0.0014	0.8627	+/- 0.0007	0.7373	+/- 0.0007
Average			0.975		0.996		0.894		0.934		0.992		0.931		0.852	
St.Dev.			0.028		0.023		0.059		0.037		0.015		0.054		0.096	

Table 16. Normalized Ratios of simulated to measured detection efficiencies for the Am(Li) sources in the poly spheres.

Am(Li) neutron detection efficinecy ratio of modeled to measured values.													
Sphere OD	**Measured**	**VDZ**		**S4C**		**IPPE**		**Thom**		**Owens**		**Werle**		**Trykov**	
0.0	1.0000	1.0000	+/- 0.0007	1.0000	+/- 0.0006	1.0000	+/- 0.0007	1.0000	+/- 0.0007	1.0000	+/- 0.0005	1.0000	+/- 0.0005	1.0000	+/- 0.0005
7.0	1.0000	0.9702	+/- 0.0007	0.9713	+/- 0.0006	0.9508	+/- 0.0007	0.9552	+/- 0.0007	0.9743	+/- 0.0007	0.9568	+/- 0.0004	0.9278	+/- 0.0005
9.7	1.0000	0.9478	+/- 0.0007	0.9612	+/- 0.0006	0.9050	+/- 0.0007	0.9198	+/- 0.0007	0.9604	+/- 0.0008	0.9181	+/- 0.0004	0.8591	+/- 0.0005
12.2	1.0000	0.9710	+/- 0.0010	1.0025	+/- 0.0009	0.9048	+/- 0.0010	0.9333	+/- 0.0010	0.9947	+/- 0.0011	0.9240	+/- 0.0007	0.8384	+/- 0.0007
15.0	1.0000	0.9339	+/- 0.0012	0.9998	+/- 0.0011	0.8524	+/- 0.0011	0.9013	+/- 0.0012	0.9804	+/- 0.0013	0.8738	+/- 0.0008	0.7709	+/- 0.0008
17.3	1.0000	0.9253	+/- 0.0014	1.0230	+/- 0.0013	0.8394	+/- 0.0014	0.9030	+/- 0.0014	0.9960	+/- 0.0015	0.8531	+/- 0.0009	0.7412	+/- 0.0009
Average		0.958		0.993		0.909		0.935		0.984		0.921		0.856	
St.Dev.		0.028		0.023		0.060		0.037		0.015		0.054		0.097	
Cd wrapped Am(Li) source located inside HDPE sphere, each sphere is centered veritically and radially within the assay cavity.															

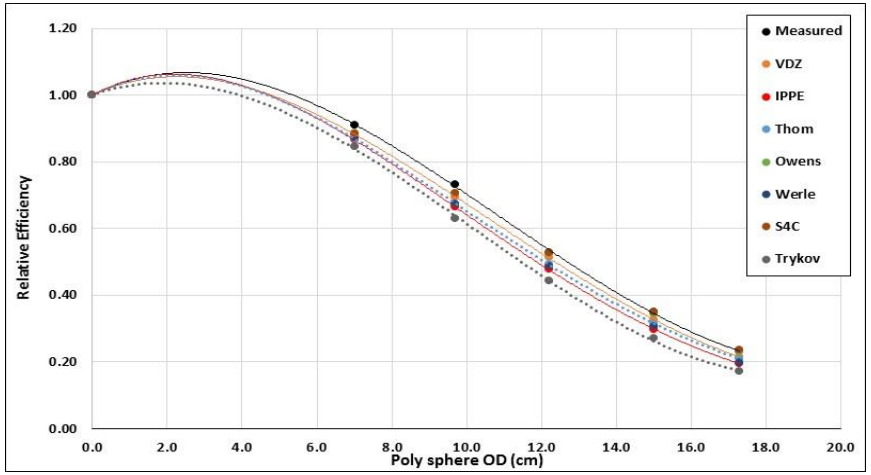

Figure 14. Relative Am(Li) neutron detection efficiency as a function of HDPE sphere OD ***(The lines represent an unweighted polynomial fit to the data and is presented as an eye guide only)*****.**

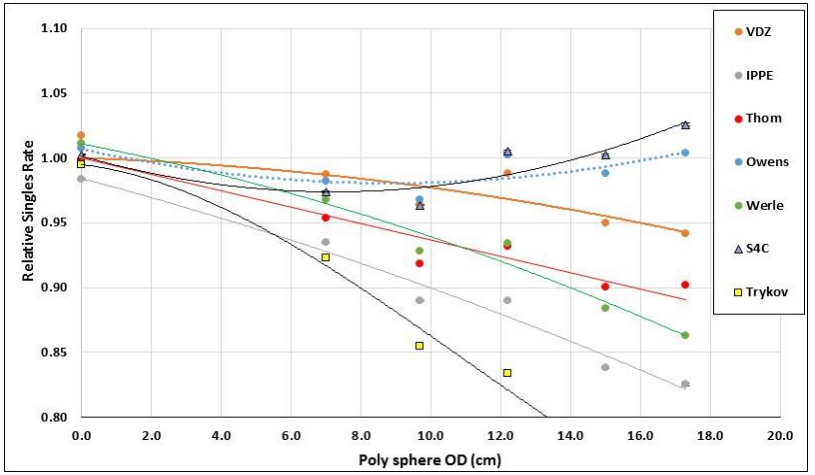

Figure 15. Am(Li) neutron detection efficiency ratio of modeled to measured values as a function of HDPE sphere OD*(The lines represent an unweighted polynomial fit to the data and is presented as an eye guide only)*.**.**

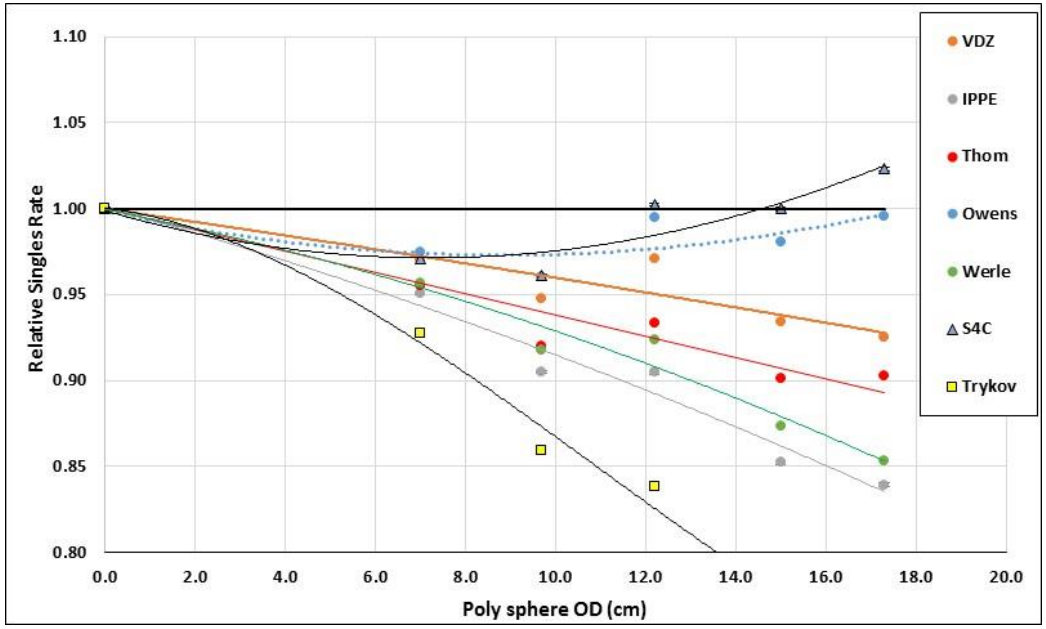

Figure 16. Am(Li) neutron detection efficiency ratio of modeled to measured values (normalized to no HDPE) ***(The lines represent an unweighted polynomial fit to the data and is presented as an eye guide only)*****.**

3.4 CONCLUSIONS – SENSITIVITY STUDY

- The Owens spectrum and the spectrum generated using Source4C reproduce the observed dependence of the efficiency on the moderator content. The Owens representation not only provides excellent overall agreement with the measured data but also reproduces the trend (i.e. lowest standard deviation).
- The ratio of simulated and measured ring ratios is consistent across the measured configurations for a given energy distribution. That is the standard deviation of the ratios is small (~0.7%) for each spectrum compared to the average biases which varied from 0.7% to 11% for a given spectrum.
- The Geiger Van der Zwan spectrum provided the best match of the limited ring ratio data.
- Although we cannot definitively select the "best" Am(Li) spectrum, our results suggest that the Trykov and IPPE spectra are poor representations of the Am(Li) neutron energy spectrum. These spectra provide the two least promising results for the sum spectrum dependence and ring ratio measurements deviating from the measured values by twice amount of the other spectra examined.
- The IPPE, Trykov and Werle distributions have a larger low energy (<100 keV) component than the more successful spectra. Arbitrarily truncating the low energy component of these spectra improves their performance.
- The three most promising spectra examined are that of Owens, Geiger and Van der Zwan and the Sources 4C representation.
- More accurate absolute neutron yield values for the Am(Li) sources would simplify the evaluation of the neutron energy distributions. If possible a more fully characterized source should be used for these analyses (e.g. measurement in a $MnSO_4$ bath).

3.5 FUTURE WORK

This study represents an initial effort to more accurately defining the interrogating neutron energy distribution from Am(Li). To continue this effort, we need to provide a more robust validation of the MCNP model of the detector and acquire data using more robust (reliable) electronics modules and analysis software. The suggested next steps are:

- Obtain data from additional Am(Li) sources: We have examined only 2 Am(Li) sources so far. These two sources were produced in the same batch by the manufacturer. Different sources are known to have difference contaminants. While we have identified better and lessor performing spectra for these two sources, it may not be true for others.

- Obtain Additional Ring Ratio Data: The ring ratio data available did not span a wide dynamic range of moderator for the Am(Li) sources.

- Obtain Additional Data using a higher efficiency, multi-ring counter that has been optimized for uniformity in energy response.

- Model Sensitivity Analysis: Examine the sensitivity of the model to fabrication assumptions (e.g. HDPE density, tube placement, and poly shell composition). The results of the sensitivity analysis will identify critical design parameters for verification (e.g. density analysis of moderating components).

- Perform a high-resolution gamma spectroscopy study to identify and quantify any impurities which could produce neutrons. This includes O and for example Be and F.

- Extend the measurements and analysis to evaluate the potential of unfolding the spectrum from a data set generated by counting HDPE encased Am(Li) sources. This includes construction energy dependent response functions.

A sensitivity analysis to the simulation choices (e.g. LV AWCC as-built materials and configuration) should be undertaken.

Part IV – Gamma Related Activities

4.1.1 Enrichment measurements performed at LASAL

Gamma-ray measurements are used to confirm the operator's U-235 enrichment declaration of nuclear material (NM) found in nuclear fuel cycle.

Since technology advances, such as hardware (detector´s, multichannel analyzers- MCA) and software (multichannel analyzers control, gamma-ray spectra acquisition and enrichment analysis), it is necessary to LASAL being updated with the state of art of nuclear material measurements.

4.1.2 Medium Resolution Gamma Spectrometry (MRGS)

Medium resolution detector´s (e.g. $LaBr_3$ scintillation) replaced the low-resolution scintillation detector (NaI) and digital MCA´s will replace analogic MCA´s.

The LASAL had available two $LaBr_3$ detectors (Ø 38×38mm) one analog MCA (GBS 166) and one digital MCA (GBS 527 base). However, the analysis software NaIGEM needed to be update to a version able to analyze medium resolution spectra ($LaBr_3$).

DOE has provided the NaIGEM v. 2.1.4 able to analyze $LaBr_3$ spectra.

A plan of measurements to compare 2 systems was established. This plan consisted on the following:

System 1

Equipment:

- Detector $LaBr_3$ Ø 38×38mm length
- Analogic MCA (GBS 166)
- Collimator 20 Ø mm×20 mm depth
- No Cd filter
- Standards SRM 969: 031; 071; 194; 295 and 446
    - 0.3166 ± 0.0002%, 0.7119 ± 0.0005%, 1.9420 ± 0.0014%, 2.9492 ± 0.0021%, 4.4623 ± 0.0021% mass enrichment in ^{235}U (from National Bureau of Standards Certificate)
- Steel attenuators: 0, 4 , 8, 12 and 16 mm

Software:

- WinSpec v. 2.04.0000
- NaIGEM v. 2.1.4

System 2 (loan by ABACC)

Equipment:

- Detector $LaBr_3$ Ø 38×38mm length
- Digital MCA (GBS 527 base)
- Collimator 30 mm Ø x 15 mm depth. Collimator is built in lead.
- Standards SRM 969: 031; 071; 194; 295 and 446
    - 0.3166 ± 0.0002%, 0.7119 ± 0.0005%, 1.9420 ± 0.0014%, 2.9492 ± 0.0021%, 4.4623 ± 0021% mass enrichment in ^{235}U
    - Steel attenuators: 0, 4 , 8, 12 and 16 mm
- 1 mm Cd filter in front of the detector

Software:

- WinSpec v. 2.04.0000
- NaIGEM v. 2.1.4

These standards and attenuators covers all the enrichments and containers of NM found in the nuclear fuel cycle. A set of 20 spectra of 600 s for each standard and attenuator were taken and analyzed. An excel spreadsheet was prepared reporting the results.

Both set of results showed the systems tested could be properly used NM U-235 enrichment measurements. The results showed a better stability for the digital MCA.

LASAL provides NDA training for Safeguards inspectors in gamma-ray U-235 enrichment. With these updates, 11 inspectors were trained up to May, 2019.

4.1.3 Results

Figures 1 & 2 summarized the results of the measurement campaigns performed. As see in the plots, the results show a reliable determination of the uranium enrichment even with thick attenuators with the reduction of the signal to the detector. Increasing the attenuator thickness increase the uncertainties associated to the determined enrichment.

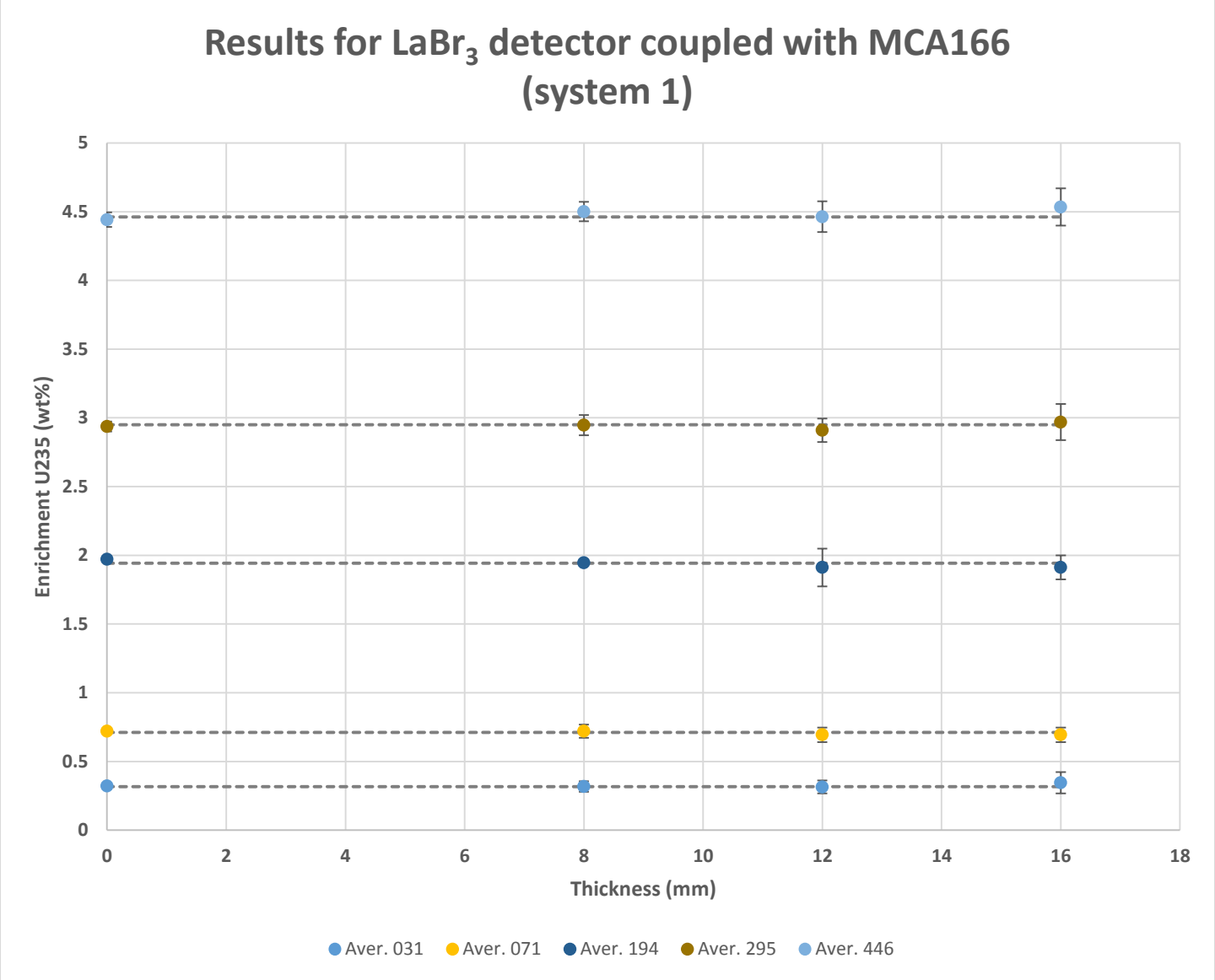

Figure 1. The plot reports the results of the enrichment extracted by the measurement, using NaIGEM for $LaBr_3$, as function of the thickness of the attenuator using system 1. Increasing the attenuator thickness the count rate is reduced and so the uncertainty increased as expected. The dash lines are added to show the expected values from the certificate and to guide the reader eyes.

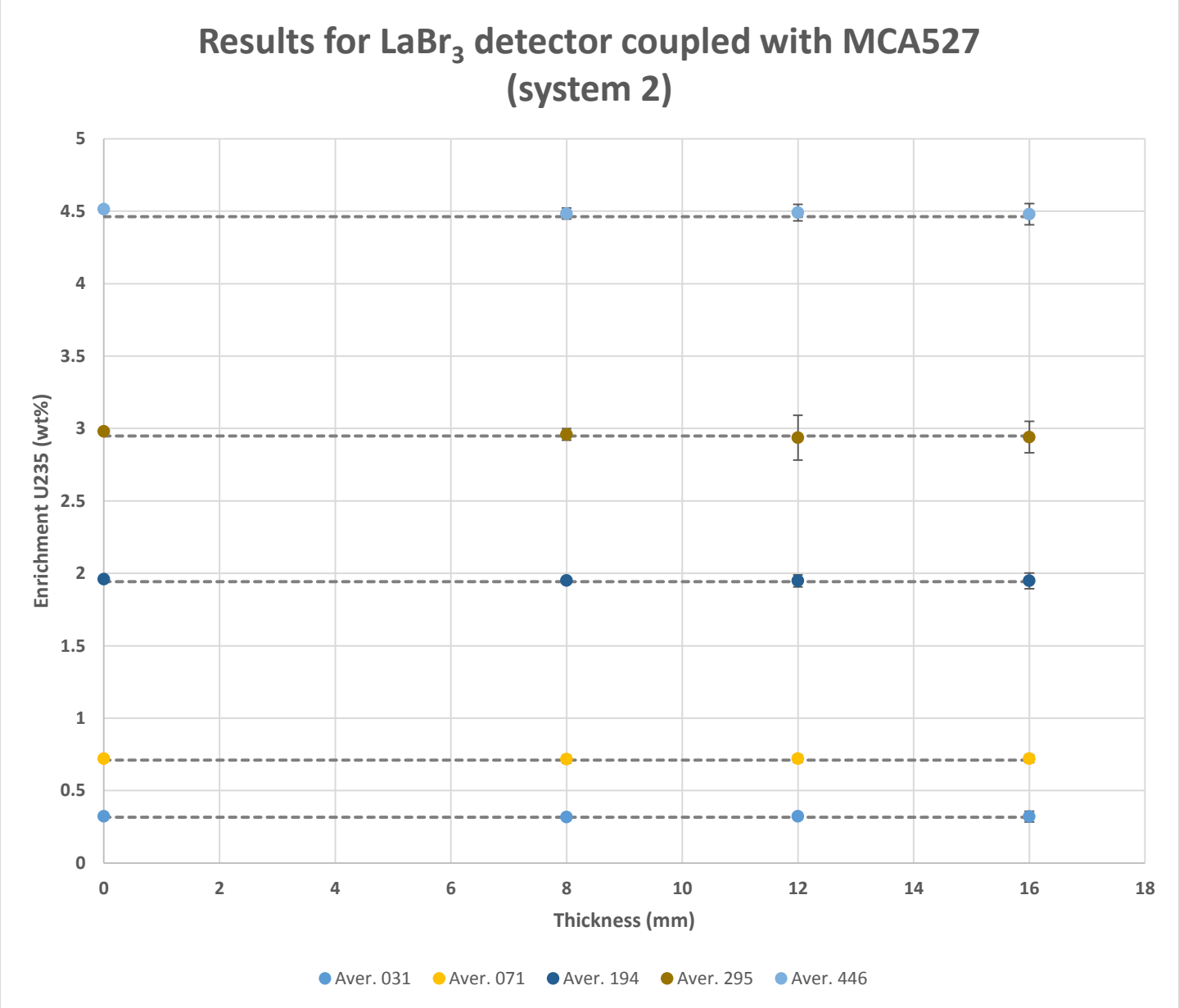

Figure 2. The plot reports results of the enrichment extracted by the measurement, using NaIGEM for $LaBr_3$, as function of the thickness of the attenuator using system 2. Increasing the attenuator thickness the count rate is reduced and so the uncertainty increased as expected. The dash lines are added to show the expected value from the certificate, and to guide the eyes.

4.1.4 High Resolution Gamma Spectrometry (HRGS)

LASAL analyses the U-235 enrichment of samples by HRGS at energies lower than 300 keV.

The results precision improves with better detector energy resolution (FWHM). To check this parameter, as well as identify x-ray and gamma ray peaks LASAL need an appropriate software.

LANL provided to LASAL the software PeakEasy to achieve LASAL demands. The software presents the state of the art in the gamma spectra analysis.

4.2 Enrichment Measurements using the NaI(Tl) Well Spectrometer

4.2.1 Abstract

Enrichment verification at the Resende nuclear fuel fabrication plant in Brazil is routinely performed using low resolution gamma spectroscopy (LRGS) on vials of solution. The overall uncertainty is strongly dependent on the quality control program used in the dissolution step, although a spectroscopic analysis likely will offer some advantages over the current region of interest (ROI) analysis, especially when gain stabilization is not employed. Bottom-up uncertainty quantification is likely to be difficult and incomplete. Fortunately there is an extensive database that can be used to perform a robust top-down uncertainty evaluation. We recommend that CNEN consider this approach.

4.2.2 Background

At the fuel fabrication facility in Resende the enrichment of U_3O_8 powder is verified by LRGS in a fixed counting geometry. The basic procedure is as follows. 2.5 grams of dry powder is dissolved in nitric acid to 25 mL. Two 10 mL samples are drawn with 5 mL spare/archive. After use the uranium is recycled. A 10 mL plastic vial of solution is placed into a shielded NaI(Tl) well counter. The solution extends above the top of the detector but an annulus of Pb on top of the end cap defines the effective height. Data acquisition is performed using the Canberra Industries INCA software with Genie2k. In 800 sec the statistical uncertainty on the net 186 keV peak feature directly from ^{235}U is typically a few tenths of % at 1-sigma. Three repeats are usually made both as a consistency check and also to reduce the random uncertainty further. The enrichment is directly proportional to the measured ^{235}U intensity. Representative standards are available for calibration including solutions prepared using IAEA certified 3.2 wt% enriched material, 4.25 wt% plant material, and various NBL certified reference materials. The operational range of the factory is quite narrow so that each unknown can be sandwiched by a pair of closely matched standards giving the enrichment determination the character of a relative measurement. This reduces systematic uncertainty. The analytical uncertainty on the reference solutions is tiny in comparison to other sources of uncertainty. The second vial of solution is used for impurity analysis and so the U/powder mass fraction is also verified. If there is a problem with the enrichment determination mass spectroscopy using the TIMS system can be used to resolve the question. This instrument is primarily used for UF_6-sample analysis but oxides can be measured with suitable analytical preparation of the sample. Following the hydrolyzation step material is loaded onto a filament which is pre-tested for conductivity before installation into the spectrometer.

4.2.3 Discussion and Recommendations

The repeat counts should ideally involve removing and repositioning the vial so as the capture the full repeatability uncertainty.

The use of light graded-Z filtering of vial using Sn/Cu would reduce x-ray and low energy contributions which don’t add useful information to the spectrum but may contribute to pile-up and other nuisance events. However

it is not practical to add filtering retrospectively because there is no space between the vial and the internal well-wall.

The overall accuracy of the method is *strongly* dependent on the powder weighing (a fundamental physical measurement) and dissolution (a simple chemical procedure) steps and also on the overall measurement control process. Consequently simple region of interest spectrum analysis provides a robust and statistically straightforward means of determining the net 186 keV peak feature counting rate which is fit for purpose. The better resolution of a $LaBr_3$(Ce)-well should offer a marginal benefit especially if used in conjunction with a spectroscopic analysis. The possible benefits of a spectroscopic analysis (e.g. the application specific code NaIGEM) should, however, be explored anyway because this offers a degree of auto-correction for temperature dependent gain and resolution drifts.

There is a 3”x3” well counter at LASAL which can be used to evaluate performance empirically. In Figure 1 we show photograph of the detector and shield arrangement at LASAL. This laboratory system provides ease of access and greater flexibility to try new things compared to experimenting on the in-plant system.

Figure 1. NaI(Tl) well detector at LASAL with the Pb-shield around it. The The Pb-annulus and shield lid are removed for viewing. On the right the top part of the shield

It is important to note that there exists already is a large data base of historical factory results which can be reanalyzed. Assessing the overall uncertainty of the enrichment determination by bottom-up analysis is likely to leave some uncertainty contributions hidden and others poorly predicted. Because of this we suggest that the best overall uncertainty estimate that can be made currently would make use of a top-down approach based on a Grubbs-type analysis of the extensive historical operator declared vs inspector measured paired data. We recommend that CNEN consider following this path, which can include a comparison of the ROI and spectroscopic (NaIGEM) algorithms. LANL/ORNL would be willing to assist in this assessment of the data

ACKNOWLEDGEMENTS

The work presented is funded by the United States Department of Energy (DOE) under action sheet AS-26 between the National Nuclear Energy Commission of Brazil (CNEN) and the United States Department of energy (DOE). The authors acknowledge the staff of Nuclear Fuel Fabrication Plant (INB) in Resende, as well as Dr. Fabio C. Dias, formerly CNEN, now ABACC, and C.R.Priest, a LANL summer student at the beginning of the project.

Appendix A - UO_2 (α,n) spectra in MCNP usable format

These spectra are determined from the data of Jacobs and Liskien (1983).

Spectra corresponding to alpha particle of 5 MeV:

SI5	SP5
H	D
0.00	0.00
0.10	0.0258554
0.20	0.0231337
0.30	0.0231337
0.40	0.0223561
0.50	0.0209953
0.60	0.0198289
0.70	0.0194401
0.80	0.0184681
0.90	0.0153577
1.00	0.0134137
1.10	0.0176905
1.20	0.0204121
1.30	0.0223561
1.40	0.0248834
1.50	0.0264386
1.60	0.0293546
1.70	0.0326594
1.80	0.0377138
1.90	0.0421851
2.00	0.0451011
2.10	0.0468507
2.20	0.0487947
2.30	0.0489891
2.40	0.0474339
2.50	0.0441291
2.60	0.0408243
2.70	0.0379082
2.80	0.0344090
2.90	0.0307154
3.00	0.0274106
3.10	0.0233281
3.20	0.0202177
3.30	0.0161353
3.40	0.0118585
3.50	0.0079705

3.60	0.0056376
3.70	0.0033048
3.80	0.0017496
3.90	0.0009720
4.00	0.0005832

Spectra corresponding to alpha particle of 4.5 MeV:

SI5	SP5
H	D
0.00	0.00
0.10	0.0115843
0.20	0.0109029
0.30	0.0091993
0.40	0.0109029
0.50	0.0115843
0.60	0.0146508
0.70	0.0132879
0.80	0.0126065
0.90	0.0166951
1.00	0.0204429
1.10	0.0197615
1.20	0.0204429
1.30	0.0224872
1.40	0.0282794
1.50	0.0330494
1.60	0.0405451
1.70	0.0459966
1.80	0.0548552
1.90	0.0620102
2.00	0.0603066
2.10	0.0603066
2.20	0.0606474
2.30	0.0599659
2.40	0.0538330
2.50	0.0477002
2.60	0.0419080
2.70	0.0364566
2.80	0.0306644
2.90	0.0248722
3.00	0.0204429
3.10	0.0146508
3.20	0.0105622

3.30	0.0088586
3.40	0.0054514
3.50	0.0027257
3.60	0.0013629

Spectra corresponding to average of 5 MeV and 4.5 MeV incident alpha particles:

SI5	SP5
H	D
0.000000E+00	0.000000E+00
1.000000E-01	1.871985E-02
2.000000E-01	1.701832E-02
3.000000E-01	1.616653E-02
4.000000E-01	1.662952E-02
5.000000E-01	1.628983E-02
6.000000E-01	1.723985E-02
7.000000E-01	1.636401E-02
8.000000E-01	1.553730E-02
9.000000E-01	1.602638E-02
1.000000E+00	1.692831E-02
1.100000E+00	1.872601E-02
1.200000E+00	2.042753E-02
1.300000E+00	2.242168E-02
1.400000E+00	2.658137E-02
1.500000E+00	2.974399E-02
1.600000E+00	3.494987E-02
1.700000E+00	3.932800E-02
1.800000E+00	4.628452E-02
1.900000E+00	5.209765E-02
2.000000E+00	5.270387E-02
2.100000E+00	5.357867E-02
2.200000E+00	5.472104E-02
2.300000E+00	5.447752E-02
2.400000E+00	5.063348E-02
2.500000E+00	4.591463E-02
2.600000E+00	4.136613E-02
2.700000E+00	3.718240E-02
2.800000E+00	3.253671E-02
2.900000E+00	2.779381E-02
3.000000E+00	2.392675E-02
3.100000E+00	1.898946E-02
3.200000E+00	1.538995E-02
3.300000E+00	1.249695E-02

3.400000E+00	8.654962E-03
3.500000E+00	5.348088E-03
3.600000E+00	3.500249E-03
3.700000E+00	1.652411E-03
3.800000E+00	8.748056E-04
3.900000E+00	4.860031E-04
4.000000E+00	2.916019E-04

Spectra corresponding to average of 5 MeV and 4.5 MeV incident alpha particles, extrapolated to 0 from 0.3 MeV:

SI5	SP5
H	D
0	0
0.10	0
0.20	0.002915559
0.30	0.005831117
0.40	0.011662234
0.50	0.015050923
0.60	0.018267598
0.70	0.017358666
0.80	0.01648201
0.90	0.016886759
1.00	0.017750334
1.10	0.019723462
1.20	0.021550047
1.30	0.023652277
1.40	0.027990202
1.50	0.031277011
1.60	0.036698327
1.70	0.041283982
1.80	0.048564158
1.90	0.054655395
2.00	0.055366313
2.10	0.056316241
2.20	0.057546176
2.30	0.057302805
2.40	0.05331816
2.50	0.048383586
2.60	0.043623471
2.70	0.03924891

2.80	0.034383248
2.90	0.029412038
3.00	0.025349759
3.10	0.020167454
3.20	0.016385183
3.30	0.013296388
3.40	0.009229749
3.50	0.005723124
3.60	0.003758717
3.70	0.001794309
3.80	0.000949928
3.90	0.000527738
4.00	0.000316643

Appendix B – Collection of initial and emergent AmLi spectra in MCNP usable format

References for AmLi spectra measurements

[Birch]
R Birch, LHJ Peaple, HJ Delafield Measurement of Neutron Spectra with Hydrogen Proportional Counters Part 1. Spectrometry System and Calibration United Kingdom Atomic Energy Authority Harwell Report AERE-R 11397 1984

[Delafield and Birch]
HJ Delfield and R Birch Neutron Spectrometry Measurements with Large Volume Cylindrical Proton Recoil Counters Developed for Use in Radiological Protection United Kingdom Atomic Energy Authority Harwell report AERE-R 13103 1989

[Geiger and van der Zwan]
KW Geiger, L van der Zwan, The neutron spectra and the resulting fluence-kerma conversions for AmLi and PoLi sources. Health Phys., 21 (1971), pp.120-123

[Ing]
H Ing et al 1981, The spectrum of neutrons from a pu-li source Health Physics 40(1981)345-350

[Obninsk] [Rinard and Menlove 1998; Rinard 2011]
[Rinard and Menlove 1998]
[Rinard, PM and Menlove, HO, "Calibration of the IAEA Active Well Coincidence Counter for Measurements of the Bruce 'A' Unirradiated Booster Rods" Los Alamos National Laboratory Report, LA-UR-98-4362,1998.
ALSO:
[Rinard 2011]
PM Rinard, Obninsk Russia IPPE, Priv. Comm. to Stephen Croft, 1st June 2011]
Also:
[Croft et al. 2011]
S. Croft, A. Favalli, M.T. Swinhoe, C. D Rael, State of the Art Monte Carlo modeling of active collar measurements and comparison with experiment, Proc. 52nd Annual INMM Meeting, July 2011 Palm Desert, CA, USA.

[Owens 0.1 and 5 Ci]
JG Owen, DR Weaver and J Walker, Neutron Spectra from Am/f and Am/Li sources. Nuclear Data for Science and Technology Proc. Of the Interantional Conf. on Nucl Data for Science and Technol., Antwerp, 6-10 Sept 1982. pp492-494

[Sources99]
Beddingfield, DH, "Application of the Sources Code in Nuclear Safeguards" Proceedings of American Nuclear Society 12th Biennial Topical Meeting of the Radiation Protection and Shielding Division, Santa Fe, NM, 2002

[3-micron (DHB); 5-micron (DHB); SGTS1; SGTS2]
DH.Beddingfield, Private Communication, July 14th 2016
Brief description of 3-micron and 5-micron: MCNP used to calculate the alpha energy escaping from 10.5 g/cm^3 AmO_2 sphere with 3 micron diameter and 5 micron diameter. Then SOURCES4C used to calculate neutron spectrum on 0.75 g/cm^3 Li_2O
Brief description of SGTS1: The response for each energy bin for UNCL and AWCC benchmark measurements of Monsanto sources Singles and Doubles were calculated. The least-squares best-fit spectrum based on the energy responses was created.
Brief description of SGTS2: The response for each energy bin for UNCL and AWCC benchmark measurements of Gammatron sources Singles and Doubles were calculated. The least-squares best-fit spectrum based on the energy responses was created.

[Tagziria2003]
H. Tagziria, N.J. Roberts, D.J. Thomas Measurement of the 241Am–Li radionuclide neutron source spectrum Nucl. Instrum. Methods Phys. Res. A, 510 (3) (2003), pp. 346–356

[Tagziria2004]
H. Tagziria, H. Klein, B. Wiegel, B. Knauf, J. Wittstock, J. Zimbal Measurement and Monte Carlo Modelling of the JRC 241AmLi(α,n) source spectrum Radiat. Prot. Dosim., 110 (1-4) (2004), pp. 129–134

[Tagziria 2012]
H Tagziria M Looman The Ideal Neutron Energy Spectrum of AmLi sources Applied Radiation and Isotopes 2012

[Trykov2mm; Trykov4mm]
Trykov, L.A., Chernov, V.A., Rabochy, S.V. Investigations of AmO2–LiH neutron sources characteristics. Private Commun. 1997

[Werle]
Werle, H., 1970. Spectrum measurements of Radioactive Neutron sources in the 10 keV to 10 MeV energy region with proton recoil proportional counters. Karlsruhe Report KFK-INR-4/70-25 ORNL-tr-2415 English translation

Spectra in MCNP usable format

Birch

R Birch, LHJ Peaple, HJ Delafield Measurement of Neutron Spectra with Hydrogen Proportional Counters Part 1. Spectrometry System and Calibration United Kingdom Atomic Energy Authority Harwell Report AERE-R 11397 1984

SI	SP (initial)	SP (emergent)
0.000E+00	0.000000E+00	0.0000000E+00
5.000E-02	8.288379E-02	8.3489474E-02
1.000E-01	7.808080E-02	7.8254161E-02
1.500E-01	7.632317E-02	7.6600904E-02
2.000E-01	7.463468E-02	7.4672104E-02
2.500E-01	5.816281E-02	5.8139535E-02
3.000E-01	5.120453E-02	5.1250964E-02
3.500E-01	5.302490E-02	5.3510416E-02
4.000E-01	5.154408E-02	5.1967376E-02
4.500E-01	4.882613E-02	4.8385319E-02
5.000E-01	4.480835E-02	4.4803262E-02
5.500E-01	4.139041E-02	4.1331423E-02
6.000E-01	3.863712E-02	3.8575995E-02
6.500E-01	3.565526E-02	3.5820567E-02
7.000E-01	3.313382E-02	3.3175355E-02
7.500E-01	3.019975E-02	3.0309710E-02
8.000E-01	2.807689E-02	2.7829825E-02
8.500E-01	2.487426E-02	2.4798854E-02
9.000E-01	2.319869E-02	2.3035380E-02
9.500E-01	2.101677E-02	2.0941254E-02
1.000E+00	1.885116E-02	1.8736912E-02
1.050E+00	1.696269E-02	1.6808112E-02
1.100E+00	1.506073E-02	1.4879312E-02
1.150E+00	1.334478E-02	1.3226055E-02

1.200E+00	1.109541E-02	1.1021713E-02
1.250E+00	9.494509E-03	9.3684559E-03
1.300E+00	7.377188E-03	7.2192219E-03
1.350E+00	5.627439E-03	5.5108564E-03
1.400E+00	3.659540E-03	3.5820567E-03
1.450E+00	1.701845E-03	1.6532569E-03
1.500E+00	1.148478E-03	1.1021713E-03

Delafield and Birch

HJ Delfield and R Birch Neutron Spectrometry Measurements with Large Volume Cylindrical Proton Recoil Counters Developed for Use in Radiological Protection United Kingdom Atomic Energy Authority Harwell report AERE-R 13103 1989

SI	SP (initial)	SP (emergent)
0.000000E+00	0.000000E+00	0.00000000E+00
7.021858E-02	6.559679E-02	6.61436243E-02
9.002553E-02	3.006804E-02	3.02853482E-02
1.104319E-01	3.110982E-02	3.10477523E-02
1.303278E-01	3.265153E-02	3.28034677E-02
1.496198E-01	3.236185E-02	3.27026406E-02
1.703508E-01	3.430763E-02	3.43253415E-02
1.835347E-01	2.092891E-02	2.14194796E-02
2.107028E-01	4.279111E-02	4.23796798E-02
2.314396E-01	2.971251E-02	2.96239272E-02
2.514252E-01	2.470051E-02	2.45324012E-02
2.620562E-01	1.018257E-02	1.02816628E-02
3.463360E-01	9.186630E-02	9.22240882E-02
4.464875E-01	1.005996E-01	1.00774984E-01
5.000000E-01	4.655573E-02	4.65497799E-02
5.476945E-01	4.012873E-02	4.00304276E-02
5.982844E-01	3.788040E-02	3.78658600E-02
6.983191E-01	7.476585E-02	7.50201778E-02
7.565299E-01	3.818747E-02	3.82122342E-02
7.950764E-01	2.101629E-02	2.09500336E-02
8.542479E-01	3.513393E-02	3.49269783E-02
9.461248E-01	4.423543E-02	4.40245353E-02
1.050780E+00	4.139158E-02	4.10544733E-02
1.147840E+00	2.817082E-02	2.78813433E-02
1.253864E+00	2.253660E-02	2.23001459E-02
1.358385E+00	1.428355E-02	1.40047154E-02
1.471618E+00	6.627197E-03	6.48847374E-03
1.600000E+00	2.209266E-03	2.14642386E-03

Geiger and van der Zwan

KW Geiger, L van der Zwan, The neutron spectra and the resulting fluence-kerma conversions for AmLi and PoLi sources. Health Phys., 21 (1971), pp.120-123

SI	SP (initial)	SP (emergent)
0.000E+00	0.000000E+00	0
1.000E-11	0.000000E+00	0
1.000E-03	3.699848E-05	3.69985E-05
2.000E-03	6.999713E-05	6.99971E-05
3.000E-03	9.099627E-05	9.09963E-05
4.000E-03	1.109954E-04	0.000110995
5.000E-03	1.259948E-04	0.000125995
6.000E-03	1.389943E-04	0.000138994
7.000E-03	1.509938E-04	0.000150994
8.000E-03	1.669932E-04	0.000166993
9.000E-03	1.799926E-04	0.000179993
1.000E-02	1.849924E-04	0.000184992
2.000E-02	2.472899E-03	0.002472899
3.000E-02	3.516856E-03	0.003516856
4.000E-02	4.601811E-03	0.004601811
5.000E-02	5.848760E-03	0.00584876
6.000E-02	7.229704E-03	0.007229704
7.000E-02	8.520651E-03	0.008520651
8.000E-02	9.661604E-03	0.009661604
9.000E-02	1.054957E-02	0.010549567
1.000E-01	1.129954E-02	0.011299537
1.100E-01	1.186951E-02	0.011869513
1.200E-01	1.241949E-02	0.012419491
1.300E-01	1.291947E-02	0.01291947
1.400E-01	1.331945E-02	0.013319454
1.500E-01	1.342945E-02	0.013429449
1.600E-01	1.332945E-02	0.013329453
1.700E-01	1.321946E-02	0.013219458
1.800E-01	1.310946E-02	0.013109463
1.900E-01	1.296947E-02	0.012969468
2.000E-01	1.283947E-02	0.012839474
2.200E-01	2.541896E-02	0.025418958
2.400E-01	2.492898E-02	0.024928978
2.600E-01	2.447900E-02	0.024478996
2.800E-01	2.403901E-02	0.024039014
3.000E-01	2.354903E-02	0.023549034
3.200E-01	2.307905E-02	0.023079054
3.400E-01	2.260907E-02	0.022609073
3.600E-01	2.214909E-02	0.022149092
3.800E-01	2.172911E-02	0.021729109

4.000E-01	2.118913E-02	0.021189131
4.200E-01	2.070915E-02	0.020709151
4.400E-01	2.033917E-02	0.020339166
4.600E-01	1.977919E-02	0.019779189
4.800E-01	1.934921E-02	0.019349207
5.000E-01	1.893922E-02	0.018939223
5.200E-01	1.843924E-02	0.018439244
5.400E-01	1.802926E-02	0.018029261
5.600E-01	1.757928E-02	0.017579279
5.800E-01	1.714930E-02	0.017149297
6.000E-01	1.675931E-02	0.016759313
6.200E-01	1.625933E-02	0.016259333
6.400E-01	1.589935E-02	0.015899348
6.600E-01	1.551936E-02	0.015519364
6.800E-01	1.510938E-02	0.015109381
7.000E-01	1.470940E-02	0.014709397
7.200E-01	1.434941E-02	0.014349412
7.400E-01	1.400943E-02	0.014009426
7.600E-01	1.362944E-02	0.013629441
7.800E-01	1.328946E-02	0.013289455
8.000E-01	1.293947E-02	0.012939469
8.200E-01	1.262948E-02	0.012629482
8.400E-01	1.229950E-02	0.012299496
8.600E-01	1.200951E-02	0.012009508
8.800E-01	1.170952E-02	0.01170952
9.000E-01	1.140953E-02	0.011409532
9.200E-01	1.109954E-02	0.011099545
9.400E-01	1.081956E-02	0.010819556
9.600E-01	1.050957E-02	0.010509569
9.800E-01	1.021958E-02	0.010219581
1.000E+00	9.946592E-03	0.009946592
1.020E+00	9.627605E-03	0.009627605
1.040E+00	9.329617E-03	0.009329617
1.060E+00	9.020630E-03	0.00902063
1.080E+00	8.678644E-03	0.008678644
1.100E+00	8.346658E-03	0.008346658
1.120E+00	7.963673E-03	0.007963673
1.140E+00	7.586689E-03	0.007586689
1.160E+00	7.178706E-03	0.007178706
1.180E+00	6.772722E-03	0.006772722
1.200E+00	6.318741E-03	0.006318741
1.220E+00	5.904758E-03	0.005904758
1.240E+00	5.499775E-03	0.005499775
1.260E+00	5.090791E-03	0.005090791
1.280E+00	4.672808E-03	0.004672808

1.300E+00	4.274825E-03	0.004274825
1.320E+00	3.864842E-03	0.003864842
1.340E+00	3.460858E-03	0.003460858
1.360E+00	3.052875E-03	0.003052875
1.380E+00	2.668891E-03	0.002668891
1.400E+00	2.280906E-03	0.002280906
1.440E+00	3.322864E-03	0.003322864
1.480E+00	1.742929E-03	0.001742929
1.500E+00	3.199869E-04	0.000319987
1.520E+00	2.499898E-05	2.4999E-05
1.540E+00	1.999918E-06	1.99992E-06

Ing

H Ing et al 1981, The spectrum of neutrons from a Pu-Li source Health Physics 40(1981)345-350

SI	SP (initial)	SP (emergent)
0.000	0.000000E+00	0.0000000E+00
0.060	8.957388E-02	9.0000496E-02
0.100	5.629348E-02	5.6719045E-02
0.150	6.319417E-02	6.3464743E-02
0.200	6.586205E-02	6.6093463E-02
0.300	1.189707E-01	1.1870318E-01
0.400	1.016882E-01	1.0307206E-01
0.500	9.447609E-02	9.3969722E-02
0.600	8.969553E-02	8.9156683E-02
0.700	7.055772E-02	7.0948879E-02
0.800	5.989466E-02	5.9745165E-02
0.900	4.956925E-02	4.9201413E-02
1.000	4.150266E-02	4.1257465E-02
1.100	3.276569E-02	3.2265197E-02
1.200	2.318456E-02	2.2929741E-02
1.300	1.379573E-02	1.3580533E-02
1.400	1.049910E-02	1.0274026E-02
1.500	5.616284E-03	5.4553209E-03
1.600	2.886581E-03	2.8066352E-03
1.700	1.201451E-03	1.1800304E-03
1.800	7.293913E-04	7.2211277E-04
1.900	6.854751E-04	6.7756370E-04
2.000	4.722687E-04	4.6529223E-04
2.100	4.984475E-04	4.9358949E-04
2.200	4.915460E-04	4.9002399E-04
2.300	4.939003E-04	4.8754009E-04
2.400	5.055188E-04	4.9996959E-04
2.500	4.935658E-04	4.8540393E-04

2.600	4.828458E-04	4.7587894E-04
2.700	4.682013E-04	4.5977045E-04
2.800	4.593790E-04	4.4844967E-04
2.900	4.270478E-04	4.1726194E-04
3.000	3.902247E-04	3.7941356E-04
3.100	3.734152E-04	3.5963373E-04
3.200	3.512583E-04	3.4125211E-04
3.300	3.286127E-04	3.1765556E-04
3.400	3.075140E-04	2.9597099E-04
3.500	2.868613E-04	2.7601275E-04
3.600	2.606932E-04	2.5246572E-04
3.700	2.396939E-04	2.3111097E-04
3.800	2.258950E-04	2.1604134E-04
3.900	2.107423E-04	2.0209810E-04
4.000	1.924894E-04	1.8169247E-04

Obninsk

Rinard, PM and Menlove, HO, "Calibration of the IAEA Active Well Coincidence Counter for Measurements of the Bruce 'A' Unirradiated Booster Rods" Los Alamos National Laboratory Report, LA-UR-98-4362,1998. ALSO maybe P Rinard, Obninsk Russia IPPE, Priv. Comm. to Stephen Croft, 1st June 2011

SI	SP (initial)	SP (emergent)
0.0000	0.000000E+00	0
0.0250	2.040117E-02	2.0671835E-02
0.0500	2.741287E-02	2.7993109E-02
0.0750	3.628829E-02	3.6175711E-02
0.1000	4.299382E-02	4.3066322E-02
0.1500	5.506415E-02	5.5555556E-02
0.2000	7.605887E-02	7.6658053E-02
0.2500	8.757187E-02	8.7424634E-02
0.3000	9.161004E-02	9.1300603E-02
0.3500	8.081774E-02	8.1395349E-02
0.4000	6.631414E-02	6.6752799E-02
0.4500	4.644526E-02	4.5650301E-02
0.5000	3.864528E-02	3.8759690E-02
0.5500	3.680567E-02	3.6606374E-02
0.6000	3.465599E-02	3.4453058E-02
0.6500	2.985083E-02	3.0146425E-02
0.7000	2.577798E-02	2.5839793E-02
0.7500	2.298947E-02	2.3255814E-02
0.8000	2.176920E-02	2.1533161E-02
0.8500	2.000485E-02	1.9810508E-02
0.9000	1.643967E-02	1.6365202E-02
0.9500	1.337838E-02	1.3350560E-02

1.0000	1.212652E-02	1.2058570E-02
1.0500	9.573580E-03	9.4745909E-03
1.1000	7.430726E-03	7.3212748E-03
1.1500	5.195640E-03	5.1679587E-03
1.2000	3.900063E-03	3.8759690E-03
1.2500	2.133527E-03	2.1533161E-03
1.3000	1.699233E-03	1.7226529E-03
1.3500	1.708769E-03	1.7226529E-03
1.4000	1.699863E-03	1.7226529E-03
1.4500	1.243697E-03	1.2919897E-03
1.5000	1.704611E-03	1.7226529E-03
1.7500	1.076700E-02	1.0766581E-02
2.0000	1.760948E-02	1.7226529E-02
2.2500	1.322126E-02	1.2919897E-02
2.5000	1.113275E-02	1.0766581E-02
3.0000	4.419223E-03	4.3066322E-03
3.5000	3.138532E-03	3.0146425E-03

Owen 0.1ci

JG Owen, DR Weaver and J Walker, Neutron Spectra from Am/f and Am/Li sources. Nuclear Data for Science and Technology Proc. Of the Interantional Conf. on Nucl Data for Science and Technol., Antwerp, 6-10 Sept 1982. pp492-494

SI	SP (initial)	SP (emergent)
0.00000	0.000000E+00	0.0000000E+00
0.02250	1.717494E-02	1.7755102E-02
0.04500	1.670294E-02	1.7755102E-02
0.06750	2.010644E-02	2.1428571E-02
0.09000	2.696512E-02	2.7806122E-02
0.11250	2.379815E-02	2.7959184E-02
0.13500	5.221057E-02	5.0918367E-02
0.15750	2.860530E-02	2.9897959E-02
0.18000	3.784834E-02	3.9285714E-02
0.20250	3.753370E-02	3.5102041E-02
0.22500	2.261509E-02	2.4489796E-02
0.24750	2.814058E-02	2.7142857E-02
0.27000	1.944181E-02	2.0510204E-02
0.29250	1.926588E-02	1.9897959E-02
0.31500	2.424690E-02	2.5255102E-02
0.33750	2.044281E-02	2.0765306E-02
0.36000	2.197608E-02	2.3724490E-02
0.38250	2.115636E-02	2.1479592E-02
0.40500	2.124454E-02	2.0918367E-02
0.42750	1.706461E-02	1.6989796E-02

0.45000	1.827996E-02	1.8061224E-02
0.47250	1.634745E-02	1.7142857E-02
0.49500	1.914396E-02	1.7959184E-02
0.51750	1.237218E-02	1.5816327E-02
0.54000	2.024817E-02	1.9387755E-02
0.56250	1.849605E-02	1.7857143E-02
0.58500	1.223649E-02	1.2295918E-02
0.60750	1.118165E-02	1.3520408E-02
0.63000	1.966416E-02	1.8622449E-02
0.65250	1.352090E-02	1.3367347E-02
0.67500	1.326159E-02	1.3112245E-02
0.69750	1.149199E-02	1.2244898E-02
0.72000	1.149140E-02	1.3163265E-02
0.74250	1.323074E-02	1.2653061E-02
0.76500	1.676504E-02	1.5510204E-02
0.78750	1.069894E-02	1.0714286E-02
0.81000	1.021835E-02	1.2755102E-02
0.83250	1.729362E-02	1.3673469E-02
0.85500	9.169148E-03	8.9285714E-03
0.87750	7.675273E-03	8.2142857E-03
0.90000	1.228646E-02	1.1530612E-02
0.92250	1.074783E-02	1.0459184E-02
0.94500	8.891009E-03	1.0969388E-02
0.96750	1.788900E-02	1.5102041E-02
0.99000	8.327314E-03	9.2346939E-03
1.01250	1.417932E-02	1.2397959E-02
1.03500	5.936753E-03	8.6734694E-03
1.05750	2.100493E-02	1.7346939E-02
1.08000	1.081543E-02	1.0051020E-02
1.10250	9.092440E-03	9.4387755E-03
1.12500	8.470622E-03	9.6938776E-03
1.14750	1.725370E-02	1.5051020E-02
1.17000	1.414361E-02	1.0714286E-02
1.19250	3.889992E-09	2.2448980E-03
1.21500	1.086487E-02	1.0612245E-02
1.23750	1.322868E-02	1.0765306E-02
1.26000	2.738778E-03	4.5918367E-03
1.28250	1.516077E-02	1.1479592E-02
1.30500	1.998881E-03	3.2653061E-03
1.32750	1.139960E-02	8.7755102E-03
1.35000	2.387106E-03	2.8061224E-03
1.37250	6.565533E-03	5.2040816E-03
1.39500	1.101815E-03	1.5306122E-03
1.41750	4.916069E-03	3.7244898E-03
1.44000	5.792403E-04	1.0204082E-03

1.46250	3.173508E-03	2.5510204E-03
1.48500	1.978507E-03	1.5306122E-03
1.50750	1.191528E-03	1.0204082E-03
1.53000	8.566970E-04	7.6530612E-04
1.55250	9.084679E-04	7.6530612E-04
1.57500	6.700644E-04	5.6122449E-04
1.59750	5.560003E-04	5.1020408E-04
1.62000	6.164246E-04	5.1020408E-04
1.64250	7.418146E-04	5.1020408E-04

Owen 5ci

JG Owen, DR Weaver and J Walker, Neutron Spectra from Am/f and Am/Li sources. Nuclear Data for Science and Technology Proc. Of the Interantional Conf. on Nucl Data for Science and Technol., Antwerp, 6-10 Sept 1982. pp492-494

SI	SP (initial)	SP (emergent)
0.00000	0.000000E+00	0.0000000E+00
0.02250	1.846260E-02	1.9104803E-02
0.04500	1.789205E-02	1.9104803E-02
0.06750	2.299527E-02	2.3799127E-02
0.09000	2.300112E-02	2.4672489E-02
0.11250	2.745595E-02	3.0021834E-02
0.13500	4.290789E-02	4.3122271E-02
0.15750	3.013342E-02	3.1386463E-02
0.18000	3.971321E-02	3.9628821E-02
0.20250	3.010630E-02	2.9203057E-02
0.22500	2.414955E-02	2.4017467E-02
0.24750	1.814914E-02	1.8558952E-02
0.27000	1.720460E-02	1.9104803E-02
0.29250	2.163880E-02	2.1288210E-02
0.31500	2.021672E-02	2.2379913E-02
0.33750	2.340732E-02	2.2379913E-02
0.36000	1.691187E-02	2.0633188E-02
0.38250	2.654597E-02	2.5109170E-02
0.40500	1.800372E-02	1.8831878E-02
0.42750	1.904106E-02	1.8831878E-02
0.45000	2.029679E-02	1.9923581E-02
0.47250	1.757077E-02	1.8286026E-02
0.49500	2.027312E-02	1.9104803E-02
0.51750	1.439359E-02	1.6648472E-02
0.54000	1.637302E-02	1.5829694E-02
0.56250	1.423943E-02	1.5010917E-02
0.58500	1.487056E-02	1.4737991E-02
0.60750	1.439342E-02	1.5283843E-02

0.63000	1.451962E-02	1.5010917E-02
0.65250	1.496356E-02	1.4737991E-02
0.67500	1.349566E-02	1.4192140E-02
0.69750	1.658710E-02	1.6266376E-02
0.72000	1.154921E-02	1.3646288E-02
0.74250	1.597976E-02	1.4082969E-02
0.76500	1.289072E-02	1.2991266E-02
0.78750	1.264827E-02	1.2008734E-02
0.81000	1.021223E-02	1.2008734E-02
0.83250	1.319628E-02	1.1353712E-02
0.85500	1.033420E-02	1.0480349E-02
0.87750	1.124169E-02	1.0917031E-02
0.90000	1.215692E-02	1.1735808E-02
0.92250	1.255058E-02	1.2008734E-02
0.94500	1.080489E-02	1.1572052E-02
0.96750	1.210688E-02	1.1462882E-02
0.99000	1.143514E-02	1.1353712E-02
1.01250	1.291915E-02	1.1735808E-02
1.03500	9.523304E-03	1.0098253E-02
1.05750	1.275701E-02	1.1572052E-02
1.08000	1.026591E-02	1.0098253E-02
1.10250	1.220113E-02	1.1735808E-02
1.12500	1.055227E-02	9.8253275E-03
1.14750	8.690976E-03	8.7336245E-03
1.17000	1.030446E-02	9.2794760E-03
1.19250	9.867462E-03	8.7336245E-03
1.21500	7.192092E-03	7.0960699E-03
1.23750	6.494881E-03	6.6593886E-03
1.26000	9.260189E-03	7.9148472E-03
1.28250	6.607256E-03	6.0043668E-03
1.30500	6.209722E-03	5.4585153E-03
1.32750	5.398631E-03	4.9126638E-03
1.35000	4.573135E-03	4.3668122E-03
1.37250	5.554043E-03	4.9126638E-03
1.39500	3.874260E-03	3.2751092E-03
1.41750	3.011550E-03	2.7292576E-03
1.44000	3.464355E-03	2.7292576E-03
1.46250	5.668228E-04	1.0917031E-03
1.48500	3.852696E-03	2.7292576E-03
1.50750	1.279722E-04	5.4585153E-04
1.53000	2.254614E-03	1.9104803E-03
1.55250	1.956574E-03	1.6375546E-03
1.57500	1.271456E-03	1.0917031E-03
1.59750	1.283952E-03	1.0917031E-03
1.62000	2.602738E-04	5.4585153E-04

1.64250	1.833762E-03	1.6375546E-03
1.66500	1.590362E-03	1.3646288E-03
1.68750	1.249759E-03	1.0917031E-03
1.71000	7.359204E-04	8.1877729E-04
1.73250	1.655711E-03	1.3646288E-03
1.75500	9.446237E-04	8.1877729E-04
1.77750	1.438388E-03	1.0917031E-03
1.80000	5.204560E-04	5.4585153E-04
1.82250	4.205154E-04	5.4585153E-04
1.84500	5.496207E-04	8.1877729E-04
1.86750	2.840851E-03	2.1834061E-03
1.89000	1.272402E-03	1.0917031E-03
1.91250	1.577144E-04	5.4585153E-04
1.93500	1.819762E-03	1.6375546E-03
1.95750	2.338902E-03	1.9104803E-03
1.98000	3.315124E-03	2.1834061E-03

Sources '99

Beddingfield, DH, "Application of the Sources Code in Nuclear Safeguards" Proceedings of American Nuclear Society 12th Biennial Topical Meeting of the Radiation Protection and Shielding Division, Santa Fe, NM, 2002

SI	SP (initial)
0.00	0.000000E+00
0.25	2.047774E-01
0.50	2.517263E-01
0.75	2.237567E-01
1.00	1.788056E-01
1.25	1.088816E-01
1.50	3.156568E-02
1.75	4.055591E-05
2.00	4.545059E-05
2.25	5.703799E-05
2.50	6.542887E-05
2.75	6.682735E-05
3.00	6.243213E-05
3.25	5.114440E-05
3.50	3.925732E-05
3.75	2.806948E-05
4.00	1.748100E-05
4.25	8.181106E-06
4.50	2.737024E-06
4.75	6.632789E-07
5.00	5.404125E-07
5.25	4.135504E-07

5.50	2.846905E-07
5.75	1.178719E-07
6.00	4.485124E-09

SGTS1

DH.Beddingfield, Private Communication, July 14th 2016
Details: The response for each energy bin for UNCL and AWCC benchmark measurements of Monsanto sources S and D were calculated. The least-squares best-fit spectrum based on the energy responses was created.

SI	SP (initial)
0.0000	0.000000E+00
0.0250	4.649547E-03
0.0500	6.299387E-03
0.0750	8.129209E-03
0.1000	9.689057E-03
0.1500	1.307873E-02
0.2000	3.899620E-02
0.2500	2.111794E-02
0.3000	1.643840E-01
0.3500	1.586845E-01
0.4000	5.399474E-02
0.4500	9.629062E-02
0.5000	8.189203E-02
0.5500	7.739246E-02
0.6000	7.259293E-02
0.6500	6.359381E-02
0.7000	5.099503E-02
0.7500	2.204785E-02
0.8000	9.929033E-03
0.8500	9.899036E-03
0.9000	4.559556E-03
0.9500	3.509658E-03
1.0000	3.179690E-03
1.0500	2.498757E-03
1.1000	1.931812E-03
1.1500	1.361867E-03
1.2000	1.022900E-03
1.2500	5.669448E-04
1.3000	4.529559E-04
1.3500	4.529559E-04
1.4000	4.529559E-04
1.4500	3.419667E-04
1.5000	4.529559E-04

1.7500	2.837724E-03
2.0000	4.529559E-03
2.2500	3.419667E-03
2.5000	2.837724E-03
3.0000	1.136889E-03
3.5000	7.949226E-04
4.0000	1.181885E-06
4.5000	1.181885E-06

SGTS2

DH.Beddingfield, Private Communication, July 14th 2016
Details: The response for each energy bin for UNCL and AWCC benchmark measurements of Gammatron sources S and D were calculated. The least-squares best-fit spectrum based on the energy responses was created.

SI	SP (initial)
0.000	0.000000E+00
0.025	2.862973E-02
0.050	3.436457E-02
0.075	4.361144E-02
0.100	4.165537E-02
0.150	4.756803E-02
0.200	5.334732E-02
0.250	5.912662E-02
0.300	6.134942E-02
0.350	4.490066E-02
0.400	3.832116E-02
0.450	2.520661E-02
0.500	2.511770E-02
0.550	3.014124E-02
0.600	3.507586E-02
0.650	3.543151E-02
0.700	3.494250E-02
0.750	3.489804E-02
0.800	3.231959E-02
0.850	3.014124E-02
0.900	2.658475E-02
0.950	2.169458E-02
1.000	1.960514E-02
1.050	1.538181E-02
1.100	1.191424E-02
1.150	8.402203E-02
1.200	6.312766E-03
1.250	3.498695E-03

1.300	2.800734E-03
1.350	2.800734E-03
1.400	2.800734E-03
1.450	2.018307E-03
1.500	2.582900E-03
1.750	1.329237E-02
2.000	2.000525E-02
2.250	1.253662E-02
2.500	9.513606E-03
3.000	3.689856E-03
3.500	2.796289E-03

Tagziria2003

H. Tagziria, N.J. Roberts, D.J. Thomas Measurement of the ^{241}Am–Li radionuclide neutron source spectrum Nucl. Instrum. Methods Phys. Res. A, 510 (3) (2003), pp. 346–356

SI	SP (initial)	SP (emergent)
0.0000E+00	0.000000E+00	0.000000E+00
1.2600E-09	0.000000E+00	0.000000E+00
2.0000E-09	7.943303E-09	7.589837E-09
3.1600E-09	0.000000E+00	0.000000E+00
5.0100E-09	3.197305E-08	5.240743E-08
7.9400E-09	1.099073E-07	1.096986E-07
1.2600E-08	3.596968E-07	3.438029E-07
2.0000E-08	5.395451E-07	6.802595E-07
3.1600E-08	1.548694E-06	1.544190E-06
5.0100E-08	3.377153E-06	3.147066E-06
7.9400E-08	6.194777E-06	5.962368E-06
1.2600E-07	1.109065E-05	1.038310E-05
2.0000E-07	1.858433E-05	1.749997E-05
3.1600E-07	2.199146E-05	2.222992E-05
5.0100E-07	3.842760E-05	3.823990E-05
7.9400E-07	5.812100E-05	5.596402E-05
1.2600E-06	8.725644E-05	8.651130E-05
1.9900E-06	1.194193E-04	1.199597E-04
3.1600E-06	1.726544E-04	1.720246E-04
5.0100E-06	2.343125E-04	2.338864E-04
7.9400E-06	3.127563E-04	3.098421E-04
1.2600E-05	4.081059E-04	4.068616E-04
2.0000E-05	5.199317E-04	5.207263E-04
3.1600E-05	6.691459E-04	6.694310E-04
5.0100E-05	8.171311E-04	8.232489E-04
7.9400E-05	1.055750E-03	1.061030E-03
1.2600E-04	1.323994E-03	1.327493E-03

2.0000E-04	1.634112E-03	1.637293E-03
3.1600E-04	2.059424E-03	2.166205E-03
5.0100E-04	2.318156E-03	2.230940E-03
7.9400E-04	3.127513E-03	3.141259E-03
1.2600E-03	3.907006E-03	3.888184E-03
2.0000E-03	4.894983E-03	4.944114E-03
3.1600E-03	5.821142E-03	5.828352E-03
5.0100E-03	7.271620E-03	7.359592E-03
7.9400E-03	8.762832E-03	9.071843E-03
1.2600E-02	1.164099E-02	1.139696E-02
2.0000E-02	1.450107E-02	1.441837E-02
3.1600E-02	1.818627E-02	1.860399E-02
5.0000E-02	2.723324E-02	2.739204E-02
6.0000E-02	1.244681E-02	1.209566E-02
7.0000E-02	1.167935E-02	1.179755E-02
8.0000E-02	1.224318E-02	1.237697E-02
9.0000E-02	1.183652E-02	1.202160E-02
1.0000E-01	1.256980E-02	1.270654E-02
1.1000E-01	1.401628E-02	1.381298E-02
1.2000E-01	1.422581E-02	1.426961E-02
1.3000E-01	1.519459E-02	1.550185E-02
1.4000E-01	1.517780E-02	1.757243E-02
1.5000E-01	1.901047E-02	1.693550E-02
1.6000E-01	1.592487E-02	1.594956E-02
1.7000E-01	1.557407E-02	1.583613E-02
1.8000E-01	1.588061E-02	1.603680E-02
1.9000E-01	1.552261E-02	1.626366E-02
2.0000E-01	1.565250E-02	1.476055E-02
2.1000E-01	1.449848E-02	1.433648E-02
2.2000E-01	1.223908E-02	1.260029E-02
2.3000E-01	1.264444E-02	1.224790E-02
2.4000E-01	1.093688E-02	1.089848E-02
2.5000E-01	9.889852E-03	9.832693E-03
2.6000E-01	9.324399E-03	9.239644E-03
2.7000E-01	8.637468E-03	8.938803E-03
2.8000E-01	8.716372E-03	8.801289E-03
2.9000E-01	9.422646E-03	9.127900E-03
3.0000E-01	9.418220E-03	9.420133E-03
3.1000E-01	9.252869E-03	9.703769E-03
3.2000E-01	9.165843E-03	9.528910E-03
3.3000E-01	9.211844E-03	8.840764E-03
3.4000E-01	9.001691E-03	8.891328E-03
3.5000E-01	8.728801E-03	8.984033E-03
3.6000E-01	8.675796E-03	9.059884E-03
3.7000E-01	9.317685E-03	9.177872E-03

3.8000E-01	9.037741E-03	9.531843E-03
3.9000E-01	9.165473E-03	9.068314E-03
4.0000E-01	8.012565E-03	8.132829E-03
4.1000E-01	8.145493E-03	8.031696E-03
4.2000E-01	8.127118E-03	7.888422E-03
4.3000E-01	7.742902E-03	7.719867E-03
4.4000E-01	7.612332E-03	7.593449E-03
4.5000E-01	7.726386E-03	7.593449E-03
4.6000E-01	7.509319E-03	7.601877E-03
4.7000E-01	7.226847E-03	7.433320E-03
4.8000E-01	7.419995E-03	7.290047E-03
4.9000E-01	7.391039E-03	7.332187E-03
5.0000E-01	7.269172E-03	7.231052E-03
5.1000E-01	6.941288E-03	6.862907E-03
5.2000E-01	6.688871E-03	6.613277E-03
5.3000E-01	6.356321E-03	6.429554E-03
5.4000E-01	6.342693E-03	6.337714E-03
5.5000E-01	6.406269E-03	6.329364E-03
5.6000E-01	6.084021E-03	6.120613E-03
5.7000E-01	6.144640E-03	6.045460E-03
5.8000E-01	6.048880E-03	5.987010E-03
5.9000E-01	6.130362E-03	6.128962E-03
6.0000E-01	6.096710E-03	6.187413E-03
6.1000E-01	6.065137E-03	6.195762E-03
6.2000E-01	6.139544E-03	6.128962E-03
6.3000E-01	6.130542E-03	6.187413E-03
6.4000E-01	6.090046E-03	6.187413E-03
6.5000E-01	5.951273E-03	6.028760E-03
6.6000E-01	5.880902E-03	5.928560E-03
6.7000E-01	5.636508E-03	5.744858E-03
6.8000E-01	5.772234E-03	5.694757E-03
6.9000E-01	5.891793E-03	5.870111E-03
7.0000E-01	6.003109E-03	6.028760E-03
7.1000E-01	5.672728E-03	5.911859E-03
7.2000E-01	5.252892E-03	5.310654E-03
7.3000E-01	5.370742E-03	5.277252E-03
7.4000E-01	5.320904E-03	5.410854E-03
7.5000E-01	5.405253E-03	5.394154E-03
7.6000E-01	5.303519E-03	5.143654E-03
7.7000E-01	4.950776E-03	5.035101E-03
7.8000E-01	4.938607E-03	4.868099E-03
7.9000E-01	4.889438E-03	4.801300E-03
8.0000E-01	4.901798E-03	4.888587E-03
8.1000E-01	4.937318E-03	4.858811E-03
8.2000E-01	4.855586E-03	4.850121E-03

8.3000E-01	4.805319E-03	4.728433E-03
8.4000E-01	4.651099E-03	4.676280E-03
8.5000E-01	4.441875E-03	4.389446E-03
8.6000E-01	4.267402E-03	4.328602E-03
8.7000E-01	4.401709E-03	4.337293E-03
8.8000E-01	4.432953E-03	4.363371E-03
8.9000E-01	4.413110E-03	4.406831E-03
9.0000E-01	4.481832E-03	4.502444E-03
9.1000E-01	4.506041E-03	4.441599E-03
9.2000E-01	4.368068E-03	4.337293E-03
9.3000E-01	4.360624E-03	4.345986E-03
9.4000E-01	4.309147E-03	4.311217E-03
9.5000E-01	4.198061E-03	4.232990E-03
9.6000E-01	4.034778E-03	4.146072E-03
9.7000E-01	4.171653E-03	4.093918E-03
9.8000E-01	3.997340E-03	3.937463E-03
9.9000E-01	3.921394E-03	3.911387E-03
1.0000E+00	3.831969E-03	3.841852E-03
1.0100E+00	3.997760E-03	3.876620E-03
1.0200E+00	3.913741E-03	3.876620E-03
1.0300E+00	3.511560E-03	3.589784E-03
1.0400E+00	3.558680E-03	3.528951E-03
1.0500E+00	3.644587E-03	3.589773E-03
1.0600E+00	3.615992E-03	3.581093E-03
1.0700E+00	3.545701E-03	3.459404E-03
1.0800E+00	3.335428E-03	3.302949E-03
1.0900E+00	3.305543E-03	3.276875E-03
1.1000E+00	3.562177E-03	3.485481E-03
1.1100E+00	3.429609E-03	3.415945E-03
1.1200E+00	3.160995E-03	3.163877E-03
1.1300E+00	3.193837E-03	3.076959E-03
1.1400E+00	2.961174E-03	2.937886E-03
1.1500E+00	2.816546E-03	2.807507E-03
1.1600E+00	2.820642E-03	2.772740E-03
1.1700E+00	2.767317E-03	2.781431E-03
1.1800E+00	2.825288E-03	2.816199E-03
1.1900E+00	2.744167E-03	2.677126E-03
1.2000E+00	2.535373E-03	2.555441E-03
1.2100E+00	2.382671E-03	2.364216E-03
1.2200E+00	2.224475E-03	2.207762E-03
1.2300E+00	2.190513E-03	2.138226E-03
1.2400E+00	2.114597E-03	2.077380E-03
1.2500E+00	2.051780E-03	2.068690E-03
1.2600E+00	2.220968E-03	2.146952E-03
1.2700E+00	2.406521E-03	2.338481E-03

1.2800E+00	2.028120E-03	1.966672E-03
1.2900E+00	1.970868E-03	1.947104E-03
1.3000E+00	1.904355E-03	1.839475E-03
1.3100E+00	1.835732E-03	1.790552E-03
1.3200E+00	1.709998E-03	1.692708E-03
1.3300E+00	1.574453E-03	1.526373E-03
1.3400E+00	1.537824E-03	1.497020E-03
1.3500E+00	1.504691E-03	1.487235E-03
1.3600E+00	1.541970E-03	1.487235E-03
1.3700E+00	1.469541E-03	1.448097E-03
1.3800E+00	1.468222E-03	1.448097E-03
1.3900E+00	1.220291E-03	1.183918E-03
1.4000E+00	1.139699E-03	1.134995E-03
1.4100E+00	1.085915E-03	1.056719E-03
1.4200E+00	1.049285E-03	1.007798E-03
1.4300E+00	9.990677E-04	9.676807E-04
1.4400E+00	9.620589E-04	9.373496E-04
1.4500E+00	9.839105E-04	9.393060E-04
1.4600E+00	7.783938E-04	7.680788E-04
1.4700E+00	7.872563E-04	7.465535E-04
1.4800E+00	8.904993E-04	8.580958E-04
1.4900E+00	9.401574E-04	8.952762E-04
1.5000E+00	4.462738E-04	4.402997E-04
1.5100E+00	2.051970E-04	2.172143E-04
1.5200E+00	3.150844E-04	3.219081E-04
1.5300E+00	4.940335E-04	4.862868E-04
1.5400E+00	4.936438E-04	4.892223E-04
1.5500E+00	4.837722E-04	4.657397E-04
1.5600E+00	5.253771E-04	5.117259E-04
1.5700E+00	5.110891E-04	4.931361E-04
1.5800E+00	4.936838E-04	4.872650E-04
1.5900E+00	4.429965E-04	4.373641E-04
1.6000E+00	4.252615E-04	4.148605E-04
1.6100E+00	4.190667E-04	4.129032E-04
1.6200E+00	3.251759E-04	3.209299E-04
1.6300E+00	2.651365E-04	2.710290E-04
1.6400E+00	5.546924E-04	5.381441E-04
1.6500E+00	5.897428E-04	5.792392E-04
1.6600E+00	5.545225E-04	5.391224E-04
1.6700E+00	5.270657E-04	5.195543E-04
1.6800E+00	4.789762E-04	4.588903E-04
1.6900E+00	4.353230E-04	4.354077E-04
1.7000E+00	4.122624E-04	4.089894E-04
1.7100E+00	3.185015E-04	3.228863E-04
1.7200E+00	3.479766E-04	3.502828E-04

1.7300E+00	7.729084E-04	7.573157E-04
1.7400E+00	8.480151E-04	8.140651E-04
1.7500E+00	3.394638E-04	3.395205E-04
1.7600E+00	1.753921E-04	1.839476E-04
1.7700E+00	4.930943E-04	4.823730E-04
1.7800E+00	7.940206E-04	7.582940E-04
1.7900E+00	6.371728E-04	6.027219E-04
1.8000E+00	1.845144E-04	1.888396E-04
1.8100E+00	1.536205E-04	1.624214E-04
1.8200E+00	6.018027E-04	5.939161E-04
1.8300E+00	8.364648E-04	8.013455E-04
1.8400E+00	3.868339E-04	3.767010E-04
1.8500E+00	0.000000E+00	0.000000E+00
1.8600E+00	3.247462E-04	3.199516E-04
1.8700E+00	5.491470E-04	5.332521E-04
1.8800E+00	5.496067E-04	5.215108E-04
1.8900E+00	5.305327E-04	4.999846E-04
1.9000E+00	4.477325E-04	4.334503E-04
1.9100E+00	0.000000E+00	0.000000E+00
1.9200E+00	0.000000E+00	0.000000E+00
1.9300E+00	3.306812E-04	3.228863E-04
1.9400E+00	4.274097E-04	4.031192E-04
1.9500E+00	4.686649E-04	4.393214E-04
1.9600E+00	4.835024E-04	4.637823E-04
1.9700E+00	4.991092E-04	4.774810E-04
1.9800E+00	5.344394E-04	5.038992E-04
1.9900E+00	4.879986E-04	4.539983E-04

Tagziria2004

H. Tagziria, H. Klein, B. Wiegel, B. Knauf, J. Wittstock, J. Zimbal Measurement and Monte Carlo Modelling of the JRC ^{241}AmLi(α,n) source spectrum Radiat. Prot. Dosim., 110 (1-4) (2004), pp. 129–134

SI	SP (initial)	SP (emergent)
0.000000E+00	0.000000E+00	0.0000000E+00
6.305000E-02	0.000000E+00	0.0000000E+00
8.459000E-02	1.979765E-02	2.1499013E-02
1.061400E-01	2.584817E-02	2.6160333E-02
1.276800E-01	2.730328E-02	2.7930099E-02
1.492300E-01	2.345222E-02	2.5374271E-02
1.707700E-01	2.986695E-02	3.0695966E-02
1.943200E-01	3.232511E-02	3.3935475E-02
2.452300E-01	6.641056E-02	6.7605133E-02
2.961400E-01	6.164156E-02	6.2470105E-02
3.470500E-01	6.544054E-02	6.7747854E-02

3.979500E-01	5.896339E-02	6.1567382E-02
4.488600E-01	5.465022E-02	5.4040276E-02
4.997700E-01	5.269486E-02	5.2930185E-02
5.506800E-01	4.713163E-02	4.6819090E-02
6.015900E-01	4.234588E-02	4.2645588E-02
6.325800E-01	2.433149E-02	2.5126844E-02
7.167700E-01	6.902127E-02	7.0069219E-02
8.009700E-01	6.298162E-02	6.1288762E-02
8.851600E-01	5.412284E-02	5.2434242E-02
9.693500E-01	4.987340E-02	4.7627436E-02
1.053550E+00	3.261114E-02	3.1457328E-02
1.137740E+00	3.441640E-02	3.1821975E-02
1.221940E+00	2.254240E-02	2.1111257E-02
1.306130E+00	1.598476E-02	1.4265009E-02
1.390320E+00	9.101416E-03	8.1323733E-03
1.474520E+00	4.813020E-03	4.1977396E-03
1.558710E+00	1.811477E-03	1.6253196E-03
1.642900E+00	1.031807E-03	9.5219251E-04
1.727100E+00	9.140001E-04	8.5800900E-04
1.811290E+00	9.905466E-04	9.1604766E-04
1.895480E+00	1.059487E-03	9.5281211E-04
1.979680E+00	9.437878E-04	8.4231510E-04
2.063870E+00	7.364344E-04	6.5650322E-04
2.148060E+00	6.160932E-04	5.5086552E-04
2.232260E+00	5.557780E-04	4.9144934E-04
2.316450E+00	5.028890E-04	4.4778910E-04
2.400650E+00	4.656693E-04	4.1222768E-04
2.484840E+00	4.319408E-04	3.8282706E-04
2.569030E+00	4.120898E-04	3.6063625E-04
2.653230E+00	3.919796E-04	3.4436064E-04
2.737420E+00	3.701866E-04	3.2575574E-04
2.821610E+00	3.494662E-04	3.0863785E-04
2.905810E+00	3.550820E-04	3.0054934E-04
2.995000E+00	3.895058E-04	3.1874677E-04

Tagziria 2012

H Tagziria, M Looman, The Ideal Neutron Energy Spectrum of AmLi sources, Applied Radiation and Isotopes, 2012

SI	SP (initial)
0.0000	0.000000E+00
0.0400	7.947906E-03
0.0800	2.380437E-02
0.1200	4.318231E-02

0.1600	6.128150E-02
0.2000	5.901910E-02
0.2400	5.183845E-02
0.2800	5.183845E-02
0.3200	4.800220E-02
0.3600	4.367414E-02
0.4000	4.229702E-02
0.4400	3.855915E-02
0.4800	3.796896E-02
0.5200	3.688694E-02
0.5600	3.088666E-02
0.6000	2.941119E-02
0.6400	2.911609E-02
0.6800	2.901773E-02
0.7200	2.783734E-02
0.7600	2.596841E-02
0.8000	2.459129E-02
0.8400	2.321418E-02
0.8800	2.341091E-02
0.9200	2.223053E-02
0.9600	2.114851E-02
1.0000	1.957467E-02
1.0400	1.918121E-02
1.0800	1.632862E-02
1.1200	1.623025E-02
1.1600	1.485314E-02
1.2000	1.288584E-02
1.2400	1.091853E-02
1.2800	1.022998E-02
1.3200	9.413547E-03
1.3600	6.619976E-03
1.4000	6.078968E-03
1.4400	3.875588E-03
1.4800	2.842753E-03
1.5200	1.564006E-03
1.5600	1.691881E-03
1.6000	1.396785E-03
1.6400	1.209892E-03
1.6800	1.573843E-03
1.7200	1.150872E-03
1.7600	1.583679E-03
1.8000	1.573843E-03
1.8400	1.514824E-03
1.8800	1.170546E-03
1.9200	8.361040E-04

1.9600	1.357439E-03
2.0000	1.209892E-03

Trykov2mm

Trykov, L.A., Chernov, V.A., Rabochy, S.V. Investigations of AmO_2–LiH neutron sources characteristics. Private Commun. 1997

SI	SP (initial)	SP (emergent)
0.000000	0.000000E+00	0.000000000E+00
0.001000	0.000000E+00	0.000000000E+00
0.002150	4.887926E-03	4.877369008E-03
0.004650	9.441399E-03	9.615384615E-03
0.010000	1.828436E-02	1.811594203E-02
0.021500	3.072902E-02	3.065774805E-02
0.046500	5.113787E-02	5.156075808E-02
0.100000	8.671456E-02	8.779264214E-02
0.200000	1.322309E-01	1.337792642E-01
0.400000	2.057967E-01	2.090301003E-01
0.500000	9.492155E-02	9.476031215E-02
0.600000	8.553180E-02	8.500557414E-02
0.700000	6.816173E-02	6.828316611E-02
0.800000	5.323683E-02	5.295429208E-02
0.900000	4.703541E-02	4.598662207E-02
1.000000	3.289871E-02	3.205128205E-02
1.100000	2.252718E-02	2.159977703E-02
1.200000	1.155270E-02	1.114827202E-02
1.300000	5.586138E-03	5.434782609E-03
1.400000	4.289519E-03	4.180602007E-03
1.500000	3.495354E-03	3.344481605E-03
2.500000	2.122214E-02	2.020624303E-02
4.000000	1.031818E-02	9.615384615E-03

Trykov4mm

Trykov, L.A., Chernov, V.A., Rabochy, S.V. Investigations of AmO_2–LiH neutron sources characteristics. Private Communication. 1997

SI	SP (initial)	SP (emergent)
0.000000	0.000000E+00	0.000000E+00
0.001000	0.000000E+00	0.000000E+00
0.002150	5.417760E-03	5.302876E-03
0.004650	8.656090E-03	8.770141E-03
0.010000	1.455885E-02	1.427697E-02
0.021500	2.257934E-02	2.243524E-02

0.046500	3.622415E-02	3.671222E-02
0.100000	6.356761E-02	6.526616E-02
0.200000	1.070767E-01	1.101367E-01
0.400000	1.822360E-01	1.896798E-01
0.500000	1.139375E-01	1.142158E-01
0.600000	1.025301E-01	1.019784E-01
0.700000	8.610646E-02	8.566184E-02
0.800000	6.620592E-02	6.526616E-02
0.900000	5.614461E-02	5.404854E-02
1.000000	3.950643E-02	3.773200E-02
1.100000	2.605989E-02	2.447481E-02
1.200000	1.525197E-02	1.427697E-02
1.300000	6.848715E-03	6.526616E-03
1.400000	5.151311E-03	4.894962E-03
1.500000	4.157348E-03	3.875178E-03
2.500000	2.547962E-02	2.345503E-02
4.000000	1.230354E-02	1.101367E-02

Werle

Werle, H., 1970. Spectrum measurements of Radioactive Neutron sources in the 10 keV to 10 MeV energy region with proton recoil proportional counters. Karlsruhe Report KFK-INR-4/70-25 ORNL-tr-2415 English translation

SI	SP (initial)	SP (emergent)
0.000	0.000000E+00	0.0000000E+00
0.010	1.033855E-02	1.0442531E-02
0.020	1.038780E-02	1.0442531E-02
0.030	9.993893E-03	1.0442531E-02
0.040	1.067331E-02	1.0442531E-02
0.050	1.403537E-02	1.4851600E-02
0.060	2.001464E-02	1.9492725E-02
0.070	2.074194E-02	2.0885063E-02
0.080	2.068260E-02	2.0885063E-02
0.090	1.866787E-02	1.8796556E-02
0.100	1.741417E-02	1.7520247E-02
0.110	1.788889E-02	1.7520247E-02
0.120	1.751527E-02	1.7520247E-02
0.130	1.684013E-02	1.7032929E-02
0.140	1.410802E-02	1.6522405E-02
0.150	1.857176E-02	1.6522405E-02
0.160	1.657725E-02	1.6522405E-02
0.170	1.540781E-02	1.5617386E-02
0.180	1.549482E-02	1.5617386E-02
0.190	1.470391E-02	1.5617386E-02

0.200	1.655686E-02	1.5617386E-02
0.210	1.471475E-02	1.4619544E-02
0.220	1.415871E-02	1.4619544E-02
0.230	1.511045E-02	1.4619544E-02
0.240	1.475151E-02	1.4619544E-02
0.250	1.161229E-02	1.1556401E-02
0.260	1.166454E-02	1.1556401E-02
0.270	1.116254E-02	1.1556401E-02
0.280	1.150790E-02	1.1556401E-02
0.290	1.196434E-02	1.1556401E-02
0.300	1.161729E-02	1.1556401E-02
0.310	1.003922E-02	1.0558559E-02
0.320	1.011474E-02	1.0558559E-02
0.330	1.100835E-02	1.0558559E-02
0.340	1.070805E-02	1.0558559E-02
0.350	1.029196E-02	1.0558559E-02
0.360	1.011774E-02	1.0558559E-02
0.370	1.073622E-02	1.0558559E-02
0.380	9.925329E-03	1.0558559E-02
0.390	1.057308E-02	1.0558559E-02
0.400	1.049756E-02	1.0558559E-02
0.410	1.087981E-02	1.0581765E-02
0.420	9.234518E-03	8.9805769E-03
0.430	9.029683E-03	8.9805769E-03
0.440	9.014278E-03	8.9805769E-03
0.450	9.186156E-03	8.9805769E-03
0.460	8.466070E-03	8.5860813E-03
0.470	8.350446E-03	8.5860813E-03
0.480	8.721235E-03	8.5860813E-03
0.490	8.658848E-03	8.5860813E-03
0.500	8.618498E-03	8.5860813E-03
0.510	8.717439E-03	8.5860813E-03
0.520	7.879655E-03	7.7738844E-03
0.530	7.675069E-03	7.7738844E-03
0.540	7.793471E-03	7.7738844E-03
0.550	7.854440E-03	7.7738844E-03
0.560	7.508470E-03	7.5418281E-03
0.570	7.679889E-03	7.5418281E-03
0.580	7.643535E-03	7.5418281E-03
0.590	7.541817E-03	7.5418281E-03
0.600	7.464434E-03	7.5418281E-03
0.610	7.388160E-03	7.5418281E-03
0.620	7.598180E-03	7.5418281E-03
0.630	7.514234E-03	7.5418281E-03
0.640	6.523950E-03	6.6600144E-03

0.650	6.563970E-03	6.6600144E-03
0.660	6.620494E-03	6.6600144E-03
0.670	6.544180E-03	6.6600144E-03
0.680	6.806038E-03	6.6600144E-03
0.690	6.712812E-03	6.6600144E-03
0.700	5.674110E-03	5.7317894E-03
0.710	5.606668E-03	5.8942288E-03
0.720	5.820084E-03	5.8942288E-03
0.730	6.017866E-03	5.8942288E-03
0.740	5.832552E-03	5.8942288E-03
0.750	5.903111E-03	5.8942288E-03
0.760	6.122582E-03	5.8942288E-03
0.770	5.902112E-03	5.8942288E-03
0.780	4.931755E-03	4.8731813E-03
0.790	4.982374E-03	4.8731813E-03
0.800	4.874692E-03	4.8731813E-03
0.810	4.931984E-03	4.8731813E-03
0.820	4.881615E-03	4.8731813E-03
0.830	4.978698E-03	4.8731813E-03
0.840	4.859067E-03	4.8731813E-03
0.850	4.972564E-03	4.8731813E-03
0.860	4.134334E-03	4.1770125E-03
0.870	4.238989E-03	4.1770125E-03
0.880	4.232526E-03	4.1770125E-03
0.890	4.189049E-03	4.1770125E-03
0.900	4.157890E-03	4.1770125E-03
0.910	4.266132E-03	4.1770125E-03
0.920	4.236032E-03	4.1770125E-03
0.930	4.232186E-03	4.1770125E-03
0.940	4.227830E-03	4.1770125E-03
0.950	4.215483E-03	4.1770125E-03
0.960	2.817621E-03	2.9007031E-03
0.970	2.943485E-03	2.9007031E-03
0.980	2.949129E-03	2.9007031E-03
0.990	2.916811E-03	2.9007031E-03
1.000	2.892985E-03	2.9007031E-03
1.010	2.931800E-03	2.8542919E-03
1.020	2.893748E-03	2.8542919E-03
1.030	2.810791E-03	2.8542919E-03
1.040	2.892270E-03	2.8542919E-03
1.050	2.916126E-03	2.8542919E-03
1.060	2.888823E-03	2.8542919E-03
1.070	2.613840E-03	2.5526188E-03
1.080	2.574470E-03	2.5526188E-03
1.090	2.576867E-03	2.5526188E-03

1.100	2.589475E-03	2.5526188E-03
1.110	2.551872E-03	2.5526188E-03
1.120	2.574120E-03	2.5526188E-03
1.130	2.671762E-03	2.5526188E-03
1.140	2.583551E-03	2.5526188E-03
1.150	2.581563E-03	2.5526188E-03
1.160	2.639245E-03	2.5526188E-03
1.170	2.588396E-03	2.5526188E-03
1.180	1.328568E-03	1.3459263E-03
1.190	1.357389E-03	1.3459263E-03
1.200	1.324921E-03	1.3459263E-03
1.210	1.359307E-03	1.3459263E-03
1.220	1.356480E-03	1.3459263E-03
1.230	1.385640E-03	1.3459263E-03
1.240	1.376470E-03	1.3459263E-03
1.250	1.350216E-03	1.3459263E-03
1.260	1.393473E-03	1.3459263E-03
1.270	1.382643E-03	1.3459263E-03
1.280	1.406909E-03	1.3459263E-03
1.290	1.382514E-03	1.3459263E-03
1.300	1.420785E-03	1.3459263E-03
1.310	5.859601E-04	5.8014063E-04
1.320	5.807253E-04	5.8014063E-04
1.330	5.920640E-04	5.8014063E-04
1.340	5.932828E-04	5.8014063E-04
1.350	5.771189E-04	5.8014063E-04
1.360	5.902758E-04	5.8014063E-04
1.370	5.765595E-04	5.8014063E-04
1.380	5.771089E-04	5.8014063E-04
1.390	5.989870E-04	5.8014063E-04
1.400	5.834326E-04	5.8014063E-04
1.410	5.901858E-04	5.8014063E-04
1.420	5.982778E-04	5.8014063E-04
1.430	5.917343E-04	5.8014063E-04
1.440	5.918841E-04	5.8014063E-04
1.450	5.992068E-04	5.8014063E-04
1.460	5.945315E-04	5.8014063E-04
1.470	6.114446E-04	5.8014063E-04
1.480	6.023437E-04	5.8014063E-04
1.490	6.050010E-04	5.8014063E-04
1.500	6.085675E-04	5.8014063E-04
1.510	2.326733E-04	2.3205625E-04
1.520	2.365295E-04	2.3205625E-04
1.530	2.392767E-04	2.3205625E-04
1.540	2.425734E-04	2.3205625E-04

1.550	2.460200E-04	2.3205625E-04
1.560	2.448911E-04	2.3205625E-04
1.570	2.473287E-04	2.3205625E-04
1.580	2.389970E-04	2.3205625E-04
1.590	2.445615E-04	2.3205625E-04
1.600	2.508951E-04	2.3205625E-04

3-micron (DHB)

DH.Beddingfield, Private Communication, July 14th 2016

Details: MCNP to calculate the alpha energy escaping from 10.5 g/cm^3 AmO_2 sphere with 3 micron diameter. Then SOURCES4C to calculate neutron spectrum on 0.75 g/cm$_3$ Li_2O.

SI	SP (initial)
0.000000	0.000000E+00
0.055600	4.905095E-03
0.111000	1.056482E-02
0.167000	1.388519E-02
0.222000	1.554538E-02
0.278000	1.972100E-02
0.333000	1.212439E-01
0.389000	1.413673E-01
0.444000	1.323118E-01
0.500000	1.172192E-01
0.556000	1.086667E-01
0.611000	9.961115E-02
0.667000	8.049386E-02
0.722000	1.926822E-02
0.778000	1.398581E-02
0.833000	1.116852E-02
0.889000	9.961115E-03
0.944000	9.256794E-03
1.000000	8.502164E-03
1.060000	7.697226E-03
1.110000	6.741361E-03
1.170000	5.785496E-03
1.220000	4.729014E-03
1.280000	3.712779E-03
1.330000	2.802193E-03
1.390000	1.941914E-03
1.440000	7.898460E-04
1.500000	3.622224E-04
1.560000	4.180650E-04
1.610000	4.427162E-04

1.670000	4.658582E-04
1.720000	4.920187E-04
1.780000	4.945342E-04
1.830000	5.383027E-04
1.890000	5.835805E-04
1.940000	6.187966E-04
2.000000	6.389200E-04
2.060000	6.741361E-04
2.110000	7.043213E-04
2.170000	7.395374E-04
2.220000	7.848152E-04
2.280000	8.049386E-04
2.330000	8.200312E-04
2.390000	8.401547E-04
2.440000	8.552473E-04
2.500000	8.653090E-04
2.560000	8.753708E-04
2.610000	8.653090E-04
2.670000	8.502164E-04
2.720000	8.451856E-04
2.780000	8.401547E-04
2.830000	8.351238E-04
2.890000	8.200312E-04
2.940000	7.848152E-04
3.000000	7.445682E-04
3.060000	7.043213E-04
3.110000	6.741361E-04
3.170000	6.489818E-04
3.220000	6.238274E-04
3.280000	5.886114E-04
3.330000	5.483644E-04
3.390000	5.081175E-04
3.440000	4.764230E-04
3.500000	4.417101E-04
3.560000	4.140403E-04
3.610000	3.853644E-04
3.670000	3.491421E-04
3.720000	3.204662E-04
3.780000	2.907841E-04
3.830000	2.616051E-04
3.890000	2.344384E-04
3.940000	2.027439E-04
4.000000	1.700433E-04
4.060000	1.398581E-04
4.110000	1.162130E-04

4.170000	9.709572E-05
4.220000	8.200312E-05
4.280000	6.741361E-05
4.330000	5.232101E-05
4.390000	3.773150E-05
4.440000	2.344384E-05
4.500000	1.152068E-05
4.560000	3.783212E-06
4.610000	3.541730E-06
4.670000	3.365650E-06
4.720000	3.219754E-06
4.780000	3.063798E-06
4.830000	2.943057E-06
4.890000	2.832378E-06
4.940000	2.721699E-06
5.000000	2.570773E-06
5.060000	2.399723E-06
5.110000	2.243766E-06
5.170000	2.087810E-06
5.220000	1.962038E-06
5.280000	1.831235E-06
5.330000	1.710495E-06
5.390000	1.504229E-06
5.440000	1.333180E-06
5.500000	1.177223E-06
5.560000	9.458029E-07
5.610000	7.546300E-07
5.670000	5.533953E-07
5.720000	3.687625E-07
5.780000	1.871482E-07
5.830000	3.270063E-08
5.890000	1.247655E-10
5.940000	0.000000E+00
6.000000	0.000000E+00

5-micron (DHB)

DH.Beddingfield, Private Communication, July 14th 2016
Details: MCNP to calculate the alpha energy escaping from 10.5 g/cm^3 AmO_2 sphere with 5 micron diameter. Then SOURCES4C to calculate neutron spectrum on 0.75 g/cm^3 Li_2O.

SI	SP (initial)
0.000000	0.000000E+00
0.055600	5.559393E-02
0.111000	1.496232E-01

0.167000	1.310919E-01
0.222000	1.228557E-01
0.278000	1.091288E-01
0.333000	3.342499E-02
0.389000	2.079625E-02
0.444000	1.853131E-02
0.500000	1.811950E-02
0.556000	1.763906E-02
0.611000	1.708999E-02
0.667000	1.654091E-02
0.722000	1.592320E-02
0.778000	1.530549E-02
0.833000	1.448188E-02
0.889000	1.358963E-02
0.944000	1.262875E-02
1.000000	1.159923E-02
1.060000	1.050108E-02
1.110000	9.197021E-03
1.170000	7.892966E-03
1.220000	6.451642E-03
1.280000	5.065225E-03
1.330000	3.822941E-03
1.390000	2.649291E-03
1.440000	1.853131E-03
1.500000	2.155123E-03
1.560000	2.244348E-03
1.610000	2.374753E-03
1.670000	2.498295E-03
1.720000	2.642428E-03
1.780000	2.786560E-03
1.830000	3.019917E-03
1.890000	3.280728E-03
1.940000	3.500359E-03
2.000000	3.617037E-03
2.060000	3.802351E-03
2.110000	3.960210E-03
2.170000	4.159250E-03
2.220000	4.420061E-03
2.280000	4.550466E-03
2.330000	4.612237E-03
2.390000	4.728916E-03
2.440000	4.818141E-03
2.500000	4.879912E-03
2.560000	4.948546E-03
2.610000	4.893639E-03

2.670000	4.804414E-03
2.720000	4.756370E-03
2.780000	4.735780E-03
2.830000	4.701462E-03
2.890000	4.639691E-03
2.940000	4.433788E-03
3.000000	4.186704E-03
3.060000	3.980800E-03
3.110000	3.809214E-03
3.170000	3.658218E-03
3.220000	3.514086E-03
3.280000	3.328773E-03
3.330000	3.102279E-03
3.390000	2.875785E-03
3.440000	2.690472E-03
3.500000	2.491432E-03
3.560000	2.333573E-03
3.610000	2.168850E-03
3.670000	1.969810E-03
3.720000	1.805087E-03
3.780000	1.640364E-03
3.830000	1.475641E-03
3.890000	1.324646E-03
3.940000	1.139332E-03
4.000000	9.608828E-04
4.060000	7.892966E-04
4.110000	6.554593E-04
4.170000	5.477032E-04
4.220000	4.632828E-04
4.280000	3.788624E-04
4.330000	2.951283E-04
4.390000	2.127669E-04
4.440000	1.317782E-04
4.500000	6.492822E-05
4.560000	5.161313E-05
4.610000	4.831868E-05
4.670000	4.591647E-05
4.720000	4.392607E-05
4.780000	4.179840E-05
4.830000	4.015117E-05
4.890000	3.864122E-05
4.940000	3.713126E-05
5.000000	3.507222E-05
5.060000	3.273865E-05
5.110000	3.061098E-05

5.170000	2.848331E-05
5.220000	2.676745E-05
5.280000	2.498295E-05
5.330000	2.333573E-05
5.390000	2.052171E-05
5.440000	1.818814E-05
5.500000	1.606047E-05
5.560000	1.290328E-05
5.610000	1.029517E-05
5.670000	7.549793E-06
5.720000	5.030908E-06
5.780000	2.553203E-06
5.830000	4.461242E-07
5.890000	1.702135E-09
5.940000	0.000000E+00
6.000000	0.000000E+00

Appendix C – Simulated count rates

^{235}U wt.%	**g U235/cm**	**Doubles [cps]** (4.5-64 μs)	**g U tot./cm**
0.20	2.787	24.409	1393.234
1.9025	26.500	124.247	1392.895
2.5	34.819	143.271	1392.776
3.1995	44.557	161.188	1392.636
3.5	48.740	168.144	1392.576
4	55.699	178.427	1392.476
4.18193	58.231	181.967	1392.440
4.5	62.657	187.727	1392.377
4.95	68.918	195.355	1392.287

Table C.1 Simulated Doubles rates for fuel without BP rods, simulated using EC Curto configuration with 80.3 cm active length

Gd rods	**Gd_2O_3 wt.% [Gd2O3/(Gd2O3+UO2)]**	**Gd rod ^{235}U wt.%**	**Fuel ^{235}U wt.%**	**Mean FA ^{235}U wt.%**	**Doubles [cps]** (4.5-64 μs)	**g U tot./cm**
0			4.250	4.250%	183.400	1392.295
4	2%	4.25	4.254	4.254%	177.016	1391.089
4	2%	2.50	4.282	4.252%	177.346	1391.084
4	5%	2.50	4.284	4.254%	176.333	1390.190
4	8%	2.50	4.286	4.255%	175.779	1389.309
4	11%	2.50	4.287	4.257%	175.329	1388.441

8	2%	4.25	4.258	4.257%	168.266	1389.882
8	2%	4.25	4.258	4.257%	166.694	1389.883
8	2%	2.50	4.316	4.254%	168.656	1389.872
8	2%	2.50	4.316	4.254%	167.179	1389.872
8	5%	2.50	4.319	4.258%	166.736	1388.085
8	5%	2.50	4.319	4.258%	164.965	1388.085
8	8%	2.50	4.323	4.261%	165.620	1386.323
8	8%	2.50	4.323	4.261%	163.994	1386.323
8	11%	2.50	4.326	4.264%	164.801	1384.588
8	11%	2.50	4.326	4.264%	163.024	1384.588
12	2%	4.25	4.262	4.261%	159.228	1388.676
12	2%	2.50	4.351	4.257%	160.261	1388.661
12	5%	2.50	4.356	4.261%	157.302	1385.979
12	8%	2.50	4.361	4.266%	155.626	1383.337
12	11%	2.50	4.366	4.271%	154.504	1380.735
16	2%	4.25	4.266	4.265%	155.018	1387.470
16	2%	2.50	4.387	4.259%	156.423	1387.450
16	5%	2.50	4.394	4.265%	152.963	1383.875
16	8%	2.50	4.400	4.271%	150.916	1380.352
16	11%	2.50	4.407	4.278%	149.771	1376.881
20	2%	4.25	4.270	4.268%	144.519	1386.264
20	2%	4.25	4.270	4.268%	152.017	1386.264
20	2%	2.50	4.424	4.261%	145.947	1386.239
20	2%	2.50	4.424	4.261%	153.497	1386.239
20	5%	2.50	4.433	4.269%	141.790	1381.769
20	5%	2.50	4.433	4.269%	149.594	1381.769
20	8%	2.50	4.441	4.277%	139.660	1377.366
20	8%	2.50	4.441	4.277%	147.523	1377.366
20	11%	2.50	4.450	4.285%	138.144	1373.028
20	11%	2.50	4.450	4.285%	146.042	1373.028
24	2%	4.25	4.275	4.272%	141.491	1385.058
24	2%	2.50	4.463	4.263%	143.398	1385.028
24	5%	2.50	4.473	4.273%	138.850	1379.664
24	8%	2.50	4.484	4.282%	136.566	1374.380
24	11%	2.50	4.494	4.292%	134.763	1369.174

Table C.2 Simulated Doubles rates for fuel with BP rods, simulated using EC Curto configuration with 80.3 cm active length